Testing Tube Model Predictions on Semi-Flexible Polymer Networks

ISOFORM- AND PTM-SPECIFIC, VISCOELASTIC SHEAR PROPERTIES OF ACTIN

Dissertation

for the award of the degree
Doctor rerum naturalium
of the Georg-August-Universität Göttingen

within the doctoral program
of the Georg-August-University School of Science (GAUSS)

Submitted by
Peter Nietmann
from Göttingen

Göttingen, 2022

Members of the Thesis Advisory Committee

Prof. Dr. Andreas Janshoff, Institut für Physikalische Chemie, Georg-August-Universität Göttingen
Prof. Dr. Sarah Köster, Fakultät für Physik, Institut für Röntgenphysik, Georg-August-Universität Göttingen
Prof. Dr. Peter Sollich, Fakultät für Physik, Institut für theoretische Physik, Georg-August-Universität Göttingen

Members of the Examination Board

Prof. Dr. Andreas Janshoff (Reviewer), Institut für Physikalische Chemie, Georg-August-Universität Göttingen
Prof. Dr. Sarah Köster (Reviewer), Fakultät für Physik, Institut für Röntgenphysik, Georg-August-Universität Göttingen
Prof. Dr. Peter Sollich, Fakultät für Physik, Institut für theoretische Physik, Georg-August-Universität Göttingen
Prof. Dr. Timo Betz, Fakultät für Physik, III. Physikalisches Institut - Biophysik, Georg-August-Universität Göttingen
Prof. Dr. Tim Salditt, Fakultät für Physik, Institut für Röntgenphysik, Georg-August-Universität Göttingen
Dr. Tim Schäfer, Institut für Physikalische Chemie, Georg-August-Universität Göttingen

Date of the oral examination:
November 14th, 2022

Declaration

I, Peter Friedrich Nietmann, hereby certify that my doctoral thesis “Testing Tube Model Predictions on Semi-Flexible Polymer Networks – Isoform- and PTM-Specific, Viscoelastic Shear Properties of Actin” has been written independently by me and with no other sources or aids than quoted.

Peter Friedrich Nietmann	Date

Abstract

The mechanical properties of simple entangled actin filament networks in eukaryotes are well understood as they are predictable with model systems. The high complexity of cellular actin structures like the cell cortex for example emerges from the dynamic interaction with a plethora of other proteins and ions, mainly actin binding proteins. This has been established knowledge for some time, but is it ultimately correct?

The tube model for semi-flexible filaments is commonly applied to predict the network properties of microfilaments with single filament bending mechanics similar to those of F-actin. It is based purely on the filaments bending stiffness and geometric considerations. Following this logic, an exchange of F-actin with similarly sized filaments and similar bending properties should not affect the overall network response to deformation. But does this logic reflect the reality?

This thesis investigated the raised questions by comparing the network shear response of DNA origami filament networks to those of F-actin networks. A clear difference could be shown. This is interesting on a theoretical level since the inter-filament interactions must be more complex than the assumed hard body interactions. Therefore, geometric considerations alone are not enough to predict network properties of semi-flexible filaments. But there are no such filaments present in the cytoplasm besides F-actin. The bending properties of other cellular filaments are vastly dissimilar from those of actin. However, there are different actin isoforms forming semi-flexible filaments in the cytoplasmic protein pool. They differ in a minuscule part of their amino acid sequence at the N-terminus, which is placed at the exterior of the filament. The comparison of entangled cytosolic γ- and β-actin networks revealed striking differences in the network stiffness.

So even small variations in the amino acid sequence can have a significant effect on the bulk properties of the network. For instance, in some cases network mechanics are altered by orders of magnitude.

Taking a closer look at the actin isoforms uncovers another layer of complexity hidden in the cellular machinery. In addition, these isoforms undergo post-translational modifications, which further differentiate actin filaments into a potential toolbox for the cell. To investigate electrostatic and steric causes of the observed phenomena, fluorecent labels were introduced and it was shown that a similar impact on the network stiffness could be achieved. The underlying causes of these different network mechanics of semi-flexible filaments are discussed and potential implications for *in vitro* as well as *in vivo* experiments

are evaluated.

Contents

Introduction

Eukaryotic cells are mainly composed of water (70%) and proteins (15%) [1] by mass. Their mechanical properties are ranging from viscous to elastic, and they have the ability to dynamically change their shape and deform like a viscous fluid. They can withstand sudden external stresses by stiffening their protein network structure. They are so-called viscoelastic materials with a complex stress-strain behavior.

These viscoelastic properties mainly originate from the mechanical properties of the actin cortex. It is a web-like structure consisting of cytoskeletal protein filaments. Understanding the properties of the cortex requires an understanding of single filament mechanics and also their interaction in a network. The basis for a systematic, theoretical description of protein filament networks is their characterization into categories, distinguished by the filaments' bending stiffness. On the length scale of a cell (smaller than the thickness of a human hair, $\sim$ 20 µm), thermal fluctuations play an important role for filaments with a diameter a thousand times smaller than the cell. They are not only the reason for thermal diffusion, the random thermal motion of molecules in a medium also induces fluctuations of larger structures like protein filaments. These fluctuations, for example bending fluctuations, are excited by the thermal energy of the heat bath ($k_\mathrm{B}T$, with the Boltzmann constant k_B and the temperature T) matching the internal bending energy of the filaments. The filaments stiffness determines the degree of bending they undergo at a certain temperature. To understand the mechanical properties of the networks they form, their interaction must be understood first. To characterize and compare mechanical properties of viscoelastic materials, it is handy to define a parameter, which describes the ratio of stress on the network to strain deforming it. For practical reasons, the most relevant type of deformation in the context of microscopic experimental setups is shear deformation with the shear modulus G as parameter. The goal is to connect this modulus with single filament properties. This is done in order to describe the network response to deformation on the filament level with easily accessible parameters like temperature, concentrations and the bending stiffness of the filaments. Models for this have already been established [2] and explain the viscoelasticity of filament networks with thermal fluctuations of single filaments. These fluctuations induce diffusion of the filaments, they undergo a random walk. The phenomenon is called Brownian motion. This motion is hindered by other filaments in their path and if the concentration of filaments is high enough, they glide through meshes formed by

other filaments. Their interaction suppresses bending fluctuations because of collisions. This essentially costs free energy and reduces diffusion of filaments. The energy cost depends on the bending stiffness of the filaments. A complex elasticity of the network emerges from this interaction. Even a tiny molar ratio of such filaments in water (1 µM or 0.004 %wt of entangled protein filaments) can give a drop of water macroscopically noticeable elastic properties. So the shear modulus depends on the bending stiffness of the filaments in some way. Filaments with a high bending stiffness, which are essentially rigid rods, form mikado-like structures [3]. Microtubules are an example. The stiff filaments are stacked over each other and strain on the network can mainly relax by filaments gliding through network meshes. This can be imagined and modeled like the deformation of a stack of mikados.

The network response to perturbations totally changes when the filaments show a low bending stiffness and are flexible. When they are flexible enough to curl up around themselves, their mechanics become more complicated. In a random walk situation (Brownian motion in a heat bath) the probability of finding the filament in a straight conformation is negligible compared to a sum of countless curled up conformations, which are individually equally likely. This makes the filaments response to deformation mainly entropic in nature. Thermal fluctuations push it back into a curled up conformation after stretching [2]. F-actin filaments, the main component of the cytoskeletal cortex, are characterized as semi-flexible. They show bending fluctuations at biologically relevant temperatures, but they don't curl up. They lie in between the aforementioned types and are treated separately model wise. The viscoelastic properties of these semi-flexible filaments in entangled networks (without crosslinking) are commonly described by the tube model or variants thereof [4]. It describes the shear properties of such a network as the result of a confinement around the filaments, formed by other filaments fluctuating around it. Besides collisions, the filaments don't interact with each other. Predictions of the tube model have been confirmed experimentally many times for actin stemming from skeletal muscle tissues [5, 6, 7].

This model assumes (at constant filament length and temperature) the shear properties to be dependent on two independent variables only, the concentration c and the persistence length (l_p) of the filaments. The latter one roughly represents the length over which the filament appears straight.

The question arises, whether knowing l_p is enough to predict the viscoelastic shear properties of semi-flexible polymer filaments under experimental conditions in general (at known actin concentration). Would two co-entangled,

semi-flexible polymers form a network with the same properties as a homogeneously composed one? This thesis investigates the viscoelastic properties of semi-flexible polymer networks like actin. In the first part of this thesis, another type of semi-flexible filament, artificially constructed and composed of DNA [8, 9], is characterized and compared to reconstituted actin networks. As it turns out, only some characteristic viscoelastic properties of DNA filament networks can be predicted correctly by the tube model. To illuminate the cause behind this anomaly further, actin-DNA co-entangled composite networks are co-polymerized. These composites are also characterized and compared to tube model predictions. The findings additionally reveal different viscoelastic behavior for different actin isoforms (chapter 3.2).

There are six actin isoforms in mammalians, from which two are cytosolic [10]. These two (γ- and β-actin) are responsible for cell motility, cellular shear response and so on. However, the vast majority of *in vitro* studies are performed with skeletal muscle actin (α-actin) due to availability. Assuming effectively the same protein properties because of very small differences in the amino acid sequence (AAS), this substitution is reasonable. But is it ultimately correct?

The cytosolic isoforms are evolutionary very conserved, locally separated [11, 12] in the cell and at least partially fulfil different biological roles [12], for example in epithelial-to-mesenchymal transitions [13, 14, 15, 16, 17, 18]. This raises the question, whether the mechanical properties are also different.

It opens up the opportunity to compare the mechanical properties of different semi-flexible polymer networks by only using actin. Are there already different types of interacting semi-flexible protein polymers present in the cell?

Different isoforms of actin are compared in this study and found to differ in their viscoelastic properties significantly, despite minuscule changes in the AAS. Their l_p and other single filament properties are compared to determine the influence on the viscoelastic properties. These viscoelastic shear properties are compared to tube model predictions. Alternative influences like electrostatic interactions between the filaments and inter-filament complexation of divalent cations are discussed. Therefore, the charge of actin filaments is altered with covalently labeled rhodamine-actin. Networks formed from those are also analyzed and compared.

There are not only six mammalian isoforms of actin, but also many post-translationally modified variants of them with unique AAS [19]. Post-translational modifications (PTMs) play an important role in many biological processes [20, 19]. For actin, some of them alter the ionic properties of the protein by exposing charges or exchanging them. An influence on the 3D-structure of the

protein is also possible. Are there not only two types of different semi-flexible protein polymers, but a whole cellular toolbox of them? Arginylated β-actin is chosen to investigate the influence of electrostatic interactions on the viscoelastic shear properties and network structure due to a high difference in the charge density at the surface of the filaments compared to regular, acetylated β-actin and potential relevance for cell mechanics. Again, single filament properties are analyzed first to determine their influence on the shear properties. Those are compared to a tube model prediction and alternative influences like electrostatic ones and inter-filament complexation of divalent cations are discussed like previously.

Is the filament bending stiffness the only important factor to predict the viscoelastic shear properties of semi-dilute, semi-flexible polymer networks? If not, does it make sense to alter the tube model by introducing a “sticky” tube surface or an effectively thicker tube wall, which would take attractive interaction or a “rough” tube surface into account? What is the potential biological relevance of differences in the viscoelastic properties of isoforms and post-translationally modified actins? Actin as a building block for the cellular machinery is – despite its simplicity on a first glance - still poorly understood regarding the relevance of its isoforms and PTMs. The underestimated influence of seemingly negligible changes in the AAS of actin and the implications for model systems to predict viscoelastic properties of semi-flexible filaments in general is the main focus of this work.

1 Theory and Biological Background

1.1 Shear Properties of Viscoelastic Materials

1.1.1 Basics - Elasticity, Viscosity and Linear Viscoelasticity)

Deformation of condensed matter is mainly characterized by a few variables. All of them are connected to the two phenomenologically observable characteristics of deformation; In the simplest case, strain ϵ measures the elongation $l - l_0 = \Delta l$ of a material relative to its initial length l_0 ($\epsilon = \frac{\Delta l}{l_0}$), whereas stress σ is the cause of that elongation, triggered by a force F acting on a defined area A ($\sigma = \frac{F}{A}$). It is intuitive, that pushing a piece of rubber will result in a different deformation, than doing the same with steel. The material properties stress and strain are connected by characteristic parameters, which can be compared. Which kind of parameter depends on the direction of stress and strain. For an uniaxial stress acting on the affected object, this parameter for the strain in the direction of the stress is called Young's modulus or elastic modulus E.

$$E = \frac{\sigma}{\epsilon} \tag{1}$$

For stress, that does not cause an elongation, but a three-dimensional change in shape, by essentially deforming one side (the area, the force is acting on) of the object against a parallel plane, the parameter is called shear modulus G. (Actually, a parameter is derived from the variable shear modulus under specific conditions. This will be explained later.) This kind of deformation is called shear deformation.

$$G = \frac{\text{shear stress}}{\text{shear strain}} = \frac{F/A}{\Delta s/h} \tag{2}$$

Where Δs is the shift of the parallel planes and h is their orthogonal distance. The previously described classifications are mainly associated with the elastic response of solids. The shear modulus is widely used to characterize the mechanical properties of bio-polymers, because controlling deformation is complicated to achieve in many experiments. Shearing a material, for example by dragging a probe through it, is typically much more practical than uniaxial deformation. General deformation fields have to be described by higher dimensional tensors though and require more mathematical formalism than presented here. Many experiments exploit ideal conditions, under which these can be condensed down to a simple, easily comparable scalar. In this case,

the scalar, which is utilized to compare material properties of entangled microfilament networks, is the plateau modulus G_0 (chapter 1.2.9), which is derived from a frequency-dependent shear modulus.
The viscous response of a fluid to deformation is characterized by dissipation of energy. Instead of storing energy from an outside load and elastically unloading it back (like an elastic solid), it dissipates it over time. If the fluid does not show any elastic response, it is an ideal Newtonian fluid. The simplest example is water. Since the induced deformation can be permanent, a proportional relation between stress and strain is not applicable anymore. Instead, there is one between stress and the strain rate $\dot{\epsilon}$ under non-turbulent flow conditions, which is called viscosity η.

$$\eta = \frac{\sigma}{\dot{\epsilon}} \tag{3}$$

Under conditions typical for biological materials, the mechanical response is neither completely elastic nor completely viscous. This phenomenon is usually a combination of both, called viscoelasticity. Materials with significant contribution of both are called viscoelastic. The response of these complex materials is time dependent. Energy is stored elastically, but also dissipated over time viscously. A good example is wheat flour dough, which responds elastically to quick, short stresses, like when it gets hit. But over longer time it deforms like a liquid if left on a flat surface. It stores energy elastically and dissipates it at the same time, with contributions of each depending on the time scale of the interaction. Biological materials can be characterized by E and by G. They are connected by a simple relation

$$\frac{G}{E} = 2 \cdot (1 + \nu) \tag{4}$$

where ν is the Poisson's ratio, characterizing the ratio of elongation in one direction and the corresponding contraction in the orthogonal direction. Atomic force microscope (AFM) measurements for example can investigate E for cells by oscillating the tip of a micro needle on a little light reflecting chip (a cantilever) against the cell membrane. Most methods, which measure mechanical properties of living matter, or parts of living matter, shear the often very small sample, so G is the property to compare. Uniaxial deformation would often not be practically possible on very small length scales. So for viscoelastic materials, the more relevant relation is [21, 22]:

$$G(t) = \frac{\sigma(t)}{\epsilon} \tag{5}$$

For viscoelastic materials the stress response becomes time dependent and most measurements involve a rotation, or oscillation of a probe, so a complex, frequency (of the oscillation of a cantilever for example) dependent shear modulus $G^*(\omega)$ with the angular frequency ω is utilized. It can be separated into a real part $G'(\omega)$ (the storage modulus) representing an elastic material response and an imaginary one $G''(\omega)$ (the loss modulus), the viscous response quantifying dissipation of energy.

$$G^*(\omega) = G'(\omega) + i \cdot G''(\omega) \tag{6}$$

1.1.2 Non-Linear Viscoelasticity

For most biological materials, ϵ can not exceed a certain, small value before the material is irreversibly changed in its structure and equation 5 does not apply anymore. Until that point the material response is considered linear because stress and strain show a classically elastic linear relationship. The stiffness of a viscoelastic material is commonly represented by G_0 and derived from linear viscoelastic properties. Deformation is reversible here and G_0 is a comparable, characteristic property of the material. Exceeding the linear regime and entering the so-called non-linear response is usually avoided. For a sample of protein filaments probed by a microparticle for example, this could manifest as accumulation of filaments on one side of the probe and thinning on the other. Deformation like this changes the material properties obviously. But it can also contain valuable information about the material. Intermediate filaments like vimentin for example play an important role in the mechanical response to extreme deformation in cells. Those filament structures can be stretched to a high degree by unfolding protein segments, giving the cell an unusually high resiliency through their non-linear strain response [23].

A frequently utilized parameter to find and quantify non-linear stress-strain-behavior is the differential modulus K. Since linear behavior is defined by a constant slope of stress against strain, it makes sense to use this slope as a parameter. As long as it is constant, the material response is linear.

$$K = \frac{d\sigma}{d\epsilon} \tag{7}$$

The absolute value of this slope is usually not important, so in order to compare just the "non-linearity" of different measurements, a relative value, the relative differential modulus K/K_0 is defined [24]. K gets divided by the initial value at

minimal deformation K_0 and thereby normalized and becomes comparable.

1.2 Biopolymer Networks

1.2.1 Actin

G-actin is a globular protein with a mass of about 42 kDa, which is found in almost all eukaryotic cells. It plays a crucial role in their structural stability, dynamic reorganization as well as motility. Muscle movement and cellular non-equilibrium processes are mainly mediated by the interaction between actin and the motor protein myosin, which can be classified as an actin-binding protein (ABP). Together, actin and all ABPs make up about 60 % of all proteins in muscle cells and 20 % in non-muscle cells. Comprehensive understanding of the biochemical and mechanical processes in which actin is involved is indispensable to understand cells as well as cellular processes. In the cytoplasm it is found in concentrations of up to 12 mg/ml (280 µM) [25, 26]. It polymerizes as a result of divalent cations binding to the monomer. The emerging F-actin has a filamentous structure consisting of two twisted helices and is 7-8 nm wide [27]. A three-dimensional structure of actin monomers combined to F-actin is shown in Figure 1 $\left(\mathrm{B}\right)$. The polymerization involves many complex interactions and is still not fully understood in detail [28]. The driving force of the process is the hydrolysis of adenosine triphosphate (ATP). Divalent metal ions such as Mg^{2+} and Ca^{2+} are a cofactor, accelerating the polymerization [29]. The current state of research describes the process as follows. Binding of ATP to actin leads to a structural change in the monomer (G-actin becomes G*-actin), which activates it for the binding of further monomers. Dimers are unstable and dissociate easily. Their dissociation is more likely than further binding. Trimer complexes are more stable and function as reaction seeds of the polymerization. As a result, there is a minimum or critical concentration for the polymerization, below which it does not proceed (the formation of trimers from dimers before their dissociation becomes unlikely). Due to the heterotropic structure of the monomers, a stable reaction nucleus grows into a structurally polar filament with two different ends. A distinction can be made between a positive (barbed end) and a negative (pointed end). They can be distinguished by the binding stability with other proteins (APBs) as well as with actin monomers. This leads to different reaction rates for polymerization and depolymerization at those ends. In the direction of the positive end, the filament grows about ten times faster with a rate of 11.6 $\mu M^{-1}s^{-1}$ [30]. This process proceeds until the concentration of monomers drops below the critical concentration and a steady

state is reached in which polymerization and depolymerization are in dynamic equilibrium. The critical concentration of the two ends differs. The one of the positive end is slightly above that of the negative end. This way, the barbed end is still growing, while the pointed end is already dissociating [25]. Theoretically, monomers can be incorporated over and over again after effectively wandering through the filament and dissociating again. This phenomenon is called treadmilling. The ATP bound to F-actin hydrolyzes with a rate constant of about 1/3.3 $s^{-}1$ to adenosine diphosphate (ADP) and free phosphate (Pi). ADP dissociates from the binding pocket in a hundredfold slower process. At the same time, ADP-actin dissociates easier than ATP-actin. At the pointed end, the concentration of ADP-actin grows, which causes a lower stability of the polymer [28].

Networks of entangled F-actin filaments represent the simplest *in vitro* model system for the investigation of the mechanical properties of cells and are indispensable for their understanding.

1.2.2 Isoforms of Mammalian Actin

Actin is a highly conserved protein (the amino acid sequence is very similar or identical across species) among eukaryotes, which assembles into diverse filamentous architectures coexisting in the cytoplasm. Together with a large number of ABPs, actin fulfills essential tasks connected to the exertion of forces in and by the cell. Although this by itself generates a tremendous degree of complexity within cellular systems, yet another layer is added by the presence of actin isoforms, which have previously been reported to be spatially segregated [31]. Six types of mammalian actin with unique amino acid sequence (AAS) are known (see Figure 1 A). The differences between α-skeletal muscle and the cytoplasmic isoforms β_{cyto}- and γ_{cyto}-actin (here referred to as β- and γ-actin), are concentrated at the N-terminus of actin. It is located at the periphery of the F-actin filament (see Figure 1 B). This leads to different interactions with ABPs [32, 10, 33, 34].
These two isoforms are very similar to each other in their AAS. Even the different amino acids at the outer part of the N-terminus have quite similar carbonic acid residues (aspartic acid and glutamic acid, see Figure 2 A and B). They also exist in the same cell types in close proximity to each other, but don't appear to be redundant. It has been shown that β-actin and γ-actin localize to different locations in the cell and tend to incorporate into different structures of the actin cytoskeleton such as stress fibers or the cortex, respectively [11, 12].

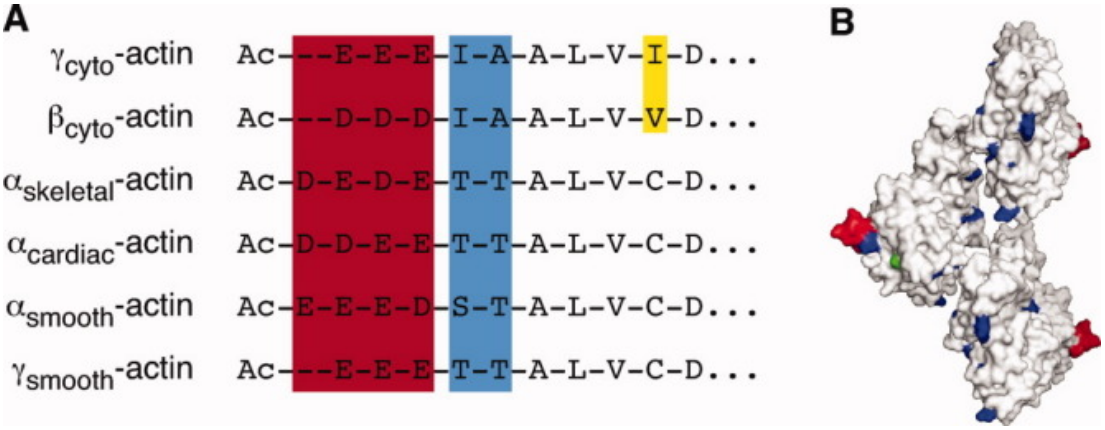

Figure 1: A) N-terminal amino acids of the six isoforms of actin (mammalians) in one letter abbreviations. Differences are marked with colors. Aspartic acid (D) and glutamic acid (E) are shown in red and dominate the differences between isoforms. B) Approximated 3D-structure of F-actin based on the work of Oda *et al*. [35]. The differences marked in A) are mapped on the 3D-structure. Adapted from Perrin et al.[10].

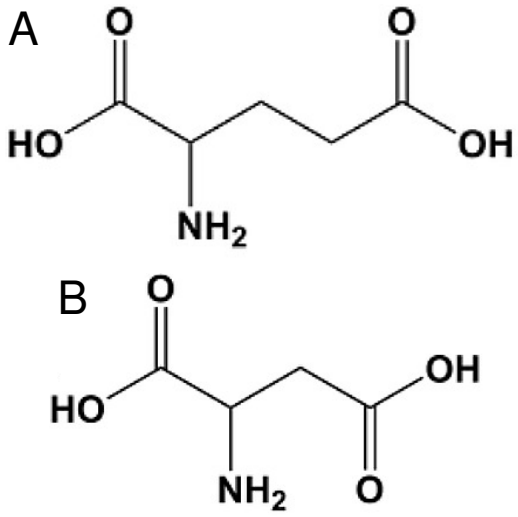

Figure 2: Structural formula for the amino acids glutamic acid A) and aspartic acid B). Both are negatively charged at physiological pH as amino acid side chains. If they are integrated into a protein or peptide, the amine group of a different amino acid attacked the carboxyl carbon atom and water was cleaved off. The own amine group attacked the next amino acids carboxyl carbon atom and water was cleaved off again. This reaction moves on from the N- to the C-terminus. The N-terminus is the amine group of the first amino acid. The carboxyl groups on the right side are deprotonated and become carboxylate groups).

Furthermore, both isoforms seem to fulfil dedicated roles regarding epithelial-to-mesenchymal transitions [13, 14, 15], cell motility [12], hearing [17, 18] and cellular junctions [16].

1.2.3 Post-Translational Modifications of Actin

Typically, when thinking of actin modifications, non-covalent interactions like the ones with a huge variety of ABPs come to mind. Examples are cofilin,

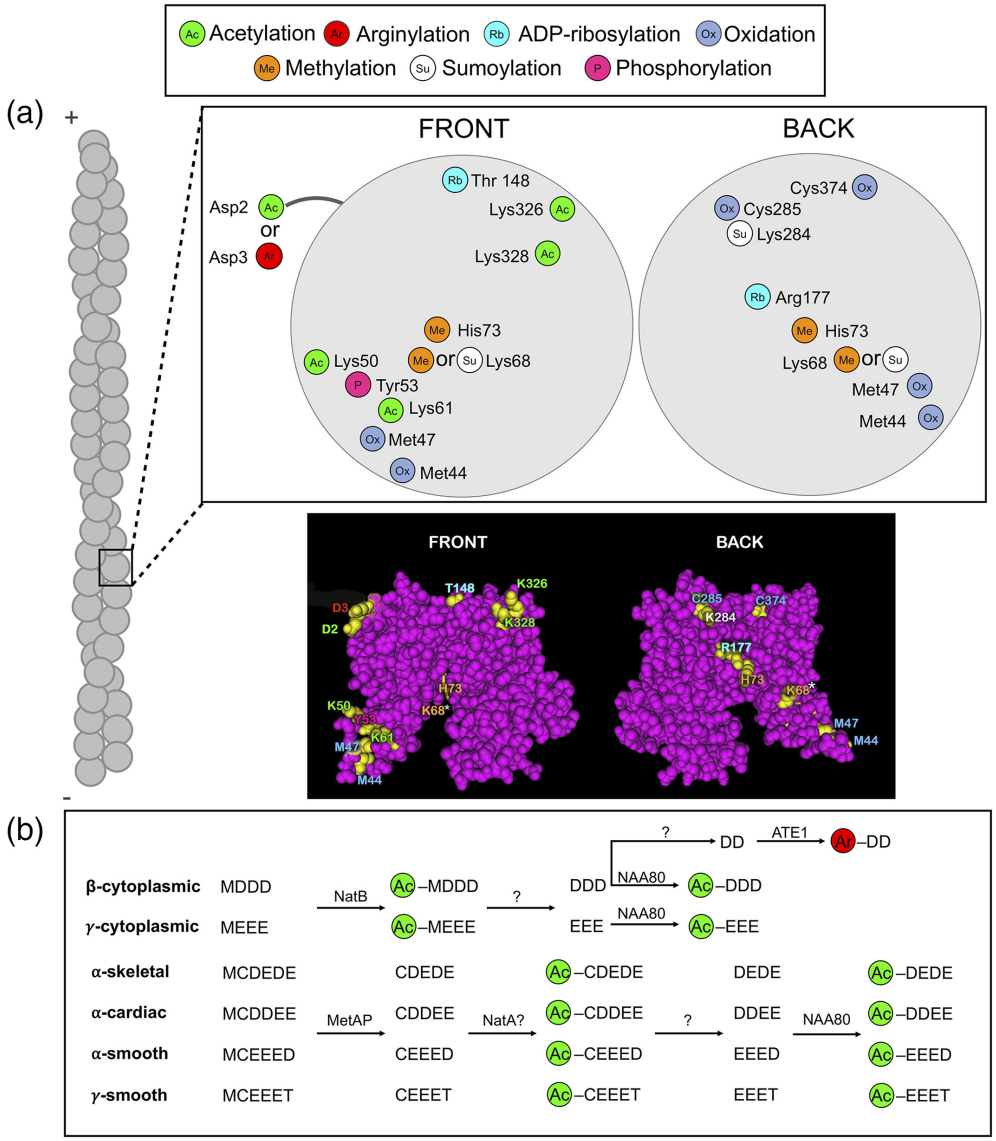

Figure 3: Actin modifications are ubiquitous in eukaryotes. a) Schematic representation of some relevant sites for post-translational modifications of actin and modification processes for actin isoforms. Schematic representation of processing at the N-terminus for different isoforms b). Originally published by MacTaggart *et al.* [36]

motor proteins like myosin and crosslinkers like fascin or α-actinin. They can change the mechanical properties of actin filaments and networks. Small molecules like divalent cations or ATP can have a similar effect [37]. Covalent modifications like post-translational modifications (PTMs) are lesser known, but very common. The first PTM for actin was found by sequencing of the protein and described in 1966. Today more than 140 specific ones are known for eukaryotic actins, which can be categorized in at least 17 types (like acetylation or arginylation for example) [20, 38]. The modification is an addition of a chemical group or even a protein to an amino acid side chain. Arginylation (a rare PTM) and acetylation (a very common PTM at the N-terminus) with added

groups and typical positions are separately listed in table 1.

PTM	chemical group	position
acetylation	$-C(O)CH_3$	**Met1**, **Asp2**, **Glu2**, Cys2, Asp3 , Lys50 , Lys52 , Lys61, Lys68, Lys113 , Lys191 , Lys193, Lys213 , Lys315 , Lys326 , Lys328
arginylation	$-C(O)CH(NH_2)(CH_2)_3CN(H)(HN)(NH_2)$	**Asp3**, Ser52 , Ser54 , Ile87, Phe90, Gly152 , Leu295 , Asn299

Table 1: Arginylation and acetylation in eukaryotes and the added chemical groups as well as the locations of the modification. amino acid positions in bold letters are relevant for cytoplasmic mammalian β-actin like the one investigated in this thesis.

These modifications are carried out at 94 different amino acid side chains, which is about half the number of theoretically possible positions. Some PTMs are rare as others are prevalent. They can also be reversible or irreversible. Besides post-translational, there are also co-translational modifications, which are typically included as PTMs. So the covalent modification can occur while the protein is translated or afterwards. It can be carried out by enzymes or through non-enzymatic mechanisms. Known effects are changes in polymerization dynamics, or in structural organization of actin [39, 40, 41, 42, 43, 44, 45, 46]. PTMs have also been shown to play in important role in diseases [47, 48]. Two modifications are in the focus of this study.

Acetylation

Most eukaryotic actins are N-terminally acetylated [49, 50]. This modification is irreversible and carried out with the transfer of an acetyl group, originating from acetyl coenzyme A at α-amino groups [51, 52]. The first step for the most relevant acetylation at the N-terminus is the removal of a methionine (Met) group by an aminopeptidase enzyme. After that, acetyltransferase enzymes add an acetyl group. This can also happen to the second or third amino acid. Although the non-acetylated variant still displays treadmilling like acetylated actin and can polymerize to filaments, it has been shown that acetylation is necessary for actin *in vivo* to form typical structures and function normally without disadvantages for the cell [49, 53, 54]. This form of acetylation is especially relevant for the interaction of F-actin with myosin in muscles and appears to facilitate it [49, 50, 53, 54].

Arginylation

Arginylation means the transfer of an arginine ($C_6H_{14}N_4O_2$) to the modified amino acid. This is mediated by the enzyme arginyltransferase and covalently finished with a peptide bond [55, 56]. In the context of this work, arginyla-

tion of β-actin at the N-terminus is studied. This modification is far away from being understood regarding its biological importance, but studies have shown a strengthening of actin networks by arginylation [56]. It appears to provide structural support for dendritic spines [57]. It also increases actin polymerization [56, 58] and a knock-out (KO) led to the collapse of lamella at the leading edge of cells, in addition, F-actin levels were reduced there without influencing the overall actin concentration much. Reintroducing arginylated actin prevents fatal effects for the KO cell. Despite the seemingly high similarity between β- and γ-actin, arginylation is only relevant for β-actin. Arginylated γ-actin is suppressed because of translation rates and further degradation, as well as a rather quick subsequent modification (ubiquitination). γ-actin appears to be translated more slowly. This is regulated by different coding sequences between the isoforms [56, 59]. A reduction or KO of arginylation affects cell migration as well as the contraction of myofibrils [60, 61, 62]. KO studies with mice have shown severe effects for the loss of arginylation. Defects in crest morphogenesis [61] and cardivascular development [63] were some of the consequences. Other studies found decreased polymerization rates in the form of slower elongation, but faster nucleation, leading to shorter filaments. Intracellular aggregates increased and the staining of F-actin was negatively effected [20, 56]. Arginylation and acetylation at the N-terminus seem to be mutually exclusive [20].

1.2.4 Single Filaments

The mechanical properties of polymer networks originate from their micro structure. Understanding them requires looking at their composition. Imagine a piece of fruit gum. Macroscopically, it is solid at room temperature. But looking at its basic structure reveals gelatin filaments forming a three-dimensional network with water or sugar solution in its pockets. In these pockets the material still is a liquid, but on a macroscopic level, the interaction between filaments keeps the system together and gives it properties of a solid.

For polymers, these basic elements are generally single filaments. In dilute and semi-dilute solutions, filaments are commonly sorted into categories depending on their thermally exited bending rigidity. Flexible filaments are deformed by the collision with solvent molecules. The movement of their ends can essentially be seen as a random walk. Therefore, in equilibrium their mean end-to-end distance over time is zero. They can entangle in themselves. This also means, that finding them in a straight configuration is extremely unlikely.

Pulling them apart results in a restoring force, which is entropic in nature. In the biological context, intermediate filaments are an example for this type of filament. Their flexible properties play an important role in cellular compression resistance and the structural integrity of the nucleus [23].
Semi-flexible polymers on the other hand have a higher bending stiffness than flexible ones. Their response to straightening by strain is a combination of entropic and enthalpic. The most likely conformation to find them in is bent but not curled up. They are, regarding their bending stiffness, in between rigid rods (tubulin) and flexible filaments (intermediate filaments, which are confusingly called that way because their diameter lies in between those of actin and tubulin). The thermal energy $k_\mathrm{B}T$ is now comparable to the filaments intrinsic bending energy. Filaments are nearly straight on length scales, where the energy required to bend them, is higher than $k_\mathrm{B}T$. A characteristic length scale is derived from the competition of bending energy and entropy, the persistence length l_p. On a phenomenological level, it is the length over which the filament appears straight.

$$l_\mathrm{p} = \frac{2}{D-1}\frac{\kappa}{k_\mathrm{B}T} \tag{8}$$

Here κ is the bending stiffness and D the spatial dimensionality of the bending [64]. Semi-flexible filaments have a contour length l_c, the total length of a straitened filament, close to l_p. The most prominent example is F-actin, which will be in the focus of this study. Actin filaments *in vivo* and *in vitro* typically have a l_c in the order of 10^{-5} m and l_p very similar to that [65]. Further information on l_p can be found in chapter 1.2.8 and 7.4.

1.2.5 Network Structures

When we take a look at cellular protein networks, one easily noticeable phenomenon is the variety of different structures of actin filaments alone. They form entangled structures, branched structures, crosslinked bundles and many more. Most of these have very different viscoelastic properties because of different filament interactions. The most relevant interactions can be crosslinks (transient and permanent) from ABPs, non-equilibrium motor protein activity, electrostatic interaction, chemical bonds or entanglements. Shearing a dense structure made of permanently crosslinked filaments results in a very elastic response, where in an entangled, low density network, filaments can slide through each other. This results in a more viscous response. Crosslinkers can simply freeze an entangled network in the time frame of the crosslinkers inverse binding rates. This increases the connectivity of the network compared to

purely entangled filaments and increases the elastic response. But crosslinks can also form different types of bundle structures, which are no longer describable on the basis of single filament properties. Crosslinked networks formed by different ABPs are shown schematically in Figure 4 (B) and (C). Fascin (B) forms straight bundles, where α-actinin (C) forms bent, more chaotic structures [66, 67].

In combination with myosin II motor protein filaments, actin filaments form active gels, which show non-thermal motion and contraction. This non-equilibrium activity (it is not caused by the surrounding heat bath) is generated by myosin filaments, shifting actin filaments against each other by hydrolyzing ATP. The resulting particle fluctuations (of filaments or probe particles) are athermal and can't be described as Gaussian white noise. This is important for microrheological analysis and structure formation of networks. Langevin equations for particle motion become more complicated and contain more than just stochastic thermal force terms (this prevents the transition from equation 47 to 48 for example) [68, 69]. Such an active, contracting network is shown in Figure 4 (D).

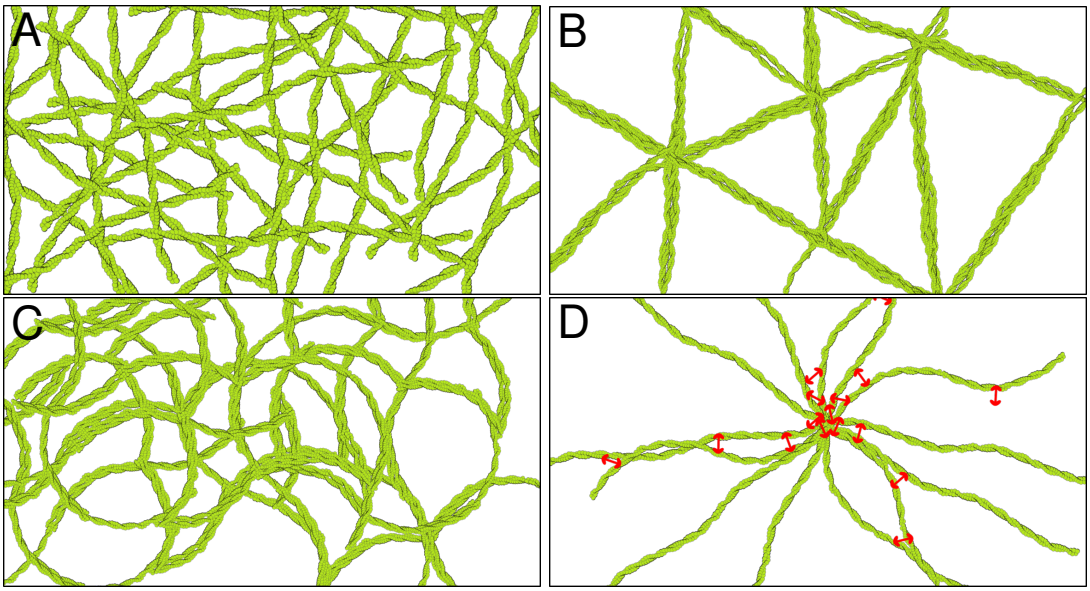

Figure 4: Schematic illustration of typical actin network structures (in a semi-dilute concentration regime). A) An entangled filament network. B) A network crosslinked by fascin. Straight bundles are formed. C) A network crosslinked by α-actinin. Curved bundles are formed. D) A network consisting of actin filaments and myosin II filaments. It is locally contracted and forms so-called asters, star like structures with actin-dense centers. Actin is depicted in green, myosin in red.

The mathematical description of the motion and viscoelastic properties of these networks obviously has to take filament interactions into account. Bundled networks and active gels, driven by motor proteins and similar to cytosolic struc-

tures, are already complicated and very hard to describe. A better starting point is the simplest system here. The entangled network (a schematic example is shown in Figure 4 $\left(\mathrm{A}\right)$, which is commonly described by the tube model (chapter 1.2.6). It is a useful tool to understand viscoelastic, semi-flexible polymer properties. It assumes purely topological interactions between the filaments. Their dynamics are a result of a competition between thermal Brownian forces deforming and moving them as well as internal bending stiffness resisting the deformation elastically. This is explained further in the following chapter.

1.2.6 The Tube Model for Semi-Flexible Polymers

The variable dominating entangled polymer solution dynamics is the connectivity. The number of entanglement points per volume, which is controlled by the monomer concentration. A model system for predicting the mechanical properties of polymer solutions was developed by de Gennes and Doi in the 70s and 80s [70, 2]. Originally, it was designed for flexible polymers and rigid rods. It was later modified to describe semi-flexible polymers, which can neither be approximated as rigid rods, nor is their structure dominated by entropic effects. Semi-flexible filaments have very little curvature on the scale of a mesh, but still show bending over their contour length, which has an influence on the mechanical properties. The so-called tube model and following modified versions still play a major role in the field of polymer physics and bio physics [71].

To reduce the immense complexity of filament network mechanics in cells, predicting characteristic properties of semi-flexible polymers from a few known variables is an important goal. These variables are primarily plateau moduli (a characteristic value of the shear modulus: further information in chapter 1.2.9), relaxation times and scaling coefficients.
A network consisting of entangled, dynamic filaments is obviously a very complicated structure. One filament is interacting with dozens or hundreds of other filaments in a time-dependent manner. The surface of those filaments also has a complex, rough shape, arising from many different amino acid residues and the folding of the protein. The first role of a model is simplification. The overall goal is to predict viscoelastic properties of the whole network. To achieve this, first we go back to the single filament level and then try to infer bulk properties from there. All filaments are assumed to have very similar properties and the system is in equilibrium.
So there is a single filament interacting with other filaments along its contour length. The first hurdle is the interaction of the filaments themselves. We simplify them to hard body interactions. Sometimes a harmonic interaction potential is used here, but that doesn't change much. The second important one is the complex, time dependent way, other filaments "hit" our filament. The surface of all filaments is simplified to be smooth. A single filament has a curvature, depending on l_p and the thermal bath energy $k_\mathrm{B}T$. The curvature of our filament is also dependent on those, but its thermal motion is restricted by a layer of filaments around it. It's diffusion constants are significantly influenced by this crowding. Translational and rotational diffusion are restricted, repta-

tional diffusion is dominating. The filament can only reptate along its contour, rotation and translation are hindered by other filaments. This type of motion in the network is therefore called reptation. The filament interactions along the contour are unified to a tube surface with walls made of filament interactions or a potential wall. The diameter of the tube is uniform. So the viscoelastic properties are determined by length scales. The first and obvious one is l_p, which for semi-flexible filaments is close to the contour length l_c.

$$l_\mathrm{c} \approx l_\mathrm{p} \tag{9}$$

It is a measure for the filaments thermal bending and therefore has an influence on the interaction with the tube wall. The tube diameter d_t is the next one. It is clearly dependent on the number of filaments per unit of volume and therefore the concentration of monomers, which is approximately the initial concentration. A high degree of polymerization is assumed. The filament has to reptate through meshes of other filaments. Simplified, a network mesh is formed by filaments enclosing a void (a space filled with solvent) and crossed in 90° angles. The average distance of parallel filaments on opposite sides of the mesh is the mesh size ξ, and approximately the tube diameter.

$$d_\mathrm{t} \approx \xi \tag{10}$$

Although l_p and d_t might seem sufficient to describe the interaction of the filament with the tube, Odijk *et al.* [72] demonstrated something else. For this type of reptation in a tube, the relevant interaction length of filament and tube is not d_t, but the so-called Odijk length l_o (or deflection length). This is the typical distance along l_c between two collisions of the filament with the tube. A schematic representation of that is shown in Figure 5. Since the filaments have a curvature, the tube also has a curvature and they diffuse (driven by thermal fluctuations) independently (on short time scales), semi-flexible filaments collide (on average) after a distance between d_t and l_c. After the collision, the filament drifts back into the inner tube, then collides again and so on. Odijk describes this length for a filament with l_p, reptating in a tube of diameter d_t. Letting the mean-square deviation σ_d from the tubes center reach the tube dimension d_t^2, led to the following scaling of l_o:

$$l_\mathrm{o} \propto l_\mathrm{p}^{1/3} \cdot d_\mathrm{t}^{2/3} \tag{11}$$

Semenov addressed the problem, that the tube diameter does not show the

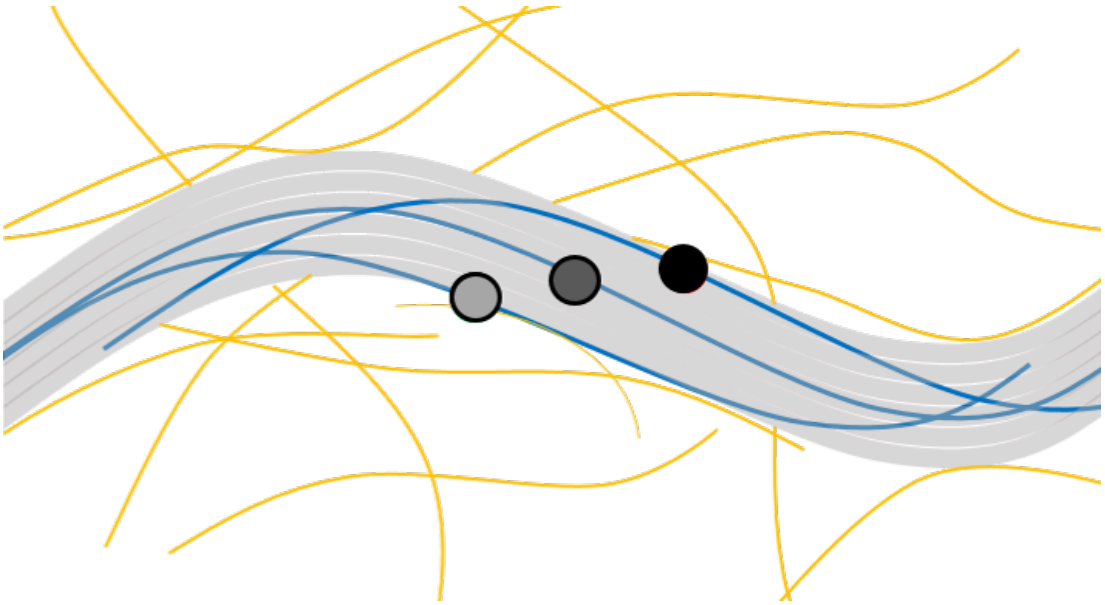

Figure 5: Schematic representation of a filament reptating through a tube, formed by the thermal fluctuations of other filaments. The reptating filament is shown in blue, the surrounding filaments in orange and the tube in grey. A dot marks the position on the filament, which is colliding with the tube walls at different points in time. The shading of the dot indicates temporal order. The filament is getting deflected from the wall at the position of first dot (light shading) to that of the third (black). The mean distance between the first and the third dot is the deflection length of this system.

same scaling behavior as the mesh size. Fluctuating filaments don't occupy overlapping volumes. Since the path of reptation is not a straight line, the filaments have to pass meshes at an angle, which reduces the effective tube diameter. At the limit of infinitely low concentrations, $d_\mathrm{t} = \xi$, with the mesh size ξ, is true. He proposed a scaling behavior of

$$d_\mathrm{t} \propto \xi^{6/5} \cdot l_\mathrm{p}^{-1/5} \propto c^{-3/5} \cdot l_\mathrm{p}^{-1/5} \tag{12}$$

with a model that describes the filament sliding through cylinders, which are connected at mesh points. From a scaling for the cylinder volume and a geometrically found scaling for the number of filaments intersecting the cylinder (both of which depend on l_p and c), he concludes equation 12 [73]. The scaling of ξ with c follows (chapter 1.2.7):

$$\xi \propto c^{-1/2} \tag{13}$$

To connect this single filament behavior with measurable, macroscopic shear properties, the next step after quantifying the number of interactions per filament length $l_\mathrm{c}/l_\mathrm{o}$, is finding one for the interaction energy.
Confining a freely fluctuating filament to a tube with a diameter smaller than

its fluctuation amplitude is connected to a cost in free energy. It was shown that every collision is increasing the free energy of the confinement by about $k_\mathrm{B}T$ [72, 74]. There have been multiple lines of reasoning, which arrived at the experimentally validated [5, 6, 7] scaling behavior of [75, 76, 77]:

$$G_0 \propto c^{7/5}. \tag{14}$$

Morse *et al.* for example argue starting from a classical theory for rigid rods introduced by Doi and Edwards [2]:

$$G_0 = 3/5 \cdot k_\mathrm{B}T \cdot \nu \tag{15}$$

with the polymer number density $\nu = 3 \cdot \xi \cdot L_\mathrm{r}$, where L_r is the average rod length. They use the relation between the tube diameter and the Odijk length (equation 11), as well as a verial expansion to identify L_r as l_O for semi-flexible polymers. They arrive at:

$$G_0 = 9/5 \cdot k_\mathrm{B}T/(\xi^2 \cdot l_\mathrm{o}) \tag{16}$$

With equation 11 and 13 we arrive at:

$$G_0 \propto c^{7/5} \cdot l_\mathrm{p}^{-1/5} \tag{17}$$

So the exponential factor of 7/5 for the concentration remains, but a weak dependency on the persistence length is added. This makes sense considering, that l_p is on the order of 10 µm for actin for example and ξ is typically 0.2-1 µm (lower mesh sizes for concentrations >2 mg/ml for entangled filaments force bundling and lower concentrations lead to non-affine networks). So on the length scale of a mesh, semi-flexible polymers are not effected by slight increases of l_p, because the change in curvature is negligible [74].
Further scaling behaviors derived from the tube model and extensions thereof are discussed in chapter 1.2.9 [78].

1.2.7 Mesh Size

The concentration dependency of the mesh size was already introduced in the previous chapter (equation 13). This assumption is purely based on geometric considerations an was presented by Schmidt *et al.* [79].
A very similar approach is presented here. Mesh sizes can be approximated by assuming a cubical network and comparing the number of molecules in one of those cubes N_mw. We can express this in dependence of its edge length a,

with the number of molecules or proteins in a volume V, N_{mv} divided by the number of cubes in that volume N_{w}, which we can also express in dependence of the edge length a. Solving towards a results in a good approximation for the average mesh size.

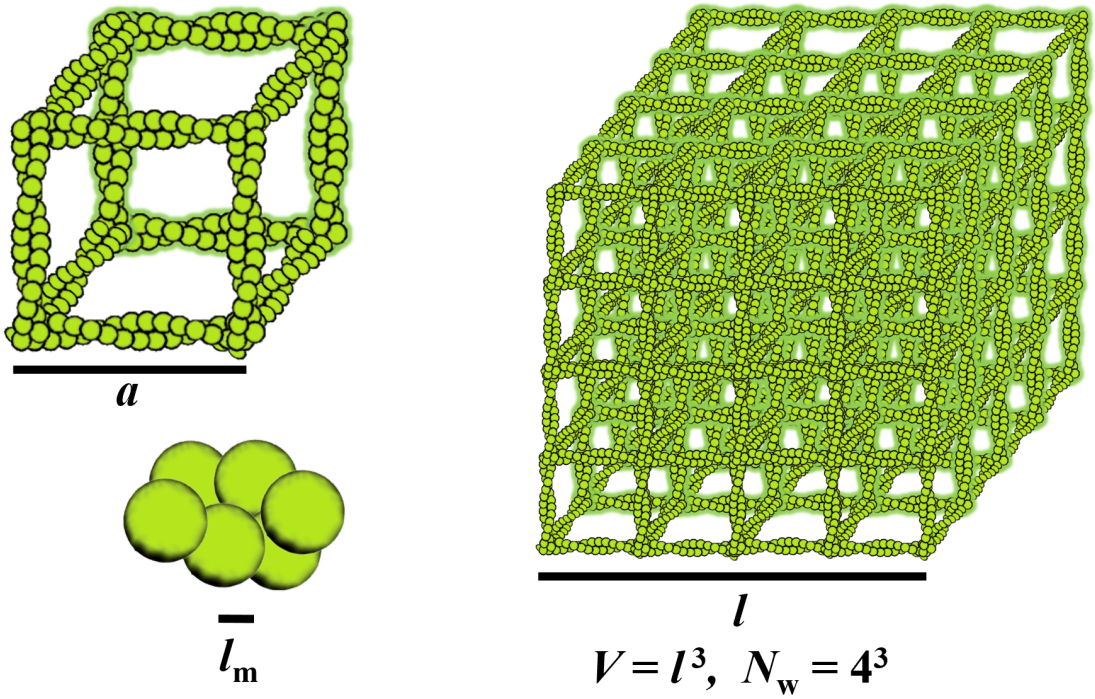

Figure 6: Schematic representation of the structure of a semi-flexible protein filament network. Purely geometrical assumptions are used to predict the mesh size of a cubical network from the protein concentration. The calculation is based on the size of a monomer and the volume fraction, a mesh cube of these filaments consisting of monomers would occupy in a network. It gets compared to the initial concentration of monomers, both of which can be related to the edge length a of a mesh cube.

$$\frac{N_{\mathsf{mv}}}{N_{\mathsf{w}}} = N_{\mathsf{mw}} \tag{18}$$

and

$$\frac{N_{\mathsf{A}} \cdot V \cdot a^3 \cdot c}{V} = \frac{a \cdot 12 \cdot 1/4 \cdot s_{\mathsf{u}}}{l_{\mathsf{m}}} \tag{19}$$

$$a = \sqrt{(\frac{3 \cdot s_{\mathsf{u}}}{N_{\mathsf{A}} \cdot l_{\mathsf{m}} \cdot c})} \tag{20}$$

For F-actin with a concentration of 24 µM, assuming a monomer length l_{m} (the effective distance of the next two monomers in the double helix along the the filament) of 2.761 nm [80] and one subunit per monomer $s_{\mathsf{u}} = 1$, this results in:

$$24 \cdot 10^{-6} \, \frac{\mathsf{mol}}{\mathsf{l}} \cdot 6.022 \cdot 10^{23} \, \frac{1}{\mathsf{mol}} \cdot a^3 = \frac{a \cdot 3 \cdot 1}{2.761 \text{ nm}} \tag{21}$$

$$\frac{24 \cdot 6.022 \cdot 10^{17} \cdot a^3}{10^{24}\ \text{nm}^3} = \frac{a \cdot 3}{2.761\ \text{nm}} \tag{22}$$

$$a = \sqrt{\frac{3 \cdot 10^7\ \text{nm}^2}{24 \cdot 6.022 \cdot 2.761}} \approx 274\ \text{nm} \approx \xi \tag{23}$$

For the DNA networks (chapter 2) with a subunit concentration of 24 µM, assuming a monomer length l_m of 14.2 nm and seven subunits per tile, this results in:

$$a = \sqrt{\frac{3 \cdot 7 \cdot 10^7\ \text{nm}^2}{24 \cdot 6.022 \cdot 14.2}} \approx 320\ \text{nm} \approx \xi \tag{24}$$

A list of relevant mesh sizes can be found in table 3.

A similar method to approximate ξ considers the volume of the filaments themselves, the partial specific volume of PSV $\approx 0.74\ cm^3/g$ [80, 79].

1.2.8 Persistence Length and the Angular Cosine Correlation

Measuring the stiffness (or the resistance to bending) of a macroscopic object just involves a force measurement for the bending process and a measurement of the deformation. For microscopic objects like protein filaments with diameters in the range of 10^{-8} m, this is not that simple anymore. Actively exerting force on single filaments is generally possible [81], but not simple and also not practical if good statistics are needed.
A practical alternative for objects of this size is using stochastic Brownian forces, which cause thermal bending fluctuations of the filaments.
So in practice, the bending fluctuations are imaged (via light microscopy or for filaments adhered to a surface additionally with AFM/EM) and the conformations are connected to the bending stiffness κ via a theoretical model. The worm-like chain (WLC) model [82] is a continuous model used to describe the resistance of (semi-flexible) polymers to bending. In the WLC model, semi-flexible polymers are assumed to be inextensible and to have an elastic bending energy, which is linear. Thermal fluctuations are effecting the polymer. The polymer is modeled with segments and the total length L. A coordinate along the filament s with the vector $\vec{r}(s)$ for chain segment positions and a unit tangent vector $\hat{r_\text{t}}(s) = \frac{d\vec{r}}{ds}$.
The connection to κ is introduced as an energy penalty E_b for filament bending:

$$E_\text{b} = (\kappa/2) \int |\frac{d\hat{r_\text{t}}}{ds}|^2 ds \tag{25}$$

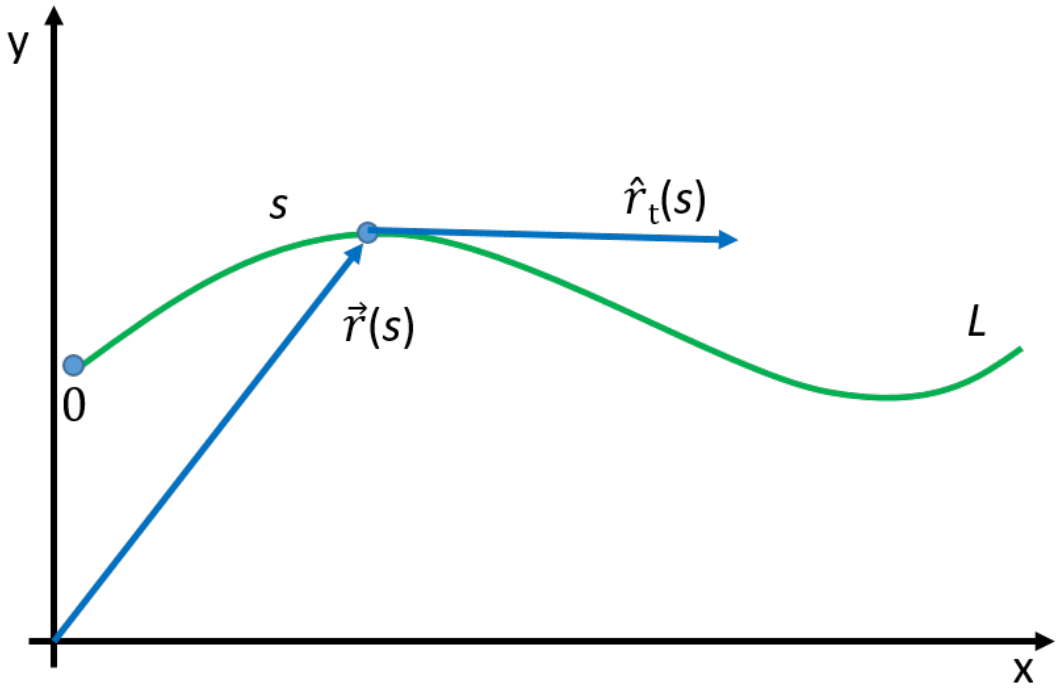

Figure 7: Schematic representation of the vectors and variables involved in the determination of the persistence length for a thermally fluctuating filament (represented with a green line).

The tangent vector autocorrelation function $C(s)$ for this WLC model can be written as:

$$C(s) = \langle \hat{r}_t(s) \cdot \hat{r}_t(0) \rangle = e^{-2s/((D-1)l_p)} \tag{26}$$

D is again the spatial dimensionality of the bending fluctuation here. For a two-dimensional system, the tangent vector can be represented with an angle $\theta(s)$ only and equation 26 becomes the cosine correlation function:

$$C(s) = \langle cos[\theta(s) \cdot \theta(0)] \rangle = e^{-2s/((D-1)l_p)} \tag{27}$$

With equation 27, l_p (compare equation 8) can be determined from a fit of $C(s)$ against s [83, 64].
On a phenomenological level, the persistence length l_p is the length, over which the filament appears straight or over which the orientation in the chain is decorrelated.

1.2.9 Frequency Spectra of the Shear Modulus

Figure 8 schematically depicts a typical frequency spectrum of the storage and the loss modulus for an entangled network of semi-flexible filaments. It

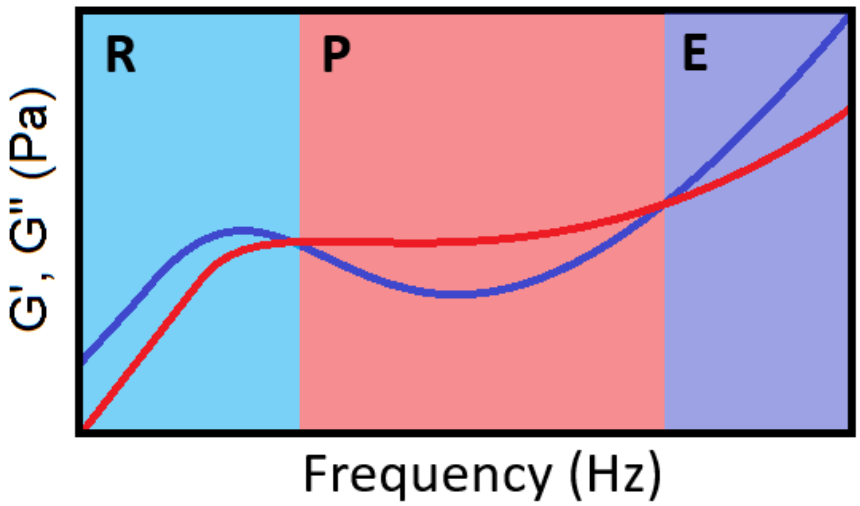

Figure 8: Schematic representation of the storage (red) and loss modulus (blue) for a typical semi-flexible, entangled polymer network in the frequency regime. Three frequency regimes, separated by the dominance of one of the moduli, are distinguished by background colors and labeling. Blue indicates a viscous network (G'' dominates), red an elastic one (G' dominates).
R (light blue) - low frequency region, reptation dominated & the crossover point is the reptation frequency ω_r ($1/\tau_r$, with the reptation time τ_r)
P (red) - plateau region, entanglement dominated (G_0 is G' at the minimum position of G'').
E (dark blue) - high frequency region, single filament mode dominated & the crossover point is the entanglement frequency ω_e ($1/\tau_e$, with the entanglement time τ_e)

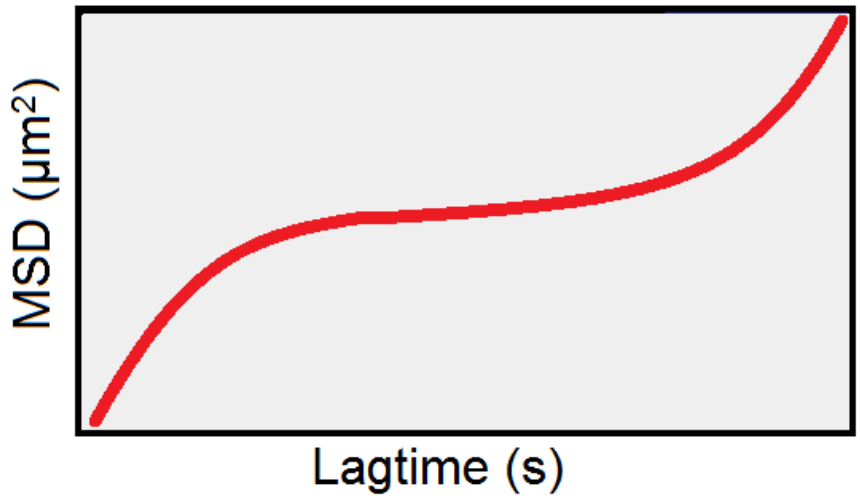

Figure 9: Schematic representation of the MSD for a microparticle in a typical semi-flexible, entangled polymer network in the lag time (τ) regime. The particle is much larger than the mesh size of the homogeneous network and (it is a quasi continuum around the particle) and the network is in equilibrium. This allows averages over time and particle numbers. Typically, high lag time increases (reptation of filaments) of the MSD are overlapped by drift (thermal drift of the instrument, thermal drift of the sample, mechanical drift of the sample...).

is separated into three frequency regimes, which are divided at the crossover points of the two moduli. They are characterized by the domination of either the loss modulus or the storage modulus. So they show either mainly viscous behavior (low and high frequency regime) or predominantly elastic behavior

(intermediate regime in the plateau region). The relaxation of the network can be understood by looking at different mechanisms happening on different time and length scales.

The plateau region (P) in the intermediate frequency regime is used to characterize a sample with the plateau modulus G_0, which is commonly defined as the storage modulus at the minimum position of the loss modulus. Although there are multiple methods to determine G_0, which have been evaluated by Liu *et al.* [84].

It is a measure for the stiffness of a material. The timescales connected to this plateau region of actin ($\sim$ 0.01-100s) are very important for interactions in biology on the length scale between a single cell and small tissues. Myosin motor activity which controls cortical tension or cellular interaction with external forces, where an elastic response is often needed, is a typical example. In the same context, the typical stiffness ranges from the mPa (cytoplasm) to the kPa (whole cells, small tissues) regime [85, 86, 87]. On a microscopic level, this elastic response can be explained by the entanglement, crosslinking or bundling of protein polymers, but in this case only entanglements are considered. On that timescale, the entanglements effectively cross connect the network, hinder deformation or flow and give it an affine behavior. Looking back at the tube model, especially transverse bending fluctuations with an amplitude

$$A_{\mathrm{bt}} \propto \sqrt{l_{\mathrm{c}}^3 / l_p} \tag{28}$$

larger than the tube diameter (compare chapter 1.2.6) [72, 88, 89] are suppressed. Introducing crosslinking proteins for example extends this plateau region into the low frequency regime (indefinitely for irreversible crosslinks and depending on the interaction time scale for transient crosslinks) because it hinders reptation of filaments and network flow even further [90]. Compare Figure 17 $\left(\mathrm{G}\right)$. Further information on the scaling behavior of the plateau modulus can be found in chapter 1.2.6.

The high frequency region (E) is dominated by single filament fluctuations (twisting, bending and coupling of both), which occur on a timescale from microseconds to seconds. They start dominating network mechanics at time scales on the order of milliseconds [91, 92, 93] and show amplitudes smaller than the entanglement length l_{e}, which is the distance between two entanglement points. The separation between this and the plateau region, is the upper crossover point of G' and G'', which is called the entanglement frequency ω_{e}. Here it is more intuitive to convert it from the frequency space to time and call

it the entanglement or disentanglement time τ_e, which can be expressed as

$$\tau_e = \beta \cdot \zeta \cdot \xi^{16/5} \cdot l_p^{-1/5}. \tag{29}$$

With the translational friction coefficient ζ

$$\zeta = \frac{4t\pi}{\ln(\xi/d_t)} \tag{30}$$

and $\beta = 1/k_B T$ [88]. A very useful transformation is

$$l_e = \xi^{4/5} \cdot l_p^{1/5} \tag{31}$$

and with $\tau_e \propto l_e^4$ as well as $l_e \propto c^{-2/5}$ we get

$$\tau_e \propto c^{-8/5}. \tag{32}$$

So doubling the concentration (in the affine, semi dilute concentration regime) results in a shift of τ_e by a factor of $2^{-8/5} \approx 0.33$.
Another important characteristic is the power law coefficient for $G(\omega)$ at $\omega > \omega_e$, which is theoretically determined as well as experimentally confirmed as ¾. This scaling behavior is the result of the network relaxing stress in the form of single filament bending fluctuations. This stress acts on filaments as tension and they get stretched or compressed. Thermal fluctuations from the surrounding water relax this tension. Gittes and MacKintosh explain this in greater detail [94].

The low frequency region (R) of $G(\omega)$ is also dominated by filament movements induced by Brownian forces. But in this case, it is a type of diffusion called reptation. Network relaxation can happen by filaments diffusing away from a source of tension and changing the network structure itself. For example on the time scale of the plateau region, a microparticle trapped in a pocket of surrounding network shows a 3D mean squared displacement (MSD, compare Figure 9) very close to the volume of that pocket. The MSD is essentially the volume (or area in 3D), the particle explores. It is the basis for the calculation of viscoelastic shear properties from particle fluctuations. The MSD shows an elastic plateau for intermediate lag times τ(the time interval, over which the particle distance is from the initial location is tracked, compare equation 54), because of the particle exploring the mesh, it is trapped in. It gets reflected by filaments when pushed against the mesh wall by Brownian forces. But over

longer times, due to filament reptation, the MSD is further increased and the particle diffuses through the network, which now behaves more like a viscous fluid. Also compare chapter 1.2.6. The timescale of this type of relaxation and thereby the lower crossover point of the storage and the loss modulus, is the reptation time τ_r. It can be estimated with:

$$\tau_\mathrm{r} \propto \beta \cdot \zeta \cdot l_\mathrm{c}^3 = \frac{4\pi}{k_\mathrm{B}T} \cdot \frac{l_\mathrm{c}^3}{\ln(\xi/d_\mathrm{t})} \tag{33}$$

where β is $\frac{1}{k_\mathrm{B}T}$. Equation 33 is very weakly concentration dependent (only in ξ). Käs *et al.* presented data for which a weak increase of $\zeta \propto c^{0.35}$ could be shown with a power-law fit [95], which is very similar to equation 33.
So a shift of τ_r should barely be observable for different concentrations of entangled actin in a logarithmic plot of $G(\omega)$. A typical timescale for τ_r is on the order of 10^3 seconds [96, 95, 97].

1.2.10 Filament-Filament Interactions

Actin monomers are highly negatively charged Molecules. α-muscle actin has a net charge of -13. Although a majority of these charges are located on the inside of the protein, the N-terminus exposes some of them as a charge density cluster. Among the first 25 of 375 amino acids, seven are negatively charged, including the very first four [98]. This leads to a strong repulsion between the monomers, which is overcome by the accumulation of cations (mainly divalent cations and primarily Mg^{2+}). The Polymerization of G-actin to F-actin is initiated this way.
Similarly, attractive inter-filament interactions of F-actin generally have to overcome this charge repulsion. There are different types of interactions, which are mostly short-lived, weak and overlapping. This makes them hard to quantify and compare. A primary goal of this study is the comparison of differently modified actins, which boils down to different interactions based on either filament bending properties, charge densities or complexation. So, understanding these inter-filament interactions in crucial. Since they induce bundling, it makes sense to compare bundling processes and bundled filaments and then infer the influence of different filament properties for different isoforms and modifications of actin.

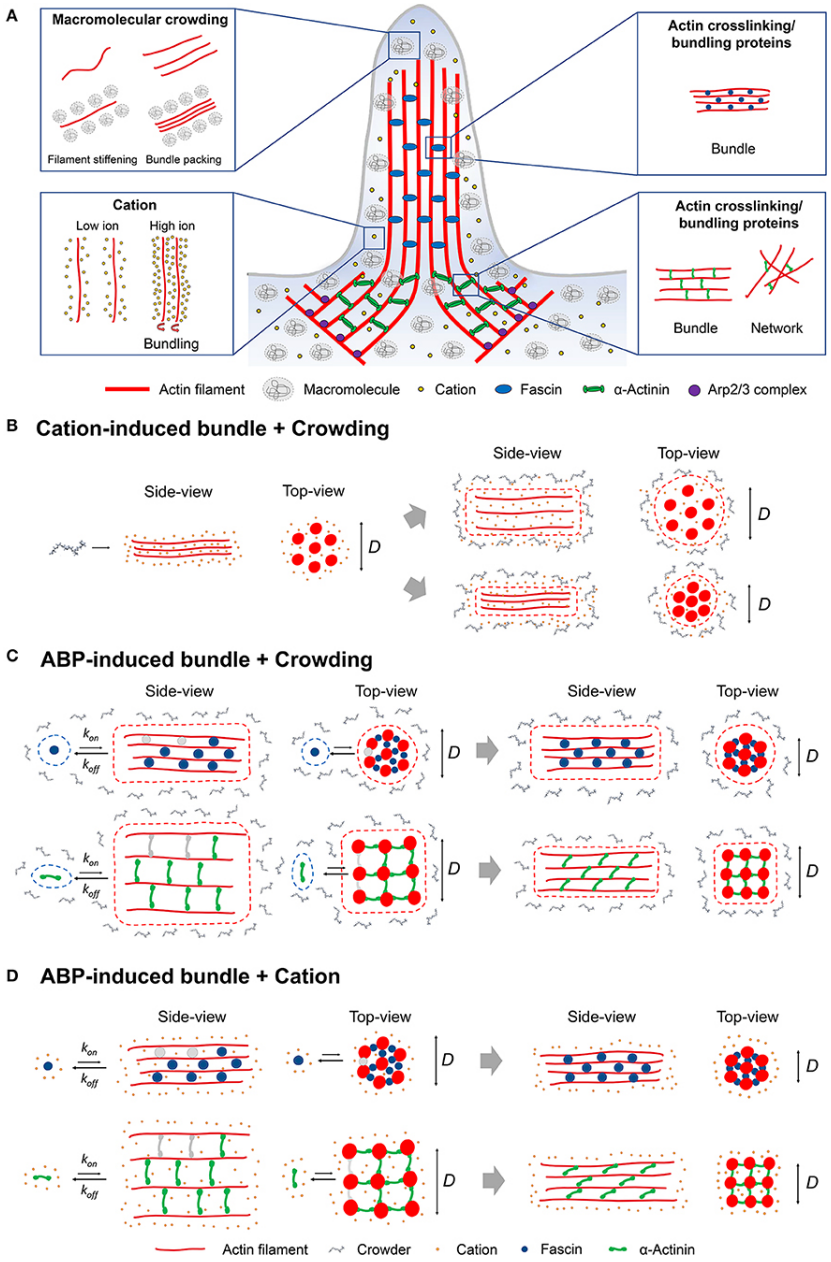

Figure 10: Schematic representation of different actin filament bundling processes relevant in the cellular environment. A) Bundling of actin filaments is highly relevant at the leading edge of cells and thereby for cell motility. Different types of bundling are present at the same time interacting with each other. These are macromolecular crowding, bundling by ABPs and counterion condensation (also called cation-induced bundling). B) Counterion condensation combined with macromolecular crowding effects. The interaction can influence the bundle diameter. C) Bundling by ABPs combined with macromolecular crowding effects. The interaction can influence the organization of the filament structure and thereby the bundle diameter. The angle between bound crosslinker and actin filament can be changed depending on the length and flexibility of the crosslinker. Shown are α-actinin in green and fascin in blue. Binding and unbinding rates can also be modified. Unbound crosslinkers are depicted in grey. D) Bundling by ABPs combined with counterion condensation. Very similarly to C) properties of the bundle and the crosslinkers can be changed by the interaction.
Originally published by Castaneda *et al.* [99].

1.2.10.1 Bundling

Bundling of actin filaments is a highly relevant process for cellular function. It is involved in many processes like cell motility [100, 101, 102, 37], membrane stabilization [103], general force generation [71] or the response of the cytoskeleton to external stresses [104, 105]. It not only changes the structure of a filament network, but also the mechanical properties by pinning multiple filaments with a certain l_p together and increasing the overall l_p. This results in longer and thicker structures with a higher bending resistance. Embedded in a network of filaments, they also change the overall response of it to deformation. Figure 4 displays a few examples. F-actin filaments in particular are highly negatively charged and repel each other strongly [98]. So bringing and keeping them into close contact in a parallel orientation requires an effect, which overcomes this repulsion. There are multiple different ways for bundle formation of F-actin and polymer filaments in general. A schematic representation can be found in Figure 10 (A). The three primary agents for bundle formation are ABPs, macromolecular crowding and electrostatic interactions [106, 107, 108, 109, 110, 111]. These bundling effects can appear combined (compare Figure 10 B-D).

In the cytoplasm, the main cause of bundle formation is the binding of **ABPs** to actin filaments. When an actin crosslinker binds two filaments in close proximity, thermal undulation orient them and bring the filament backbone closer together eventually. Then the next crosslinker can bind in between them, which again increases the likelihood of further ones binding along the parallely or antiparallely oriented filaments. This could be called a zipper-mechanism [112, 113].

Macromolecular crowding is also relevant in the highly crowded cytoplasm [114, 115]. It can bundle filaments via depletion forces from excluded volume effects [106, 116, 117].

Another mechanism for bundle formation is **counterion condensation** [111, 118]. It is driven by electrostatic interactions between the negatively charged filaments and cations (mainly divalent cations). Some studies show the buildup of charge density waves (CDW) between filaments in bundles [111, 119]. The filaments form a hexagonal tunnel with divalent cations in between. These CDWs are shaped by the electrostatic potential of the filament backbones, their helical twist and their orientation to each other. Angelini *et al.* report the formation of knots in these waves. These are comprised of ions, which are restricted in their mobility compared to ions in solution. They are localized to

some degree in so-called "liquid ion patches" (LIPs). A higher density of these is found at actin subdomain 1, where the N-terminus is located [19].

1.2.10.2 Static and Transient Crosslinking

As already discussed before, living cells need to resist external forces and deformation caused by them. ABPs and in particular crosslinking proteins are an important part of this strain response. They stiffen actin networks by increasing the filament inter-connectivity and distribute stress over a wider range of filaments. Static crosslinking would be a problem for the cell though, because permanently increased stiffness and a static shape would severely limit its motility and ability to react to a changing environment. The solution to this are transient crosslinks, which have an on-rate k_{on} and an off-rate k_{off}. They increase the connectivity of the network, but still allow for dynamic remodeling over time [120, 121]. Static crosslinking has been shown to increase the plateau stiffness of actin networks with

$$G_0 \propto R^{1.2} \tag{34}$$

where R is the total number of crosslinks. The shape of the shear modulus is changed significantly by this. G_0 increases with the crosslinker concentration, the plateau slope decreases, τ_{e} also decreases due to the average length scale for single filament relaxation being reduced from l_{e} to the crosslink distance l_{c}. τ_{r} is shifted theoretically to infinitely high times if all filaments are connected. A good real example is shown in Figure 23 $\big(\mathsf{C}\big)$ [122, 123, 124]. Transient crosslinking on the other hand, shifts τ_{r} depending on k_{on} and k_{off}. Reptation is still possible, just slowed down. In that case, the plateau stiffness of actin networks increases with

$$G_0 \propto R_{\mathsf{eff}}^{1.2} \tag{35}$$

where $R_{\mathsf{eff}}^{1.2}$ is the effectively bound total number of crosslinks [125].

1.3 Rheology and Microrheology

1.3.1 Bulk Rheology - Plate Rheometers

Plate rheometers can be used to access the shear properties of viscoelastic materials. There are multiple types of geometries for rheometers, but the simplest and very often used ones have two parallel plates. One of those plates gets rotated and a sample is sheared between them. The control variable can

be the rotation speed or the measured torque T_m.

$$T_\mathsf{m} = T_\mathsf{I} + T_\mathsf{S} \tag{36}$$

The inertial torque T_I can be calculated as follows

$$T_\mathsf{I} = I\omega^2\Theta(i\omega) \tag{37}$$

with the moment of inertia I and the sample deformation $\Theta(i\omega)$. The second part of T_m is the sample torque T_S

$$T_\mathsf{S} = g^*(i\omega)\Theta(i\omega) = \frac{G^*}{k_\mathsf{g}}(i\omega)\Theta(i\omega) \tag{38}$$

with a geometry specific constant k_g. Rheometers basically measure stress-train relations like described in chapters 1.1.1 and 1.1.2. They measure the bulk properties of a sample, local inhomogeneities are averaged out [126].

1.3.2 Microrheology

Extracting or synthesizing proteins can be very time, work and cost intensive. Often, the limiting factor in *in vitro* experiments with them is the sample volume. A good example for this are artificial actin isoforms, extracted from a yeast culture, which are discussed in chapter 3.2 and 3.8. On the one hand, sample volumes are in the low µl range, which makes classical plate rheometry impractical or even impossible. On the other hand, surface and non-linear effects can easily have a relevant influence on the structure of a polymer fluid. Microrheology typically only needs a fraction of a rheometers sample volume. Video particle tracking microrheology (VPTMR) for example can be done with a microliter or even a fraction of that.

Semi-dilute polymer solutions form meshworks with length scale dependent properties. This is mostly the case for biological protein-filament solutions used in *in vitro* studies. The backbone structure for example can have elastic properties, at least on certain time scales, but the solvent (usually water or an aqueous salt solution) inside of a meshes has purely viscous properties. The size and surface properties of the probe can influence the measured properties [127, 128, 129]. Different types of microrheology (one- and two-particle microrheology) can explore local microscopic properties of the complex fluid, as well as bulk properties [130]. This can also probe local inhomogeneities.

1.3.2.1 Active Microrheology

Active microrheology typically induces an oscillatory motion in microparticle probes. This is done for example with optical tweezers or magnetic tweezers. The general principle is similar to bulk rheology performed with a plate rheometer. An oscillatory strain is applied and the frequency-dependent stress is measured as a dampened oscillation of the probe particle together with the phase shift between probe and the stimulating field. Usually the oscillation of the driving force is also measured for accuracy reasons. From these, the viscoelastic shear properties of the sample can be calculated via a generalized Stokes-Einstein equation. The first general assumption is

$$G^*(\omega) = \frac{\sigma_\mathsf{A}}{\epsilon_\mathsf{A}} \cdot e^{i \cdot \delta_\mathsf{p}(\omega)} \tag{39}$$

with σ_A and ϵ_A as the amplitudes of stress and strain respectively as well as the phase shift $\delta_\mathsf{p}(\omega)$, which is characteristically between 0 (elastic) and 90° (viscous) for viscoelastic materials.
The starting point for a quantitative description of the (spherical) particles motion is a Langevin equation.

$$m\ddot{x} = -6\pi a \eta^*(\omega)\dot{x} + f_\mathsf{R}(t) - \kappa_\mathsf{t} x + \kappa_\mathsf{t}(Ae^{i\omega t}) \tag{40}$$

When a microscopic particle is actively oscillated in a thermal bath in one direction, the inertial term $m\ddot{x}$ can be described by a statistical random forces $f_\mathsf{R}(t)$, a drag force $-6\pi a\eta^*(\omega)\dot{x}$ and the active forces $\kappa_\mathsf{t}(A_\mathsf{d} \cdot e^{i\omega t} - x)$, which are acting on it. The involved variables are the particle radius a, a complex viscosity $\eta^*(\omega)$, the particle position in regards to the focus of the driving force x, the force constant of the driving force κ_t and the amplitude of the driving forces motion A_d.
The equation is solved with a dampened and phase shifted sinusoidal motion:

$$x(t) = D(\omega)e^{i(\omega t - \delta(\omega))} \tag{41}$$

where D is the amplitude of the particle motion.
Neglecting the random forces and the inertia term $\frac{m\omega^2}{\kappa_\mathsf{t}}$ for low oscillation frequencies (< 100 Hz), we can use a generalized Stokes-Einstein equation to connect the complex shear modulus $G^*(\omega)$ with $\eta^*(\omega)$.

$$\eta^*(\omega) = \frac{G^*(\omega)}{i\omega} \tag{42}$$

We arrive at an expression for G^* with D and δ as only remaining unknowns. These are determined by a sinusoidal fit of the trap motion as well as the particle motion:

$$G^*(\omega) = \frac{\kappa_t}{6\pi a}\left(\frac{A}{D}(\cos(\delta(\omega) + i\sin(\delta(\omega)))) - 1\right) \tag{43}$$

This complex term can of course be split up into a storage modulus $G'(\omega)$ and a loss modulus $G''(\omega)$.

$$G'(\omega) = \frac{\kappa_t}{6\pi a}\left(\frac{A}{D}(\cos(\delta(\omega))) - 1\right) \tag{44}$$

$$G''(\omega) = \frac{\kappa_t}{6\pi a}\left(\frac{A}{D}(\sin(\delta(\omega)))\right) \tag{45}$$

A more detailed description can be found in the literature [131, 132, 133, 134].

1.3.2.2 Passive Microrheology

Passive microrheology can be applied to avoid some of the disadvantages of the active variant. For example it is much more effective if good sample statistics are required. Active microrheology is a very versatile and accurate tool for the measurement of biological samples. But a downside is, that one particle has to be oscillated at a time. With passive microrheology, viscoelastic material properties can be calculated from thermal particle trajectories alone, which allows for many particles to be tracked at the same time. The fluctuation-dissipation theorem (FDT) can be applied to the recorded traces of embedded microparticles, undergoing thermal fluctuations. The FDT equates the response of a system to random thermal fluctuations with its response to external perturbations. This is possible for equilibrium systems obeying detailed balance. For example: actively moving a particle with optical tweezers in such a fluid dissipates kinetic energy via drag to heat. This heat results in Brownian motion of molecules.
The goal is to formulate an equation, which relates directly measurable properties to the shear modulus $G^*(\omega)$. The first step is again a Langevin equation for particle motion with the lag time and a memory function $\zeta_f(t)$, which can be interpreted as friction, but without a driving force.

$$m\dot{v} = f_R - \int_0^t \zeta_f(t-\tau)\cdot v(\tau)d\tau \tag{46}$$

Via an unilateral Fourier transform (F_u), this can be related to the velocity au-

tocorrelation function.

$$v^*(\omega) = \frac{f_{\mathsf{R}}^*(\omega) + mv(0)}{mi\omega + \zeta_{\mathsf{f}}^*(\omega)} \tag{47}$$

Where the velocity of the particle is v. Taking the ensemble average, neglecting inertia, applying the equipartition theorem ($m\langle v(t)v(t)\rangle = k_{\mathsf{B}}T$) and using $m\langle v(0)f_{\mathsf{R}}(t)\rangle = 0$ (random forces average out to zero) gives:

$$\langle v(0)v^*(\omega)\rangle = \frac{k_{\mathsf{B}}T}{[mi\omega + \zeta_{\mathsf{f}}^*(\omega)]} \tag{48}$$

The relation

$$\mathscr{F}_{\mathsf{u}}\{\langle \Delta r^2(\tau)\rangle\} = \frac{6}{(i\omega)^2}\mathscr{F}_{\mathsf{u}}\{\langle v(0)v(t)\rangle\} \tag{49}$$

gives

$$\zeta_{\mathsf{f}}^*(\omega) = \frac{6k_{\mathsf{B}}T}{(i\omega)^2\mathscr{F}_{\mathsf{u}}\{\langle \Delta\vec{r}^2(\tau)\rangle\}} \tag{50}$$

with the position vector $\vec{r}$ for three-dimensional motion. And with equation 42 as well as

$$\zeta_{\mathsf{f}}^*(\omega) = 6\pi a\eta^* \tag{51}$$

one arrives at

$$G^*(\omega) = \frac{k_{\mathsf{B}}T}{\pi a(i\omega)\mathscr{F}_{\mathsf{u}}\{\langle \Delta\vec{r}^2(\tau)\rangle\}} \tag{52}$$

for a particle trajectory in $N = 3$ dimensions. Since practically the accessible data is mostly two dimensional, the general equation is:

$$G^*(\omega) = \frac{Nk_{\mathsf{B}}T}{3\pi a(i\omega)\mathscr{F}_{\mathsf{u}}\{\langle \Delta\vec{r}^2(\tau)\rangle\}}. \tag{53}$$

After measuring a particle trajectory, equation 53 can be accessed via the mean squared displacement (MSD):

$$\mathsf{MSD} = \frac{1}{N}\sum_{i=1}^{N}(x_{\mathsf{i}}(t+\tau) - x_{\mathsf{i}}(t))^2 = \langle \Delta\vec{r}^2(\tau)\rangle. \tag{54}$$

Mason *et al.* [135, 136, 97] approach this from the Laplace transformed viscoelastic shear modulus $\tilde{G}(s)$ with $s = i\omega$.

$$\tilde{G}(s) = \frac{k_{\mathsf{B}}T}{\pi as\langle \Delta\tilde{r}^2(s)\rangle} \tag{55}$$

The difficulty lies in the Laplace transformation of the data over a limited fre-

quency range, which can distort it through truncation errors. To avoid this, $\langle \Delta\tilde{r}^2(\tau)\rangle$ is substituted into an algebraic Stokes-Einstein equation:

$$\tilde{G}(s) = \frac{k_B T}{\pi a \langle \Delta\tilde{r}^2(\tau)\rangle \Gamma[1 + (\delta \ \ln \ \langle \Delta\tilde{r}^2(\tau)\rangle / \delta \ \ln \ \tau)]}\Big|_{\tau=1/s} \tag{56}$$

Γ denotes the gamma function. To obtain $G^*(\omega)$ Mason *et al.* fit $\tilde{G}(s)$ as a functional form with a real s, and then obtain $G^*(\omega)$ by analytic continuation. They substitute $i\omega$ for s in the fit.

The transformation from $\tilde{G}(s)$ to $G^*(\omega)$ is explained in the literature in greater detail [137, 135, 136, 138]. They fit the MSD with a local power law and estimate $G^*(\omega)$ algebraically this way. The local power law is determined from the logarithmic time derivative of the MSD. To improve the performance of the method, Weitz *et al.* [139] modify it empirically by adding second order logarithmic time derivatives.

Other approaches to calculate shear moduli from the MSD have been taken since then [140, 139, 131, 141], but typically the improvements are minimal or only effect certain frequency ranges.

1.3.3 Methods of Rheology and Microrheology in Comparison

Method	estimated frequency range / Hz	estimated stiffness range / Pa
Rheometry (plate)	$10^{-5} - 10^{2}$	$10^{-1} - 10^{6}$
AFM	$10^{-2} - 10^{5}$	$10^{-2} - 10^{4}$
DWS	$10^{0} - 10^{7}$	$10^{-1} - 10^{4}$
DLS	$10^{-1} - 10^{6}$	$10^{-3} - 10^{4}$
VPT	$10^{-3} - 10^{2}$	$10^{-5} - 10^{1}$
OT active	$10^{-2} - 10^{4}$	$10^{-3} - 10^{2}$
OT passive	$10^{-3} - 10^{4}$	$10^{-5} - 10^{1}$
MT	$10^{-2} - 10^{3}$	$10^{-3} - 10^{4}$

Table 2: A comparison of the frequency and stiffness ranges accessible by different methods of rheology. The methods are plate rheometry (Rheometry (plate)), atomic force spectroscopy (AFM), diffusing wave spectroscopy (DWS), dynamic light scattering (DLS), video particle tracking (VPT), active and passive microrheology with optical tweezers (OT) and microrheology with magnetic tweezers (MT) [123, 93, 136, 143, 134, 144, 132, 145, 146, 142].

2 Actin-DNA Hybrid Networks

2.1 Introduction

The first aim of this thesis is an evaluation of a commonly used model to predict the viscoelastic properties of semi-flexible filament networks, the tube model. It describes the shear properties of an entangled network as the result of a confinement around the filament, formed by other filaments (theory chapter 1.2.6). Predictions of the tube model have been confirmed many times experimentally [147, 148, 96].

According to this model, (assuming constant temperature and a mean filament length close to the persistence length, which can be controlled) the shear properties are only dependent on two independent variables. The persistence length (l_p) of the filaments and their initial monomer concentration c. The model has been proven to accurately predict the mechanical properties of reconstituted actin filaments, but is knowing c and l_p enough to predict the viscoelastic shear properties of semi-flexible polymer filaments under experimental conditions in general?

It is not a given that artificial cells or even simple model systems contain actin filaments to fulfil its typical cellular role. The cellular muscle, motile engine, dynamic support structure (and so on) could be constructed from a different semi-flexible polymer with more favorable or easier to control properties *in vitro*. A combination of multiple semi-flexible polymers is also a possibility. Cells consist of many interlinked and not clearly separated composite materials already [149, 150].

Composite materials are a combination of materials with different chemical or physical properties. The combination gives rise to a mixture of those properties or even entirely new ones. Reinforced concrete is a good example of this. Where concrete alone has a high compressive strength but low tensile strength, steel shows a high tensile strength. The composite combines the advantageous properties of both and is a very resilient construction material. These also exist in nature. A very common composite is a combination of cellulose fibers and lignin called wood. Biological cells also possess composite structures and properties. They are microscopic compartments of many different protein structures, mainly composed of F-actin, microtubules and intermediate filaments. They are mostly treated as completely separate objects, which don't interact with each other in regard to mechanical properties. But as mentioned, *in vivo* they form partially interwoven structures. Studies have

shown reconstituted combinations of these filament networks to display biologically relevant composite properties [151, 152].
Understanding the mechanical properties is key to understand or even recreate biological structures with a primarily mechanical purpose. So looking back at the tube model, the question arises, whether two co-entangled semi-flexible polymers form a network with the same properties as a homogeneously composed one.
To investigate this, first semi-flexible DNA filament networks [8, 9] are compared to reconstituted actin networks. These DNA filaments consist of interconnected tiles, which themselves consist of seven DNA-strands on average. In addition to being semi-flexible, they have very promising properties, making them a perfect basic building block for more complex structures. These artificial filaments are more tunable and modifiable than their biological counterparts. They can be tuned in their mechanical as well as chemical and electrostatic properties, without the issue of having to keep protein folding in mind. They can be modified with side chains, which could form links to other structures for example. The possibilities are manifold. The analysis will be shown and explained further in subchapter 2.2. The chosen methods are mainly MR and to bulk rheology in the form of rheometry to determine linear viscoelastic shear properties. It will be shown, that only some characteristic viscoelastic properties of DNA filament networks can be predicted correctly by the tube model.
A very important characteristic for most of the measurements is a homogeneous network. Since it is not always easy to distinguish optically between filamenteous and bundled microfilament networks, Figure 11 shows examples for both. Both the filaments' and bundles' diameters are typically below the resolution limit of a fluorescence microscope and even a confocal laser scanning microscope (CLSM). Because of this, structures consisting of hundreds of filaments can appear very similar to just one.

Co-entangled composite networks with actin are co-polymerized to explore the root cause of this further in the following subchapters. Micro- and macrorheological experiments are performed with video-particle tracking and a rheometer to compare linear rheology as well as drag force experiments with optical tweezers to analyze nonlinear stress-strain behavior. They reveal shear resistance of the networks emerging from the interaction of different types of filaments as composite properties.
Purely entangled filament structures are a good model system to investigate mechanical properties in a bottom-up approach, but they are rare amongst

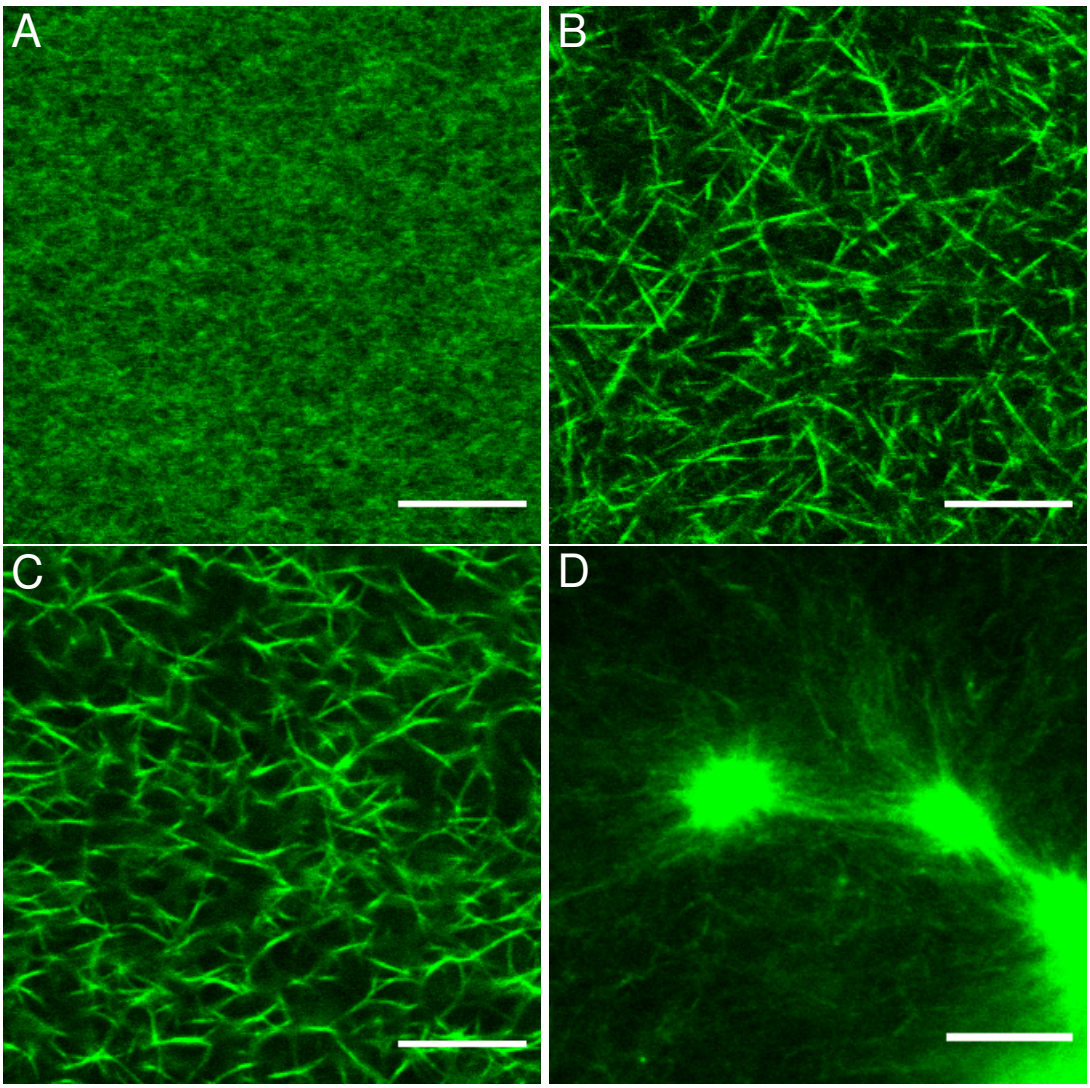

Figure 11: Confocal laser scanning microscope (CLSM) images of typical α-skeletal muscle actin networks at 24 µM. A) An entangled network. B) A crosslinked network with 2.4 µM fascin. Straight bundles are formed. C) A crosslinked network with 2.4 µM α-actinin. Curved bundles are formed. D) A network supplemented with 2.4 µM α-skeletal muscle myosin II filaments. The network is locally contracted and forms so-called asters. Scale bars are 10 µm

naturally occurring Network structures. To explore structures resembling *in vivo* conditions more, experiments with crosslinkers and motor proteins are done additionally. They address questions about the influence of additional, co-entangled semi-flexible networks on basic structure elements and the processes forming them. Are bundling by ABPs and contraction by motor proteins effected by an additional network, or are the DNA filaments just increasing the concentration of semi-flexible filaments? These questions are addressed in the following subchapter 2.5.

2.2 Characterizing the Mechanical Properties of DNA Filament Networks

Utilizing these artificial DNA structures [8, 9] requires a characterization of their properties and their interaction with biological systems first. They can be used either for artificial, biological systems or for the analysis of fundamental biological properties of cells like cortex mechanics for example or as model systems for *in vitro* measurements. To achieve this, micro- and macrorheological measurements are performed. Shear moduli as well as relaxation dynamics for DNA networks are analyzed and compared to reconstituted actin networks. These are combined with confocal images of fluorescently labeled networks in order to determine homogeneity and bundling. In the following steps, co-entanglement with naturally occurring cytoskeletal filaments (actin) is achieved and the resulting composite properties are analyzed. Lastly, their interaction with ABPs, motor proteins and divalent cations is investigated.

2.2.1 DNA Filaments and Networks

Jahnke *et al*. [8] adapted a protocol from Rothemund *et al*. [9] and assembled filaments with an average length of 6.8 µm from prepurchased strands in a thermocycler. Filaments in solution are received from them. Figure 12 shows these filaments in a diluted form on a poly-D-lysine-coated (PDL-coated) surface (A), where single filaments are visible. At higher concentrations, filament networks visually similar to those of actin are formed (B). We analyze these and co-entangled variants with F-actin for their mechanical properties. The filaments are co-polymerized and become randomly oriented.

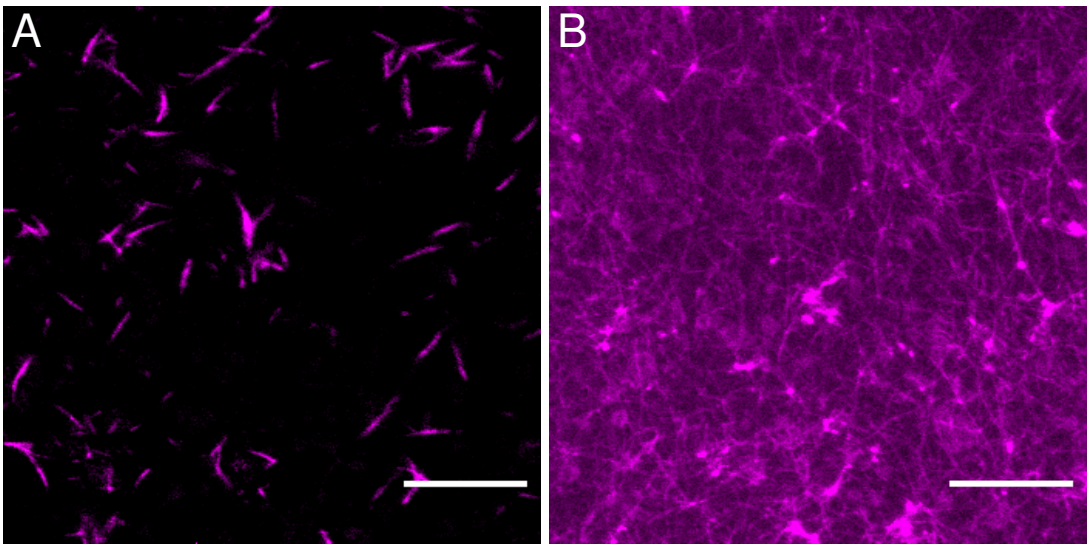

Figure 12: DNA filaments form network structures similar to those of cellular protein filaments. A) Diluted (from 10 µM by a factor of 2000) and washed DNA-filaments are immobilized on a PDL-coated glass slide. Single filaments are visible. B) At higher concentrations (here 40 µM) stable, entangled network structures, which resemble protein filament networks, are formed. Scale bars: 10 µm.

2.2.2 Semi-Flexible DNA Filaments

Considering the persistence length published by Jahnke *et al*. the filaments can be categorized as semi-flexible, similar to the semi-flexible protein filament actin. They measured a persistence length of 6.46 $\pm$ 0.26 µm [8]. Although this value should be considered carefully, since it is very close to the average filament length of 6.8 $\pm$ 4.3 µm and errors might be very large. The filaments appear to possess very little curvature over their contour length, which makes the cosine correlation [153] analysis questionable, since bending is barely measurable and image artifacts in the skeletonization process have a very high impact on the result. Filaments with higher contour lengths (a densely populated distribution with l_c that are multiples of l_p) would be preferable and probably necessary to find a reliable value. But assuming $l_p \approx l_c$ seems still reasonable. The single filaments don't show enough curvature on length scales of microns to count as flexible. Further indication can be found in the relaxation times (crossover points of G' and G'') of networks measured by microrheology as frequency-dependent shear moduli in the following subchapters.

2.2.3 Mesh Size

Besides l_p, the most relevant parameter to compare polymer networks with, is the mesh size. Even in non-crosslinked, entangled networks, it contributes

with an exponential factor of -3 to the network stiffness [94]. This means doubling a networks mesh size makes it six times softer. Based on a cubic network assumption, the mesh sizes can be calculated with equation 20. Compared to actin networks (equation 23), the monomer length and number of subunits per monomer differ for DNA networks. The networks are homogeneous to a high degree, just show some bundling and clustering, which can be seen in Figure 12. This makes the use of an average mesh size reasonable. All calculated mesh sizes relevant to this study are collected in table 3. In the following chapters, networks will be compared by their mesh size rather than their monomer- or filament concentration. This is done to ensure the comparability of different types of networks with tube model (theory chapter 1.2.6) predictions. A direct comparison of DNA and F-actin networks can be seen in Figure 17 $\big(\mathrm{A}\big)$ and $\big(\mathrm{B}\big)$. This is done, to test the assumptions from this subchapter experimentally. The mesh sizes are roughly analyzed like described in the materials and methods chapter. They are found to be $\xi_{\mathrm{DNA}} = 1.65 \pm 0.22$ µm and $\xi_{\mathrm{actin}} = 1.54 \pm 0.18$ µm. This is slightly more than the calculated 1.11 µm and 1.10 µm. The deviation is due to low image quality, but the relative similarity confirms very similar mesh sizes, homogeneous networks and the general applicability of the assumptions made here.

c_{DNA} (µM)	ξ_{DNA} DNA (nm)
40	248
24	320
20	350
16.4	387
12.3	449
10	496
8.2	547
4.1	774
2	1110

Table 3: Relevant DNA concentrations and associated mesh sizes.

2.2.4 Network Stiffness and Relaxation Times

To characterize DNA filament structures' linear mechanical properties on a network level, VPTMR is applied. Tracking the two-dimensional position of an embedded microparticle with high spatial and temporal resolution gives lag time dependent MSDs of the particles. Assuming the applicability of the FDT and comparing an approximation of its Laplace transform to the generalized Stokes-Einstein equation (theory chapter 1.3.2), gives shear moduli in the fre-

quency domain. From the shear moduli as well as the MSDs, further information like for example the plateau stiffness of the material, relaxation times or general fluidity can be drawn. Among those, relaxation times can be used to draw conclusions about single filament properties and close the information gap left open about the bending stiffness of DNA-filaments (DNA subchapter 2.2.2).

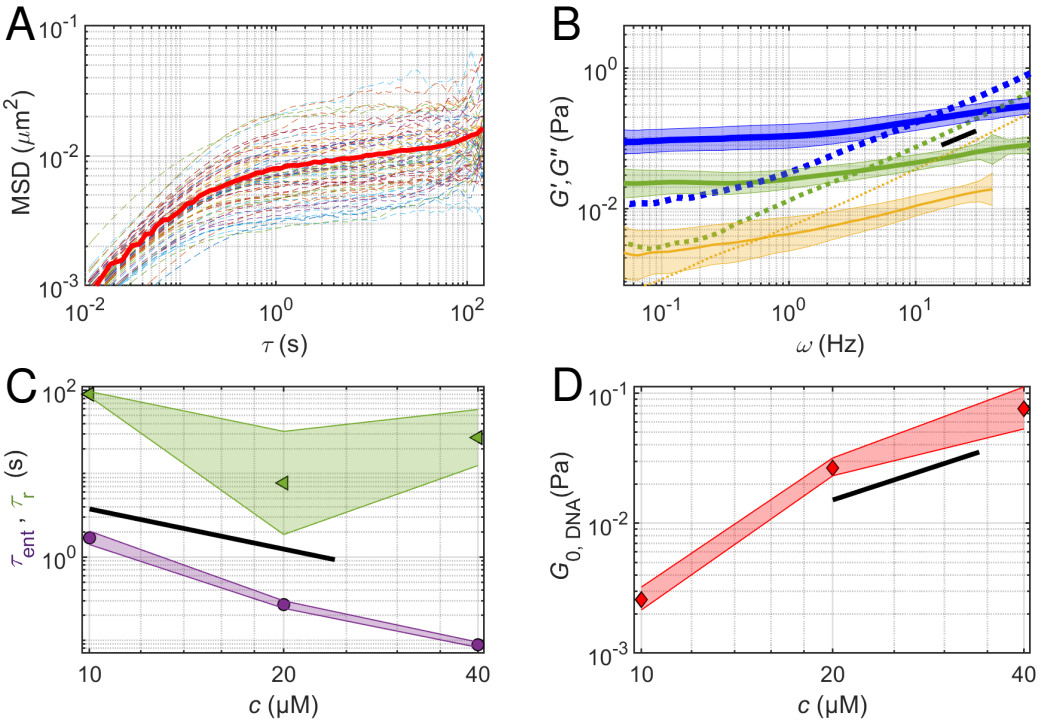

Figure 13: Mechanical properties of entangled DNA-networks at concentrations of 10, 20 and 40 µM investigated by VPTMR. They show a viscoelastic behavior similar to that of reconstituted actin networks. A) Mean squared displacement of a 40 µM DNA network with a mean shown as a thicker line in red and a distribution of single MSDs with dashed lines. B) Frequency dependent complex shear modulus $G^*(\omega)$ of different DNA filament concentrations, split up into real and imaginary contribution. G' is represented by a straight line, G'' by a dashed one. Smaller concentrations are indicated by thinner lines and different colors (10 µM orange, 20 µM green and 40 µM blue). A slope of $\omega^{3/4}$ is shown in black. C) Reptation time τ_r (green) and entanglement time τ_e (purple) against the actin concentration. A slope of $c^{-8/5}$ is shown in black. D) Plateau moduli for different concentrations (red) and a slope of $c^{7/5}$ in black.

The mechanical properties between a concentration of 10 and 40 µM are very typically viscoelastic. Looking at Figure 13 (A), the MSD of embedded microparticles displays a nearly linear, fluid-like increase with an exponential coefficient of approximately $\alpha = 0.4$ in the low lag time regime until ~0.1 s. Up to this timescale, the particle experiences the viscous properties of the surrounding medium and interacts with bending modes of the filament cage it is trapped in. So this regime extends to the borders of the relaxation time belonging to these modes. Over longer τ, the MSD creeps into a plateau region, where

the particle is trapped in an elastic filament cage, hold together by entanglements until the reptation time is approached at between 100 and 1000 s of lag time. The high lag time region is not completely reached, but an increase of the MSDs slope is clearly noticeable over τ =50 s. Here, over longer time scales, the particle diffuses through the meshes, which slowly open up by the reptation of filaments. This leads to a fluid-like linear increase of the MSD over high lag times. The formation of such a s-shape in MSD-τ graphs is typical for a viscoelastic polymer fluid.

In (B), the frequency dependent, complex shear moduli of different concentrations show a plateau region between approximately 0.01 and 10 Hz with two crossover points of G' and G''. This is a very clear sign of a dynamic, entangled network, which shows filament reptation – also a good indication for homogeneous networks, which are neither significantly bundled, nor crosslinked. These phenomena severely decrease the viscous flow of the structure, reduce or stop reptation, decrease the slope of G' in the plateau region and shift the reptation crossover point to lower frequencies. Here, the slope of G' slightly decreases with rising concentration, as the elastic properties more and more dominate the viscous ones, since the reptation of the filaments through a network of increasing density raises more friction. For very similar reasons, the plateau region gets wider in the frequency regime in both directions with higher density and smaller mesh size. The high frequency behavior of G'' has an exponential factor of approximately 3/4 and the plateau modulus G_0 has a concentration dependency with an exponential factor α of about 7/5 (D). The concentration dependency of the entanglement time τ_e (C) is stronger than the expected exponential factor of –8/5, but reasonably close, where the reptation time τ_r is barely concentration dependent. One noticeable deviation from the expectation is network plateau-stiffness, which is significantly lower than for a comparable F-actin network. A DNA-network with a concentration of 40 µM has a slightly smaller mesh size (248 nm) than a muscle actin network with 24 µM (274 nm). Considering similar filament lengths, this should result in a slightly higher G_0 for the DNA-networks (compare Figure 13 (B) and Figure 15 (A)). The found value is $G_{0,\mathrm{actin}} \approx 4 \cdot G_{0,\mathrm{DNA}}$. The combined findings, summarized in table 4, give (with one exception) a consistent picture of an entangled, viscoelastic network, which can be described with a tube model. Compare theory chapters 1.2.6 and 1.2.9. Most of the measurements are repeated with other instruments to confirm general validity. The results of that are presented in Figure 14 for two types of active measurements, active MR with optical tweezers (A) and rheometry with a plate-plate rheometer

Parameter (DNA networks, VPTMR)	expected	found α
$G''(\omega_{\text{high}})$	$\sim \omega^{3/4}$	$\sim 3/4$
$G_0(c)$	$\sim c^{7/5}$	1.81 ± 0.32
$\tau_{\text{e}}(c)$	$\sim c^{-8/5}$	-2.10 ± 0.30
$\tau_{\text{r}}(c)$	$\sim c^0 - c^{-1}$	-0.87 ± 1.5

Table 4: Expected and found characteristic exponential factors for a characterization of the viscoelastic properties of semi-flexible DNA filament networks measured by VPTMR.

$\big(\text{B}\big)$. The concentration dependency of G_0 is shown in $\big(\text{C}\big)$. The results are generally similar, $G_0(c)$ has an exponential factor a little bit higher than the expected 7/5 for plate-rheometer measurements, which could be the result of small amounts of bundles in the sample. These should form more easily with higher concentrations (40 µM) due to crowding (Figure 14 $\big(\text{C}\big)$, compare theory chapter 1.2.10.1). The G_0 values themselves increase slightly by one order of magnitude from local, linear MR (VPTMR) over linear active MR (OT) to macrorheology (rheometer), which is also an indication for inhomogeneities caused by bundles. Surface effects at the edge of the water sample or shear thickening might contribute to bundle formation between the rheometer plates. The average local response accessed by microparticles (radius $r = 1$ µm) can't reflect the relaxation of structures, which are many microns apart from each other when only a few bundles are formed. A plate rheometer measures bulk properties, so the whole network is probed. Additional results are shown in table 5.

Parameter (DNA networks, other instruments)	expected	found α
$G''(\omega_{\text{high}})$	$\sim \omega^{3/4}$	$\sim 3/4$
$G_{0,\text{Rh}}(c)$	$\sim c^{7/5}$	2.27 ± 0.47
$G_{0,\text{OT}}(c)$	$\sim c^{7/5}$	1.74 ± 0.04

Table 5: Expected and found characteristic exponential factors for a characterization of the viscoelastic properties of semi-flexible DNA filament networks measured by a plate-rheometer and OT.

Bundling slows reptation down and also pushes filament relaxation to higher frequencies. This happens due to the average length scale for single filament relaxation being reduced from l_{e} to the crosslink distance l_{cr} (compare theory chapter 1.2.10.2). Bundling can function as quasi-crosslinking in this context by pinning filament ends together in a zipper-like counter-ion condensation. An example for a crosslinking-shifted τ_{e} for actin is shown in Figure 17 $\big(\text{D}\big)$. This can be compared to an equivalent, non-crosslinked network in Figure 15 $\big(\text{A}\big)$. τ_{e} (or here $\omega_{\text{e}} = 1/\tau_{\text{e}}$) is shifted by strong rigor HMM crosslinking by at least a

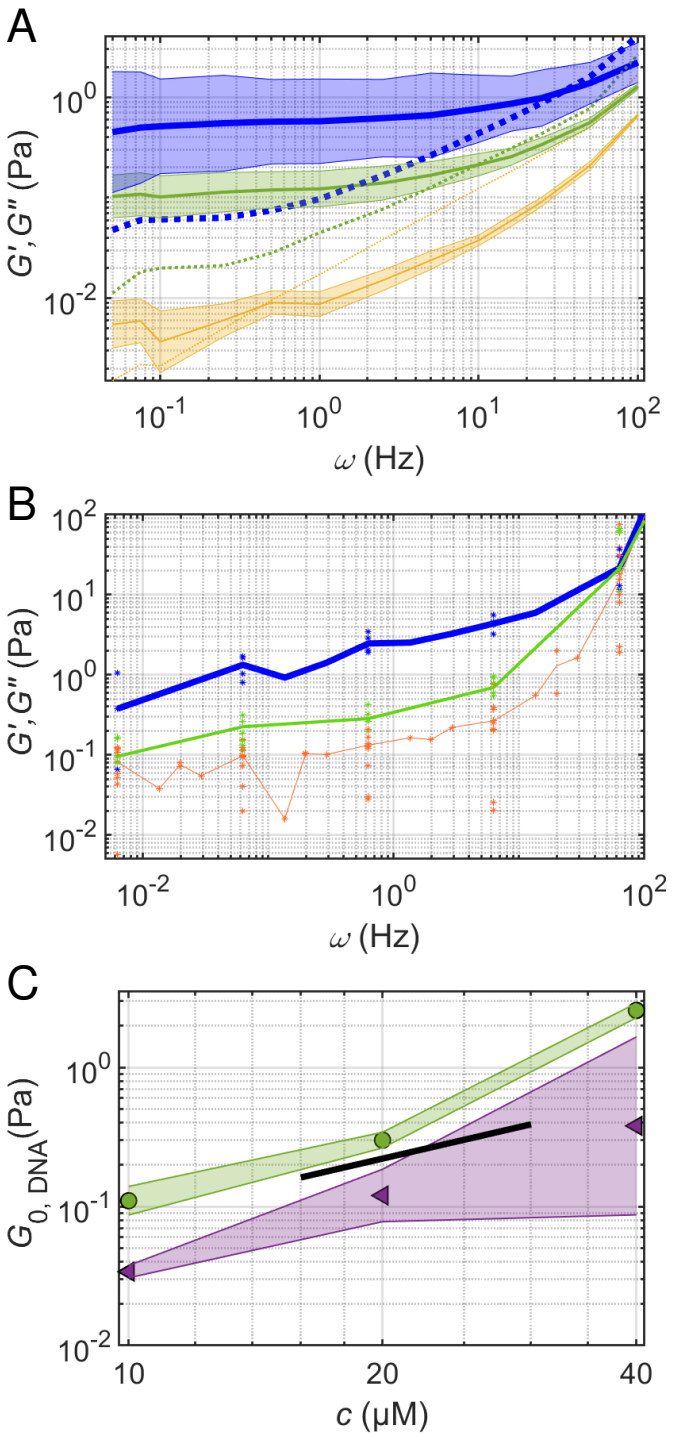

Figure 14: Other instruments confirm typical viscoelastic properties for semi-flexible filaments for DNA structures, similar to the VPTMR measurements. Mechanical properties of entangled DNA networks are shown for concentrations of 10, 20 and 40 µM. A) and B) are frequency dependent complex shear moduli $G^*(\omega)$ of different DNA-filament concentrations spit up into real and imaginary contribution. G' is represented by a straight line, G'' by a dotted one. Smaller concentrations are indicated by thinner lines and different colors (10 µM orange, 20 µM green and 40 µM blue). Shear moduli are measured with optical tweezers A) and a plate rheometer B). For the rheometer only G' is shown. C) Plateau moduli for OT (triangles, purple) and Rh (circles, green) against the DNA concentration. A slope of $c^{7/5}$ is shown in black.

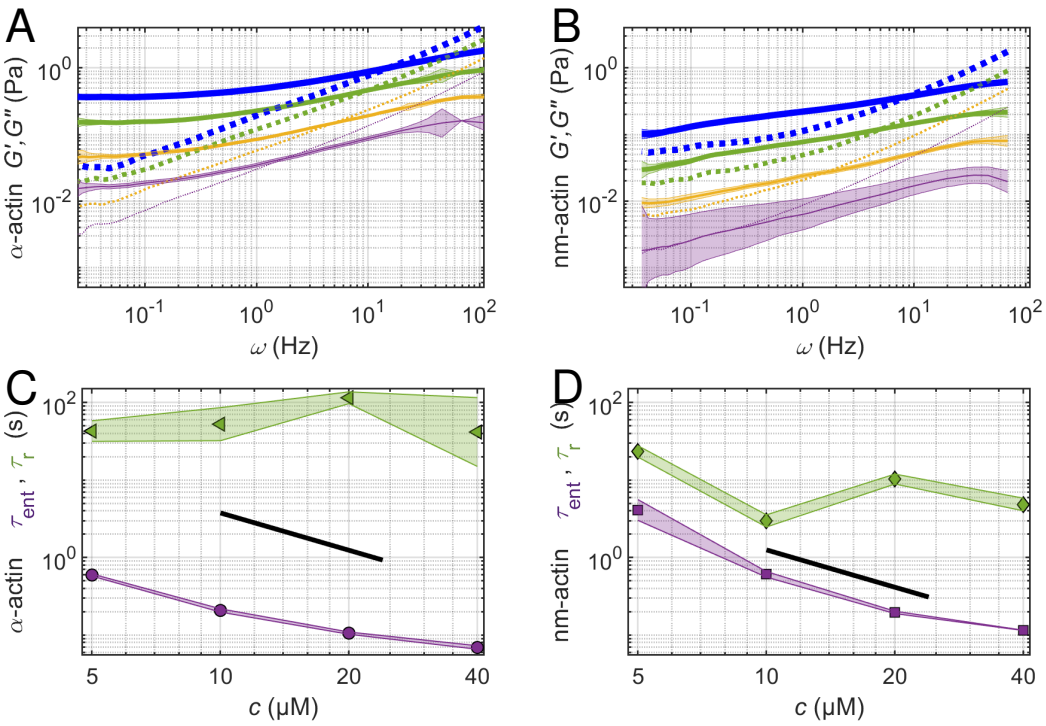

Figure 15: Mechanical properties of entangled F-actin networks consisting of the two isoforms α–skeletal muscle actin (α-actin) and non-muscle actin (nm-actin, a mixture of 85% β- and 15% γ-actin) at concentrations of 5, 10, 20 and 40 µM analyzed by VPTMR. A, B) Frequency dependent G' and G'' of different α- and nm-actin concentrations. α-actin is shown in A) and nm-actin in B). G' is represented by a straight line, G'' by a dotted one. Smaller concentrations are indicated by thinner lines and different colors. The concentrations are 5 (purple), 10 (orange), 20 (green) and 40 µM (blue). A slope of $\omega^{3/4}$ is shown as a black line. C) and D) show the reptation time τ_r (green) and the entanglement time τ_e (purple) against the actin concentration. A slope of $c^{-8/5}$ is illustrated in black for α-actin C) and nm-actin D).

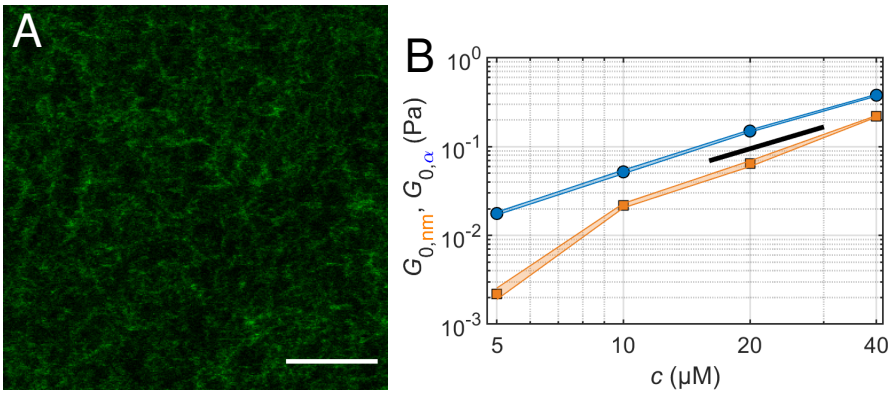

Figure 16: Direct comparison between the concentration dependency of G_0 between the two isoforms in entangled networks consisting of α-actin and nm-actin at concentrations of 5, 10, 20 and 40 µM analyzed by VPTMR. A) depicts an α-actin network at 12 µM for the comparison with DNA networks. Scale bar is 10 µm. B) Plateau moduli for different concentrations. α-actin is represented by a blue line, nm-actin by an orange line, and a slope of $c^{7/5}$ is shown in black.

decade to smaller times (higher frequencies)

[88, 77]. Overall, the DNA networks resemble actin networks to a very high degree, but the G_0 values are generally lower for comparable concentrations.

The results are summarized in table 5.
The same type of measurements for F-actin are depicted in Figure 15 and Figure 16. MR data is shown for two actin isoforms. These are well described by the tube model predictions with $G_0 \sim c^{7/5}$, $\tau_e \sim c^{-8/5}$ and $\tau_r \sim c^0$. The concentration dependency of the plateau modulus for nm-actin is an outlier, but it is distorted by G_0 for 5 µM actin. That value is probably underestimated due to a very thin, soft network, which allows mesh hopping of probe particles. The higher concentrations have a slope much closer to 7/5. The results are summarized in table 6. A very interesting observation is the difference in G_0 of these isoforms under the same experimental conditions. The buffer conditions are the same and protein concentrations as well as degree of polymerization differ only by a few percent (>95 % for both). Despite not directly influencing the comparison with DNA-networks, a further investigation of this makes sense. It potentially opens up the opportunity to compare different Semi-flexible filament networks not only in a completely artificial model system, but also in directly biologically relevant reconstituted systems. A further investigation of this phenomenon is executed in chapter 3.2 with cytoskeletal actin isoforms, extracted from genetically modified yeast.

Parameter (DNA networks, VPTMR)	expected	found α
α-actin		
$G''(\omega_{\text{high}})$	$\sim \omega^{3/4}$	$\sim 3/4$
$G_0(c)$	$\sim c^{7/5}$	1.48 ± 0.08
$\tau_e(c)$	$\sim c^{-8/5}$	-1.03 ± 0.31
$\tau_r(c)$	$\sim c^0 - c^{-1}$	0.10 ± 0.81
nm-actin		
$G''(\omega_{\text{high}})$	$\sim \omega^{3/4}$	$\sim 3/4$
$G_0(c)$	$\sim c^{7/5}$	2.15 ± 0.61
$\tau_e(c)$	$\sim c^{-8/5}$	-1.71 ± 0.69
$\tau_r(c)$	$\sim c^0 - c^{-1}$	-0.50 ± 1.36

Table 6: Expected and found characteristic exponential factors for a characterization of the viscoelastic properties of entangled semi-flexible actin filament networks measured by VPTMR for m- and nm-actin.

Looking back at the single filament properties, the analysis of shear moduli also shines light on the uncertain persistence length of the DNA filaments. Despite not being able to measure it with high enough accuracy because of their short contour length, the rheological data and especially the τ_e show a good resemblance to those for comparable actin networks. Since the bending stiffness of filaments controls their bending mode relaxation, similar relaxation

times are a good indication for similar bending stiffnesses and thereby persistence lengths. Comparing concentrations with similar mesh sizes like 40 µM DNA (247 nm) and 24 µM F-actin (274 nm) , gives a τ_e of 0.07-0.09 s (DNA) and 0.1-0.2 s (F-actin, phalloidin). So assuming an $l_{p,\,DNA}$= 1-2 times $l_{p,\,F\text{-}actin,\,phalloidin} \approx$ 17-34 µm seems reasonable [65, 154, 92] (compare table 3 and equation 23).

In summary, the analyzed DNA-filaments can be classified as semi-flexible. They form viscoelastic entangled networks from semi-dilute solutions, resembling those of also semi-flexible cellular protein filament networks of F-actin. Their mechanical properties are mainly predicted accurately by the tube model for semi-flexible polymers. One exception is a very low base plateau modulus compared to actin networks with the same mesh size. This will be addressed in the following subchapters. The DNA filaments appear to be a good choice as second semi-flexible polymer for the analysis of co-entangled networks with F-actin.

2.3 Linear Viscoelastic Behavior of Composite Networks

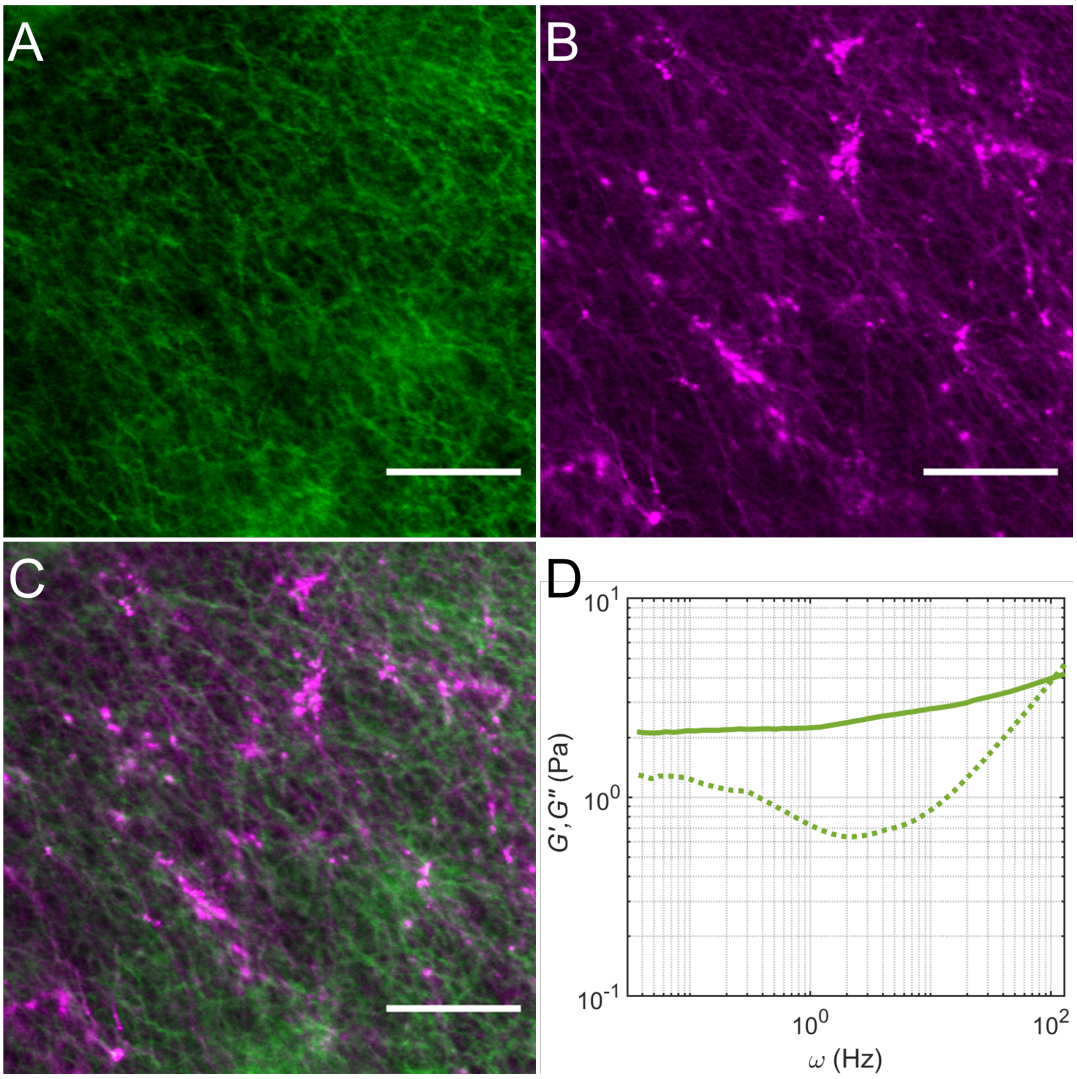

Figure 17: Actin and DNA composite networks are interwoven, but not interlinked structures. CLSM images visualize the non-colocalized networks. A), B) and C) show the actin channel, the DNA channel and an overlap of both respectively for a composite network. Scale bars are 10 µm. D) Muscle F-actin network at 24 µM strongly crosslinked with rigor HMM (2.4 µM) as example for crosslinker mediated shift of the plateau region of G' (straight green line, compare Figure 15).

Figure 17 shows a composite network of the two semi-flexible filament types, F-actin and DNA. The concentrations are chosen to produce networks with similar mesh sizes. They form separate and interwoven, homogeneous networks, which still show the afore mentioned signs of viscoelastic properties of an entangled network. They don't form combined bundles, and they are not crosslinked. This can be concluded from the comparison of the shear moduli from entangled, pure DNA filaments, pure F-actin filaments and the combination of both (compare Figure 17 (C) and Figure 18). Just like the mono-

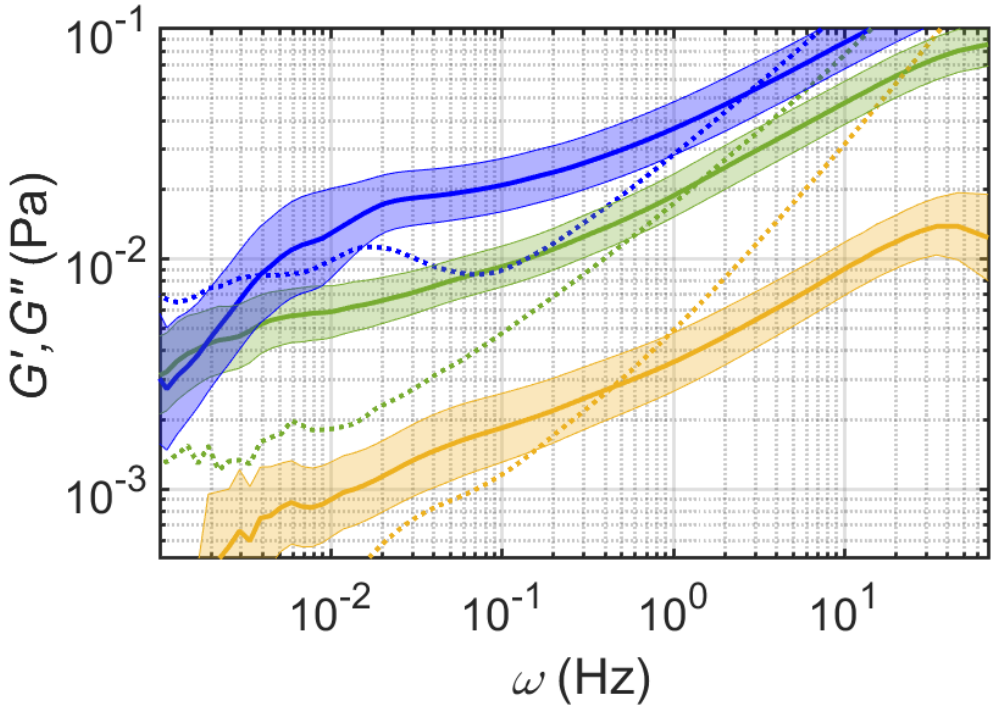

Figure 18: Actin and DNA composite networks are interwoven, but not interlinked structures. Microrheology data reveals viscoelastic properties similar to mono-component networks. Frequency dependent complex shear moduli of individual networks of α-actin at 1.5 µM (green), DNA-filaments at a concentration of 2 µM (orange) and a composite network with the same concentrations combined (blue). G' is represented by a straight line, G'' by a dotted one.

component networks, the composite has a plateau, two crossover points at frequencies similar to the single networks, and a typical $\omega^{3/4}$-behavior at high frequencies. The shape and magnitude of the moduli are also similar. The relaxation of the network does not seem to be hindered by the interaction, but appears to be dominated by F-actin reptation, which can be concluded from the shape of the plateau region with $G' > G''$ and the low frequency regime. These resemble the ones of pure actin networks ($\tau_{e,\,A}$) much more. $\tau_{e,\,comp}$ is smaller by a factor of three for the composite, compared to actin, but considering that the concentration of filaments is effectively doubled with the addition of DNA, $\tau_{e,\,comp} \approx \tau_{e,\,A} \cdot 2^{-8/5} \approx 3 \cdot \tau_{e,\,A}$ (compare theory chapter 1.2.6) makes sense. One noticeable anomaly is the very high plateau value G_0 of the composite. Using the same assumption as previously and probably overestimating here, because $G_{0,DNA}$ (0.003 Pa) is smaller than $G_{0,A}$ (0.005 Pa) by a factor of nearly two, we expect: $G_{0,comp} \approx G_{0,A} \cdot 2^{7/5} \approx 0.013$ Pa. With an overestimation, this is still only half of the measured value of 0.025 Pa. This unexpected composite behavior can't be explained by the mesh sizes and bundling is also very unlikely with the same arguments as mentioned in the previous chapter (expected change in τ_e, no increase of τ_r, no significant change in shape

of $G(\omega)$ and no visible bundling in CLSM images). Additionally, the protein concentrations of 1-2 µM are very small, which also reduces the likelihood drastically (compare theory chapter 1.2.10.1). Another explanation is needed to understand this deviation from the tube model expectation. After examining this one combination of concentrations, the next logical step is investigating the concentration dependency of this phenomenon, which is done in the following subchapter.

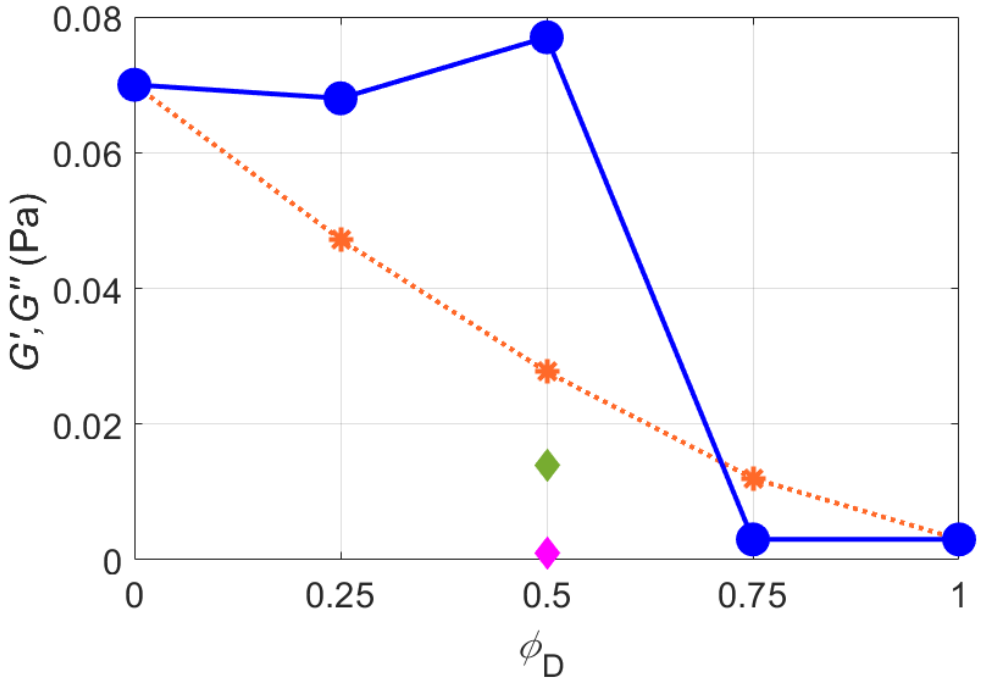

Figure 19: Composite properties of F-actin-DNA hybrid networks. Combined structures are significantly stiffer than the sum of both components' plateau moduli. The plateau moduli of the composites are plotted against the relative mesh concentration $\phi_D = \xi_D/(\xi_A + \xi_D)$ of DNA. The dark blue circle symbols connected by a line show the observed plateau moduli from VPT measurements. The orange star symbols connected by a dotted line are expected results from non-interacting networks on the basis of the tube model with $G_0 \sim c^{7/5}$. The single data points are for mixtures of varying compositions of co-polymerized DNA and muscle F-actin filaments. The concentrations and resulting mesh sizes are shown in table 7. The green and magenta diamond symbols demark the measured plateau moduli for 6 and 8.2 µM F-actin and DNA, respectively.

The mechanical properties of the networks are neither completely independent of each other, nor simply add up to a sum. The linear stiffness of composite networks comprised of different proportions of muscle F-actin and DNA are shown in Figure 19. Plateau moduli of pure F-actin networks on the left are more than an order of magnitude higher than for the equivalent DNA-network. Like previously, mesh sizes of the prepared structures are calculated with equation 20. The combinations of concentrations are chosen to add up to a comparable ef-

Concentration (µM)	ξ_{DNA} (nm)	$\xi_{\alpha\text{-actin}}$ (nm)
DNA Actin		
16.4 0	387	0
12.3 3	449	776
8.2 6	547	547
4.1 9	774	448
0 12	0	388

Table 7: Effective mesh sizes ξ of actin and DNA in composite networks, calculated with the assumption of a cubic mesh (equation 20).

fective mesh size. F-actin concentrations range from 12 to 0 µM and those of DNA from 0 to 16.4 µM. The resulting single mesh sizes are collected in table 7, effective combined mesh sizes add up to about 387 nm. The first expectation using tube model predictions would be a straight line, since the overall mesh size doesn't change and both filaments are semi-flexible with similar filament lengths. This is obviously not the case, the two networks are significantly different in their stiffness at the same mesh size. The prediction is already wrong at this point, there is something missing. So the next step is, taking the difference into account. To simplify the communication, a relative mesh concentration

$$\phi_{\text{D}} = \xi_{\text{DNA}} / (\xi_{\alpha\text{-actin}} + \xi_{\text{DNA}}) \tag{57}$$

of DNA is implemented. For non-interacting networks, the expectation with increasing ϕ_{DNA} would be a decay with

$$G_{0,\text{comp}}(c) \approx G_{0,\alpha\text{-actin,12 µM}} / \left(\frac{12\ \mu\text{M}}{c_{\alpha\text{-actin}}} \right)^{7/5} + G_{0,\text{DNA,16.4 }\mu\text{M}} / \left(\frac{16.4\ \mu\text{M}}{c_{\text{DNA}}} \right)^{7/5} \tag{58}$$

[77], so a monotonous decline for $\phi_{\text{D}} \rightarrow 1$ ($c_{\alpha\text{-actin}} \rightarrow 0$ µM and $c_{\text{DNA}} \rightarrow$ 16.4 µM) because of actin's higher base stiffness. This calculation is shown with orange star symbols and a the dashed line. Using the same assumption as before (equation 14) and modifying $G_{0,\text{A,12 }\mu\text{M}}$ with the effective mesh size would, as already mentioned, result in a straight line through $G_{0,\text{A,12 }\mu\text{M}}$ with a slope of 0. The behavior found here is a very different one. The networks seem to interact synergistically regarding the resistance to shear forces, and an unexpectedly high plateau stiffness emerges from the co-entanglement. This can clearly be seen between 12 and 6 µM actin, where the plateau modulus increases instead of the expected sharp decrease with a maximum at $\phi_{\text{D}} = 0.5$ (c_{DNA}=8.2 µM). A suppression of actin bending fluctuations by a decreased mesh size is one explanation, but this is not sufficient, since the effective mesh

size should be more or less constant over the variation of the relative mesh concentration of DNA. Increasing ϕ_D decreases the mean filament contour length in the network slightly (subchapter 2.2), which would also lead to the expectation of a decreasing G_0, using tube model predictions. This is not the case between $\phi_D = 0$ to $\phi_D = 0.5$.

Esue *et al.* report a very similar behavior for an actin-vimentin network [155]. They found a sharp peak of the elastic modulus for a molar ratio of 1:3 actin:vimentin. This translates to approximately the same mesh size for both filament types, since the segment sizes are different and vimentin has multiple monomers per segment in a filament [156]. It is essentially the same result found here for DNA-actin composites at similar mesh sizes. It is further evidence for the biological relevancy of emergent composite effects. Although it has to be noted, that vimentin is classified as flexible filament and the interaction might be of a different nature.
After excluding all obvious explanations for the unexpectedly high G_0 values of composites, that could be drawn from these findings, the next reasonable seems to be a friction between the filaments. Different charge densities on the surface of the filaments might fill the gap and explain the unexpected change in the mechanical properties. Charged filament protrusions can interact directly attractively or repulsively. They have a repeating pattern of charges on the filament surface, so the interaction changes from the assumed smooth surface hard body interaction to something with minima and maxima on both filaments, which interact with each other to create friction. These come to be due to the repetitive and in case of actin helical structure of the filaments. It would increase the "felt" roughness of the filaments while gliding through each other. This would imply an increase of τ_r for the composite though, which was not observed. τ_r could be a little bit more unreliable than τ_e, because of the worse statistics for long τ. The relatively high standard errors found before for τ_r support this. Assuming reliable data (reasonable due to increases in τ_r easily being visible for crosslinked systems, as previously shown), the elastic properties of meshes are effected, but reptation is apparently not, or not significantly. It could be a transient pinning of the filaments to each other in meshes of co-entangled filaments, which becomes irrelevant on longer time scales. This could be imagined as a high concentration of weak cross-linkers with a very high unbinding rate. That again would lead to an increase in G_0 and a decrease of the plateau-slope, but without removing the second crossover point necessarily (chapter 1.2.10.2), which is generally what is observed in Figure 18

in contrast to the effectively permanently crosslinked network in Figure 17 $\left(\mathrm{D}\right)$ for example. The maximum at ϕ_{D}=0.5 is also a good indication for this hypothesis, since a 50/50 distribution of the filaments would maximize the interaction by maximizing the number of different interaction partners around one filament type. One major argument against this, is the change of τ_{e} in accordance with the tube model expectation, as discussed in the context of Figure 18. The increase of G_0 could also be attributed to a suppression of bending/twisting fluctuations or the coupling of those, but this would also result in a shift of τ_{e}, which does not seem to be the case. So there are multiple potential explanations, which are hard to evaluate against each other at this point. Further information is necessary. This will be discussed again in the following chapters (isoforms of actin and post-translational modifications of actin).
A biological relevance of composite material effects like the here observed one appears to be convincing, since biological cells consist of many different composite materials (compare subchapter 2.4 and 2.3).

In summary, the linear viscoelastic shear behavior of F-actin-DNA composite networks is also that of a semi-diluted, entangled polymer network of semi-flexible filaments. A peculiarity is an emergent composite property. Composites show a significantly increased plateau stiffness compared to the tube model expectation, which can hardly be explained by bundling or similar static effects, because the viscous properties are not or not significantly affected. This stiffness anomaly is dependent on the relative composition of the composite. Relative concentrations, which result in the same mesh size, show the strongest increase in stiffness. A solid mechanistic explanation for this behavior requires further information, after which it will be discussed in the chapter's summary. After examining the linear viscoelastic properties of DNA-networks and composites with F-actin, the non-linear mechanics are the next step to be explored. Understanding the network response to higher strains, which induce nonlinear deformation, might give insights into potential strain stiffening or shear thinning not present in mono-component networks. In addition to the general biological relevance of strain stiffening in composite materials [23], relaxation behaviors and filament interactions can potentially be inferred from there. These can be used to find an explanation for the deviations from the tube model expectations.

2.4 Nonlinear Viscoelastic Behavior of Composite Networks

Nonlinear behavior is a relevant part of cellular mechanics [157]. Prestress stemming from the contraction of myosin motors in the cytoskeleton is the main cause of that and the overall stiffness of the cell. The cytoskeleton and the underlying cytoplasm are composed of structures and materials, which demonstrate a complex, time dependent behavior under stress. They can respond by fluidizing or stiffening [158, 159, 160]. Control of the resistance to external forces seems to play an important role in biological matter. The ability to withstand abrupt stresses and avoid damage by stiffening or move through structural barriers by fluidizing over longer periods of time is crucial to the survival of a cell. It is also something, which is not fully understood yet. DNA filaments not only modify the linear viscoelastic response of an F-actin network, they also change the non-linear regime by increasing stress response overproportionally under strain. The non-linear mechanical behavior of F-actin-DNA composite networks is investigated here with optical tweezers. Microparticles are dragged through the sample with the laser under a moderate and constant displacement rate (2 µm/s), greater than the intrinsic relaxation rates of the networks, discussed previously (subchapter 2.2.4). It is smaller than the crossover point observed by Gurmessa *et al.* [24], where strain softening from shear thinning switches to strain stiffening induced by entanglement tube dilation. The goal is to perturb the system away from an equilibrium state and study non-linear effects.

Figure 20 displays the relative differential modulus (K/K_0) against strain graphs for an entangled F-actin network (A), a DNA-network (B) and a composite-network (E). Below that are drag forces F_D against the displacement of the dragged particle Δx_D as examples in (C), (D) and (G). An overlay of (A), (B) and (E) is shown in (F), mean drag forces against displacement graph in (H). While, as expected, there is no strain stiffening for pure actin [24, 96] and DNA at this strain rate (2 µm/s), for the composite, a clear nonlinear strain stiffening is visible with a relative differential modulus >1. The force against displacement graphs confirm this. The composite essentially displays the behavior of the actin network with additional nonlinear behavior producing peaks with a sudden break-off back to the baseline. Peaks in the force response are clearly maximized in the composite networks. Purely entangled F-actin networks don't display this at all, and for DNA networks it has a rarer occurrence. This is probably due to different relaxation behaviors on the one hand

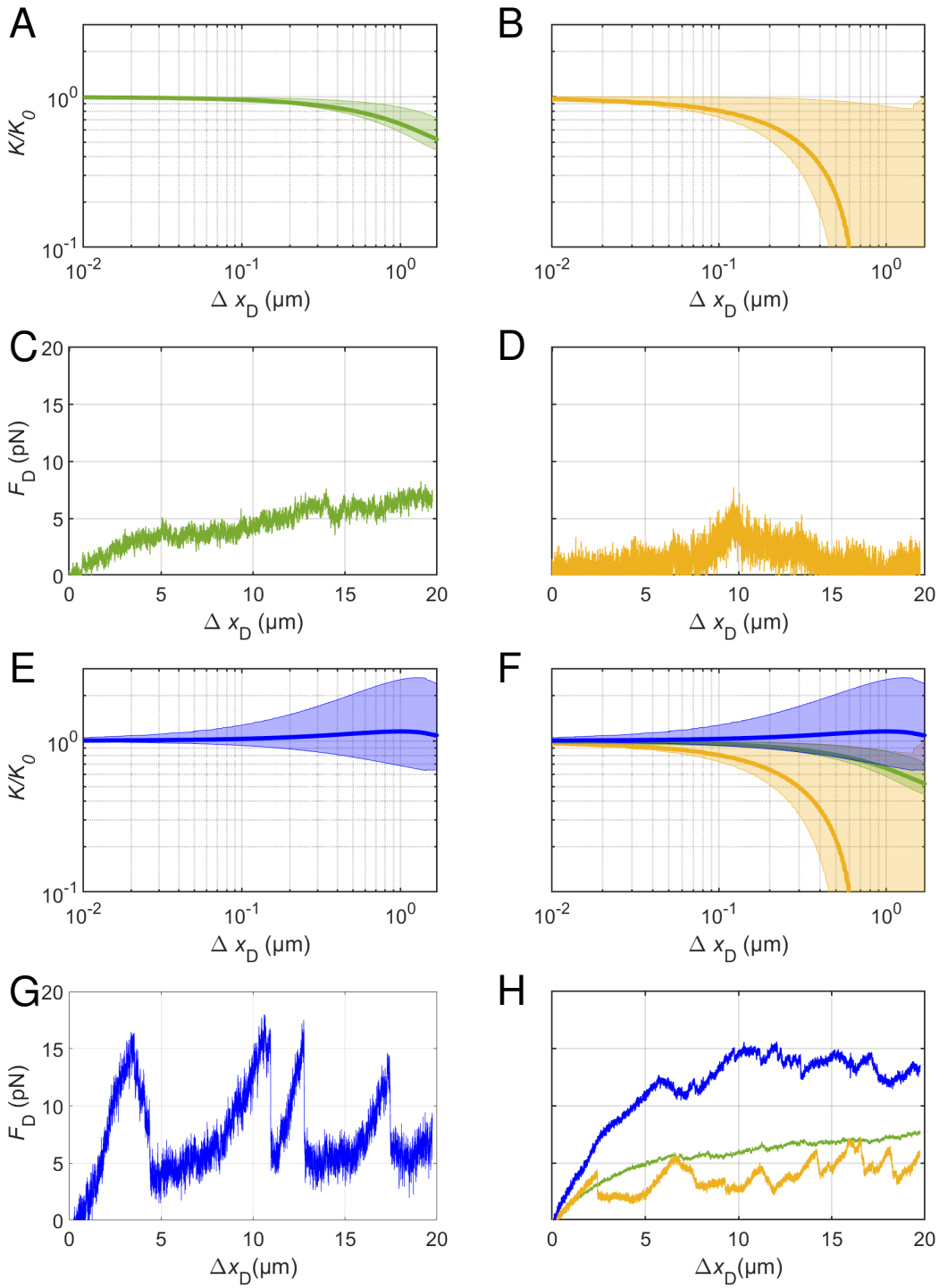

Figure 20: Nonlinear strain stiffening of F-actin-DNA composite networks. The relative differential modulus (K/K_0, where K_0 is the linear differential modulus at low strain), is plotted against the displacement Δx_D for A) a pure actin network at 12 µM (green), B) 16 µM DNA (orange), E) an actin-DNA composite network at 6 and 8 µM respectively (blue) and an overlay of all K/K0 is shown in F). The force curves below them show examples for corresponding drag force (F_D) curves against displacement data in C), D) and G). Mean force curves are shown in H) with different colors for each composition, ranging 12 µM actin and 0 µM DNA (green) over 0 µM actin and 16 µM DNA (orange) to 6 µM actin and 8.2 µM DNA (blue).

and microparticles slipping through meshes and releasing stress to produce break-off events on the other. Where entangled actin networks as well as DNA networks can freely relax stress, induced by the dragged microparticle at this displacement rate, the composite network can't. This is despite mesh sizes should be very similar as discussed in chapter 2.2.3. The different relaxation behaviors may not combine well and reduce the overall network flow. A possible explanation could be a compression of one network, while the other one is already relaxing the stress by filament gliding. This would then be hindered by the buildup of the first network in front of the particle, which further increases the buildup of tension until it is released by rupture or other forms of nonlinear network deformation. The peaks in Figure 20 $\left(\mathrm{G}\right)$ are an indication of this. Interestingly, the long-term fluidity of the composite does not seem to be effected very much, since the low frequency behavior of the shear modulus shows clear signs of network relaxation by reptation. This reptation also seems to be very similar to the one for mono-component networks as discussed in chapter 2.2.4.
Ricketts *et al.* [151] report a transition in a co-entangled actin-microtubule network from strain softening to strain stiffening with an increasing fraction of microtubules in the structure. They attributed this to a change in pyroclastic relaxation arising from different pore sizes. This was again stemming from different mesh sizes of the two filament types and also suppressed actin bending fluctuations. The results are similar to the here presented findings. An indication for comparability are the force curves of purely entangled actin. These are quite similar with average maximal forces around 10 pN. It appears important to point out, that they also performed optical tweezer measurements, so local microrheology.
Golde *et al.* [156] investigated actin-vimentin co-polymer networks and found linear as well as non-linear effects, which they explained with two non-interacting structures. They found a strong increase in strain stiffening from pure actin over increasing the fraction of vimentin to pure vimentin. The mechanics of the composites were analyzed with an inelastic glassy WLC model, which was able to predict the rheological data. This data was obtained with a plate rheometer, so it represents bulk properties from macrorheology. In essence, they did not find emerging composite behavior. Interestingly, their measurements of shear moduli for those composite networks, as well as for pure mono-filament types, did not show typical plateau behavior. This was despite them spanning over three orders of magnitude in stiffness.
In contrast and prior to that, Esue *et al.* [155] reported a very clear emergent composite behavior (as mentioned before) also for an actin-vimentin network.

They found a sharp increase in the elastic shear modulus G' for a molar composition of 1/3 actin and vimentin with rheometer measurements.
Similarly, Lin *et al.* demonstrated nonlinear stiffening of F-actin networks by the addition of microtubules [161].

In summary, F-actin-DNA composite networks display significant strain stiffening, which is neither present in pure F-actin nor DNA-networks. This has potential biological relevance, since cellular composite networks also alter the non-linear mechanics of the involved structures. It is also an additional indication for the hetero-filament interaction being stronger than the homo-filament one.

2.5 Interaction of Composite Networks with ABPs, Motor Proteins and High Cation Concentrations

This chapter explores the interaction of interwoven DNA-actin networks under the influence of motor proteins, ABPs and divalent cations. All of them induce some kind of network contraction. Comparing these contractions to those of pure actin equivalents can give an insight into filament interactions and potentially the interaction with other proteins and cations. Additionally, the biological relevance and usefulness of the composite material in biological model systems is discussed.

Actin filament polymerization and depolymerization controlled by Arp2/3 has a very important role in the motility of cells [162, 163, 164]. It is utilized to push the cell membrane forward, where then focal adhesions anchor the substrate to permanent actin structures, so-called stress fibers. These also consist of actin, but the filaments are bundled by crosslinker proteins like α-actinin mostly in an antiparallel manner. Motor protein filaments (myosin II) embedded in them are then able to contract the stress fibers by pulling on filaments and letting them slide against each other. This generates traction and for example enables the cell to either push itself further along the surface or stabilize it on the substrate. The point is, to control filament structures on a microscopic level locally and dynamically, other proteins are needed. This makes it important to study the interaction of an artificial model system with them or agents, which fulfil comparable roles. In this case, ABPs, motor proteins and biologically relevant divalent cations like Mg^{2+} and Ca^{2+} are investigated. Figure 21 shows three composite networks, one combined with myosin II, which contracts and in rigor state

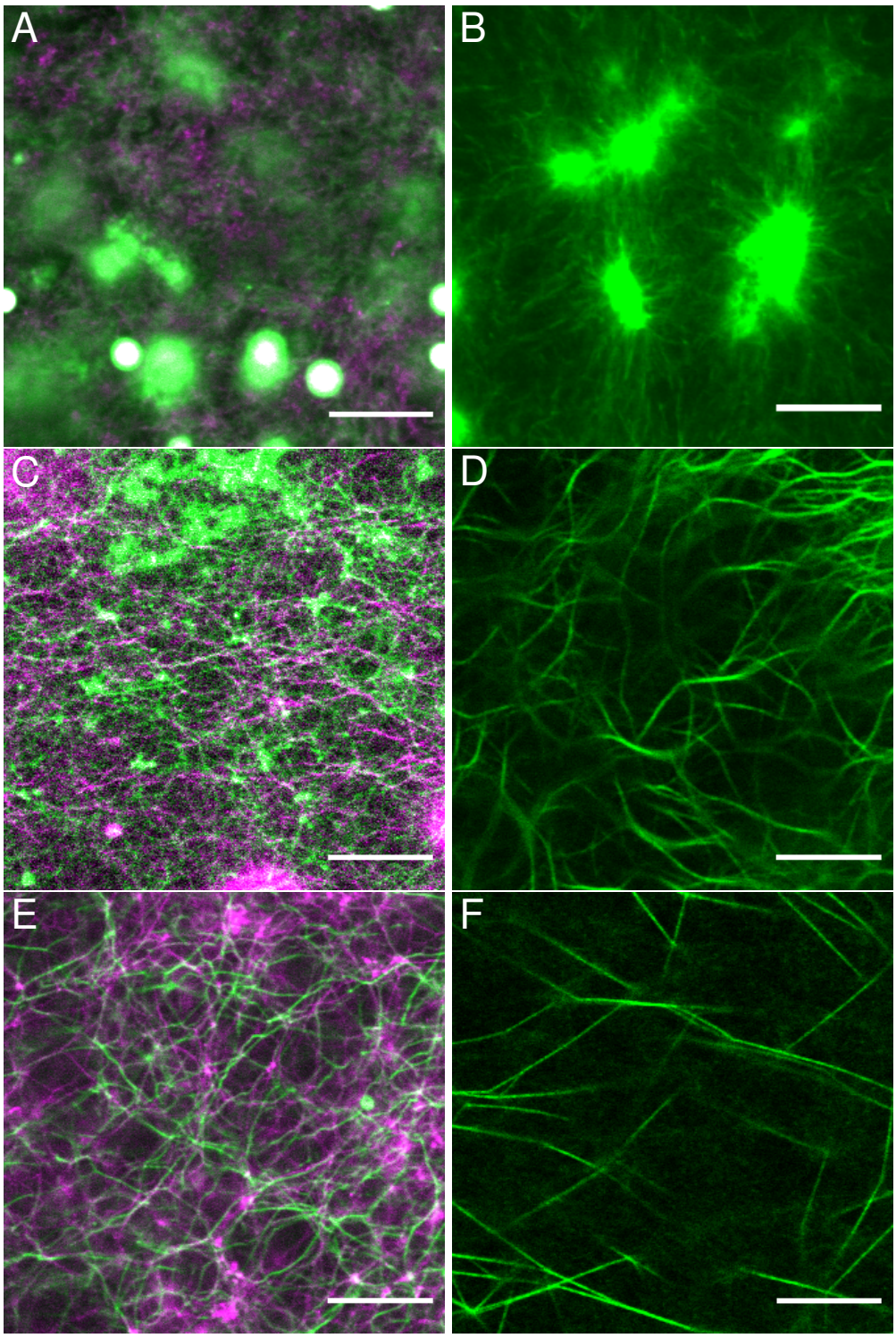

Figure 21: DNA-networks significantly change the contraction and bundling properties of F-actin. A) An actomyosin network with 24 µM actin, 2.2 µM myosin and 24 µM DNA. Bright green dots are 2 µm fluorescent microparticles for VPTMR. C), E) Bundled actin-DNA composite networks with 24 µM actin and 24 µM DNA. In C) the bundling is induced by 2 µM α-actinin, in E) by 30 mM Mg^{2+}-ions as counterion condensation. B), D) and F) show comparable actin networks without DNA structures. Scale bars are 10 µm.

crosslinks F-actin (A). Then another one with α-actinin, which crosslinks F-actin to thick bundles at high concentrations (C). And (E) shows a third composite network with an increased Mg^{2+}-concentration, which induces bundling of both networks by counterion condensation. On the right side of that the corresponding F-actin networks with the same composition, except for the DNA-structure, which is missing. The myosin II network in (B) displays typical contraction in the form of dense, bright, star-shaped aster structures. Here, the motor proteins hydrolyze ATP with a low duty ratio of the head groups until the ATP concentration is low enough to increase the duty ratio and pull on the actin filaments. These are now pulled in random directions until ATP is used up, or local accumulations of myosin filaments form. There the actin structure gets extremely dense and the number of myosin heads so high, that no more bundles of actin filaments with the connected myosin filaments can escape. More actin is pulled in instead, increasing the inner density further and further until all myosin heads are "jammed" with surrounding F-actin. Because of this jamming, the process can stop even before the ATP concentration gets exhausted. An interesting property of living things is the non-equilibrium state they are in.One hurdle when doing passive MR with cells is their non-thermal cytosolic activity, which increases thermal Brownian motion of the involved micro objects in a certain frequency range by a non-thermal, motor-driven one. Quantifying this has been the goal of some studies *in vivo* and *in vitro* [165], but there is still a lot poorly understand and to illuminate yet. One big hurdle in *in vitro* reconstructions of this phenomenon is the network contraction, which creates extreme, local inhomogeneities or stops the process altogether and thereby can make analysis very complicated. To understand motor activity on a network level more accurately, a homogeneous, non-contracting, but still dense enough to transmit stresses, network would be preferable. The composite structure shown in (A) seems to fulfil these requirements. Despite a very high myosin II concentration ($\sim$10 %), no aster formation is observed.

Another important property to control in the formation of specific sub-structures of networks, is bundling. (D) and (F) show bundled networks, one from crosslinking and one from counterion condensation. Both contain thick bundle meshes with mesh sizes partially well above 10 µM and a number of filaments per bundle in the order of 500 (concluded from known concentration of actin and again a cubic mesh assumption). These are on the one hand hard to measure by MR because of the high mesh size and on the other hardly biologically relevant, because they don't resemble *in vivo* structures. This is despite comparably or even higher cellular concentrations of actin [25, 26]. Whole cells

could easily slip through the meshes. The DNA acts as a support structure and decreases resulting mesh sizes from crosslinking significantly by an order of magnitude (C), even when bundled itself by counterion condensation (E). The mechanical properties of the types of networks depicted in Figure 22 are shown in Figure 23. (B) and (C) are a crosslinked and an actomyosin-DNA network respectively with corresponding shear moduli in Figure 23. In (A) a comparable composite network without other additives is depicted and an overlay of the shear moduli in Figure 23. The stiffness of the crosslinked networks is strongly increased compared to the entangled network, but the samples are easily measurable (the mesh size is not increased too much by bundling).

In summary, DNA networks can be utilized for controlling the dynamic microstructure of *in vitro* reconstructions of complex cytoskeletal structures and even for the analysis of non-equilibrium dynamics of motor proteins. They can be a useful tool to suppress contraction or analyze the forces involved in contraction processes.
Looking back at the previous subchapters, the results presented in this one also point towards a stronger hetero-filament interaction, which emerges as a composite property. The DNA-network is much softer than the actin network, but still able to stabilize it against contraction very effectively. It suppresses aster formation and reduces mesh sizes of bundle structures. Large asters like in Figure 21 (A), as well as bundles made of hundreds of filaments, are not present in eukaryotic cells. A similar composite effect stemming from the interaction of different filament networks is conceivable.

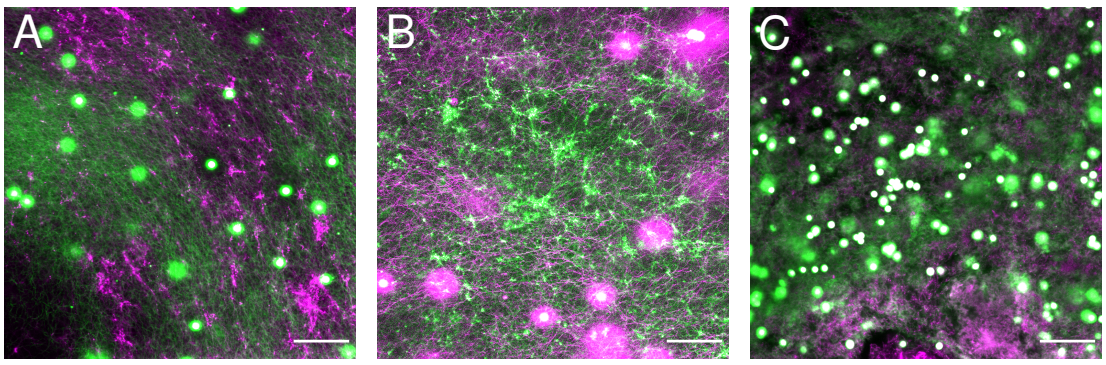

Figure 22: Micrographes of the crosslinked and contracted actin-DNA structures. A), B), C) are CLSM images of actin-DNA networks at 24 µM each. A) shows a purely entangled network, B) one with additional α–actinin (2 µM) as well as Myosin II (2.2 µM) in C). Bright green dots are 2 µm fluorescent microparticles for VPTMR. Scale bars are 20 µm.

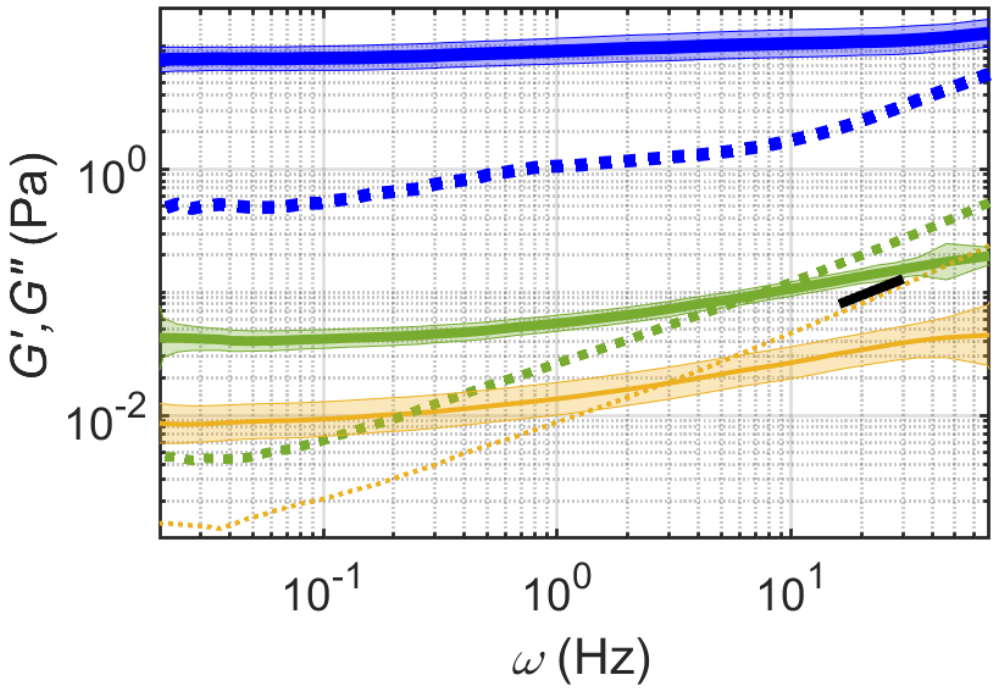

Figure 23: Mechanical properties of the crosslinked and contracted actin-DNA structures shown in the previous figure. The shear moduli G' (straight line) and G'' (dotted line) measured by VPT corresponding to Figure 22 are shown. The orange lines belong to A) and show a purely co-entangled actin network at 24 µM, the green lines to B) with additional crosslinkers (2 µM α-actinin) and the blue lines to C) with additional motor proteins (2.2 µM Myosin). A slope of $\omega^{3/4}$ is shown as a black line.

Figure 24 shows a thin (< 1 µm), compressed and floating actomyosin (rigor myosin) structure with stabilized by microparticles ($d = 15$ µm, silica) below it. The mesh size of the network is very small (between a few hundred nanometers and something below the resolution limit of the CLSM, ≈150 nm). Optically, this reconstituted structure resembles that of a cellular cortex already quite well [166, 167]. Myosin activity like contraction or restructuring would deform the structure inhomogeniously and result in asters and holes. The incorporation of DNA filaments into the structure like shown in Figure 22 could overcome this issue and pave the way for 2D-non-equilibrium cortex models.

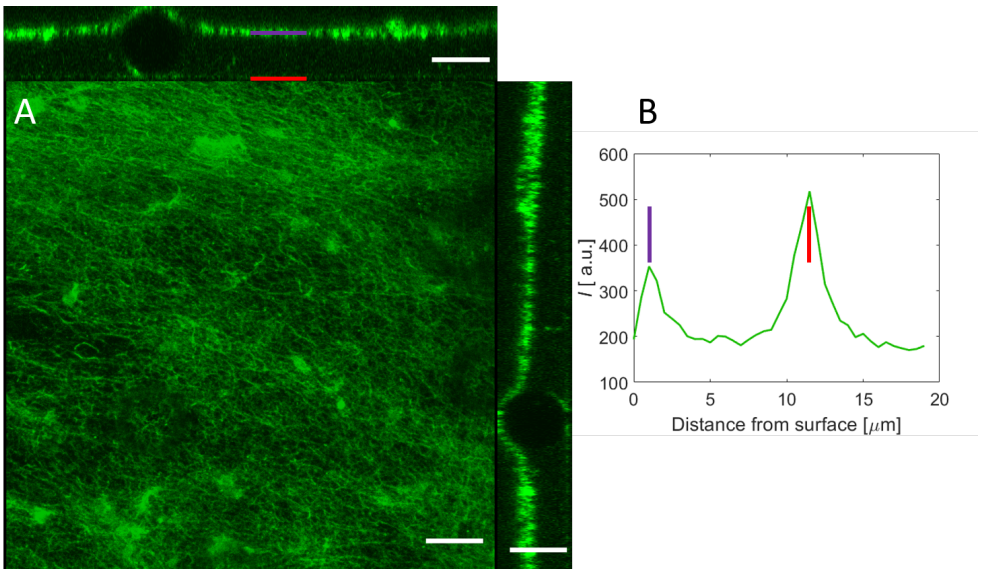

Figure 24: Support-free 2D-actomyosin carpet network. A) Reconstituted network structure of α-actin filaments connected by myosin minifilaments. It is floating in G-buffer between microparticles ($d = 15$ µm, silica) and was compressed by pouring a saturated sucrose solution over a 3D-actimyosin network, polymerized on a solid and thin ($d = 15$ µm) sucrose crystal structure. The sucrose was finally washed away with G-buffer. Approximately 50 µm of 10 µM actin and 1 µM Myosin were compressed to the thin (< 1 µm) structure. The z-stack side views above and on the right of the panel show the distance from the surface and a microparticle below the structure. B) CLSM fluorescence plot perpendicular to the carpet network plane. It shows the distence of the network from the glas chamber surface and the thickness of the structure. Scale bars: 15 µm.

2.6 Summary

The main goal of the experiments presented in this chapter was to investigate a scenario with two different semi-flexible filaments in networks, resembling structures found in eukaryotic cells on a basic level. The cytoskeleton is typically thought of as a combination of three different filament networks with individual and separated viscoelastic properties. They get categorized in three different types, distinguished by their bending properties (their persistence length) into flexible, semi-flexible and rigid rod like filaments. In recent time, cytoskeletal structures they form are more and more understood as composite materials with mechanical properties, which can't directly be attributed to one of the components, but arise from the interaction. [150, 149]

These three types of filaments significantly differ in their mechanical properties. The theories describing and predicting their viscoelastic properties have been established as individual models [2]. These usually treat the filaments as smooth, uniform bodies with a hard shell or a harmonic potential separating them from each other. Is that a good assumption in general? For semi-flexible actin filaments, the predictions have been confirmed with quite well [147, 148,

96]. But can the tube model (theory chapter 1.2.6) predict the properties of other semi-flexible filaments accurately? And then, in the next step, is it possible to predict them for a composite network consisting of different semi-flexible filaments? Following the assumptions of the tube model, at least in an entangled network, they should co-entangle. The additional second type of filament should in principle just increase the concentration of the other. Predicting the resulting properties via the tube model should be possible after correcting for different (they should still be in the same order of magnitude) monomer and filament dimensions.

The first question is addressed in chapter 2.2. The characterization of the analyzed DNA-filaments reveals them to be semi-flexible. The reported persistence length [8] of 6.46 ± 0.26 µm can not be confirmed due to the very short average filament length. It does appear rather small due to reasons presented in chapter 2.2.2. A l_p of $\sim$17-34 µm is estimated in chapter 2.2.4, which keeps it in the semi-flexible regime.
The filaments form mostly homogeneous, viscoelastic networks in semi-dilute solutions, which are very similar to semi-flexible protein filament networks of F-actin found in eukaryotic cells. This leads to the expectation of predictability of mechanical properties by the tube model for semi-flexible polymers. This expectation is well met as shown by VPTMR data. G_0 increases approximately with $c_\mathrm{DNA}^{7/5}$ and τ_e as well as τ_r (the crossover points of G' and G'') similarly follow the expected $c_\mathrm{DNA}^{-8/5}$ and $c_\mathrm{DNA}^{<1}$ behavior respectively. This is also presented in chapter 2.2.4.
So the first conclusion is: The investigated DNA-filaments are semi-flexible and form networks similar to those of F-actin. They can be described and predicted by the tube model.

After a characterization of the DNA networks, the next step is creating composites from two semi-flexible filaments. DNA-actin networks are co-polymerized and their linear viscoelastic properties are compared to tube model predictions. This is presented in chapter 2.3.
DNA-actin composites are co-polymerized with concentrations leading to similar mesh sizes of the co-entangled networks. This is done in order to account for different monomer lengths and subunit numbers (chapter 1.2.7). Molar and mass-concentration equivalents would not result in comparable networks. The optimal molar ratio of concentrations is calculated as 4.1/3 DNA/actin for similar mesh sizes. Composites with this ratio are compared to mono-component

networks and their viscoelastic properties are evaluated. This reveals a network with properties very similar to the single networks. The composites are also viscoelastic, entangled networks. They form interwoven structures, which don't clump or bundle together without an increase of ion concentrations. They also don't pin each other together. The characteristic crossover points of the shear moduli clearly demonstrate viscous flow in the low frequency regime. These crossover points have concentration dependencies similar to the mono-component networks.

One peculiarity separates the composite from the single filament type networks though. G_0 is found to be significantly higher than expected (predictions based on the tube model are shown in Figure 19 and explained in the subchapter). For further investigation in order to understand the found anomaly, the network composition is shifted incrementally from one mono-component network to the other. The phenomenon is observed to be dependent on the relative concentration and peaks - compared to expected G_0 - at a molar ratio of 4.1/3 DNA/actin. This leads to the conclusion, that entanglements between DNA-filaments and actin filaments have a stronger interaction than mono-component entanglements. At that ratio, both structures have the same total filament length per mesh, they contribute equally to the overall network structure and therefore also have a maximum overlap.

Besides the linear viscoelastic shear behavior, non-linear deformation of the networks is also analyzed via drag experiments. For this reason, microparticles are dragged with optical tweezers through DNA-actin composite networks and comparable mono-component networks, shown in chapter 2.4.

In addition to significantly higher drag forces, the composites display strain-stiffening, where actin and DNA on their own strain-softening. Strain-stiffening occurs in entangles actin networks only at much higher concentrations, strain rates or with ABP-crosslinking [158, 159, 160]. This is further evidence for a stronger interaction of the two types of filament, emerging as a composite property.

In addition to entangled networks, the effects of motor proteins, ABPs and counterion condensation are also explored in chapter 2.5. On the one hand, this is done to accumulate more information in order to explain the unexpected composite behavior, on the other hand to explore more cell like conditions in the presence of other proteins.

The primary effect of the composite's interaction with ABPs, as well as higher concentrations of divalent cations (counterion condensation above $\sim$20 mM), is found to be a stabilization of the homogeneous actin filament network. Net-

work Contraction by myosin II filaments is suppressed even at high concentrations of myosin (dense networks around 24 µM (1 mg/ml) actin and 2.2 µM myosin II filaments). Bundling by ABPs and divalent cations is also reduced. The bundled networks have smaller mesh sizes and have therefore lower numbers of filaments per bundle than the corresponding mono-component networks. Again, this is evidence for a stronger interaction of the entangled filament networks compared to the mono-component networks. The DNA-filaments don't introduce longer filaments into the network, on average they have a similar or smaller contour length (chapter 2.2), which otherwise would increase G_0 and the network's resistance to deformation in general. A direct interaction of DNA filaments and motor proteins or ABP is very unlikely, since they don't possess binding sites for either [8].
Comparing different isoforms of actin to DNA-networks led to the discovery of a significant difference in the viscoelastic shear properties of muscle and non-muscle actin. These are further explored in chapter 3.2, which in turn gives a new perspective on some of the phenomena investigated in this chapter. It is furthermore a perfect opportunity to investigate more semi-flexible filament networks and compare them to the results presented here. The finding also lays ground to the speculation, that there are different cellular protein polymer networks hidden in very similar structures in eukaryotic cells. Maybe the mechanical properties of actin filament networks are not as simple as it seems. Most experiments investigating reconstituted actin networks in some form or another are performed with muscle actin, neglecting potential differences for non-muscle actin isoforms. And if non-muscle actin is used, it is mostly purchased or isolated as a mixture of γ- and β-actin. This again neglects potential differences in those isoforms. Additionally, potential composite effects are also not explored. Further investigation of mechanical differences between actin isoforms will be presented in the following chapter.

So in conclusion, the viscoelastic properties of networks formed from the semi-flexible polymer actin and the also semi-flexible DNA-filaments can be predicted with the tube model to a high degree except for the overall plateau modulus, which is significantly lower than expected for DNA (depending on the concentration). Composite networks of both show higher shear moduli than predicted and also strain stiffening, where the entangled mono-component filament networks don't. As already demonstrated, the two types of filaments form interwoven networks, but they don't stick together or bundle at low Mg^{2+}-concentrations (below $\sim$ 20 mM). The networks show clear signs of flow and

filament reptation. So excluding bundling and static network pinning (similar to permanent crosslinking), there are multiple possible explanations for the unexpectedly high shear response of the network:
1. Direct electrostatic interactions of the filaments via amino acid residues or DNA side chains.
2. Direct steric interactions of the filaments.
3. Inter-filament complexation of divalent cations by amino acids and DNA side chains, which would function as short-lived (transient) quasi crosslinking.
Steric interactions are highly unlikely, due to relatively smooth filament surfaces on the one hand and very small filament diameters compared to the mesh sizes. Both filaments lack large (compared to the filament diameter) protrusions from the filament backbone (compare Figure 1). The filament diameters are below 10 nm, compared to mesh sizes between 200 and 1000 nm. This combined with persistence lengths much larger than the mesh size would give the filaments more than enough space to avoid the steric interactions between potential protrusions smaller than 1 nm. The other points will be discussed further in the summary of the following chapters, after additional information has been presented.

3 Actin Isoforms

3.1 Introduction

Actin is a family of globular structural filament-forming proteins found in all eukaryotic cells. It is a major component of the cytoskeleton and one of the five most abundant proteins in eukaryotes [168]. The filaments are semi-flexible with an exceptionally large persistence length of $\approx$ 10 µm with a diameter of only 7 nm [168, 169, 170]. Actin together with myosin and its many actin-binding proteins is pivotal for a variety of important cellular processes, including muscle contraction, cell motility, adhesion, cell shape, cell division, and embryogenesis [171, 172]. A common association with actin is its high degree of sequence conservation [11]. This conservation is not limited to the comparison between organisms, but also extends to its different isoforms. Some of these isoforms can even copolymerize [11]. This is puzzling, since such obvious redundancies should have disappeared in the course of evolution due to evolutionary pressure. Therefore, a good evolutionary reason for continuity should exist.

Two of the most closely related actin isoforms are non-muscle β-actin and γ-actin, which are encoded by different genes but produce nearly identical proteins except for four residues at their N-termini [11]. Despite their close similarity and their occurrence in the same cell types, the two isoforms do not appear to be redundant. For example, it has been shown that β-actin and γ-actin localize to different parts of the cell and tend to incorporate into different actin cytoskeletal structures such as the cortex and stress fibers, respectively [11, 12]. Furthermore, both isoforms seem to have dedicated roles regarding cell motility [12], epithelial-to-mesenchymal transitions [13, 14, 15], cellular junctions [16] and hearing [17, 18].

While this is evidence for the importance of small differences in isoform-specific amino acid sequence, our understanding of how these almost identical proteins could perform such different tasks is still incomplete. Previously, it has been shown that in contrast to γ-actin, only β-actin mRNA gets spatially targeted to the cell periphery [173]. However, the reason for this behavior is not likely to originate from the amino acid sequence, but rather is a result of different gene translation [174]. Recently, it has been shown that editing of the β-actin coding sequence to encode γ-actin instead leads to vital mice with unaffected phenotype, but not *vice versa*, showing that the two isoforms might be to some degree interchangeable [173].

It remains to be elucidated how this small exchange of amino acids affects protein structure and binding sites that mainly control the mechanical properties of filaments and tasks fulfilled by the cell. Consistent variations in the AAS should therefore encourage the search for different mechanical properties and functionalities.
Here, the controversy is addressed of whether different actin isoforms have indeed unique mechanical properties or are interchangeable in that regard. For this purpose, the mechanics of actin filaments are examined. This is done on different length scales and also in the presence of various crosslinkers. The overwhelming majority of studies on the mechanical properties of reconstituted actin structures has been done with α-skeletal muscle actin [175, 176, 177] and some with a commercially available mixture of cytoplasmic γ- and β-actin (15/85, here referred to as nm-actin, chapter 7.2) from human platelets [178]. Therefore, experiments are also performed with these particular actin isoforms and mixtures and the results are compared.
While single filament behavior follows the expectation of from the conserved sequence, substantial differences in plateau moduli and contractility between the different isoforms are found when forming entangled networks. The emerging picture paints β-actin as forming softer, less resilient networks with more locally dispersed contraction foci. In contrast, γ-actin builds stiffer networks but asters are larger. This is indicative of higher contractility and connectivity compared to networks composed of β-actin. The study clearly shows that actin-actin as well as actin-crosslinker interactions are considerably modified by a change of the AAS at the N-terminus of Actin.

3.2 Actin Isoforms, AAS of β- and γ-actin

Most of the actin isoforms differ only by very subtle sequence variations. In particular, the differences between cytoplasmatic β- and γ-actin are limited merely to four amino acids at the N-terminus, where aspartate appears in β-actin and glutamate in γ-actin, respectively.
Since it was found that the different isoactins are unable to replace each other without loss of function, an intracellular specialization for different mechanical tasks is inferred.

3.3 Localization of Actin Isoforms in Living Cells

Figure 25 (A)-(C) shows confocal images after immunostaining of the two prominent cytoplasmic actin isoforms β- and γ-actin in MDCK II and SK-OV-3 cells, respectively. MDCK-II cells have been used extensively to study the mechanical properties of the cytoskeleton, particularly the contribution of the cortex to resistance against external deformation [179, 180]. The images confirm the very distinct localization patterns in both cell lines, as previously predicted [12]. β-actin (green) is found exclusively in basolaterally forming stress fibers, while γ-actin (red) constitutes the apical cortex. This is in line with previous findings, which also reported a similar spatial segregation pattern for MDCK II cells [12]. Figure 25 (D) shows the sequence at the N-terminus of the three isoforms investigated in this study. Interestingly, as visualized in Figure 25 (E), the relevant positions are highly exposed along the filament.

3.4 Isoform-Specific Network Architecture and Mechanics

Since actin isoforms occupy different locations within cells, the question arose whether networks formed from pure isoforms already exhibit visible differences in architecture for reconstituted networks. The commonly used α-actin, found in muscle cells, was also included in this study as well as non-muscle actin, a mixture of β- and γ-actin. Figure 26 (left) shows confocal images of the three different F-actin networks in solution. No visually observable difference between the isoforms forming these purely entangled actin networks is found. Despite their obvious structural similarity, passive micromotion measurements are performed on the different networks to investigate their mechanical properties (Figure 26 center). The viscoelastic spectra are obtained from Laplace transformation of the mean square displacement following a standard procedure that has been described elsewhere [182, 147]. Additional information can be found in chapter 1.3.2 and 7.3. Typically, the plateau modulus arising from filament entanglement at intermediate time scales is in the range of 0.1 to 0.01 Pa. This is in good agreement with previous studies using solutions made from α-actin [182]. Surprisingly, the comparison of the mean spectra clearly shows that β-actin forms substantially softer networks with a plateau modulus G_0 almost one order of magnitude smaller than that of networks formed by γ-actin. This is a prime example of how seemingly small variations at the molecular level lead to significant mechanical consequences on the mesoscopic length scale.

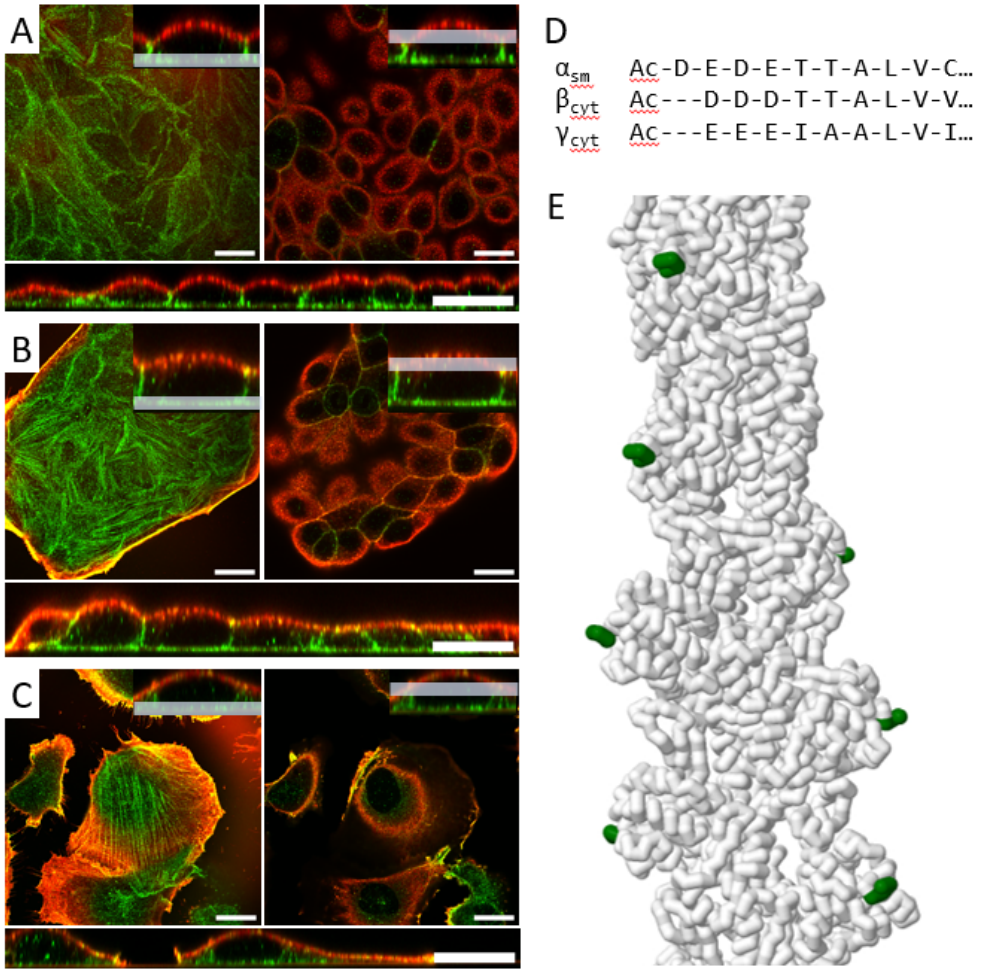

Figure 25: β-actin (green) and γ-actin (red) are locally segregated in MDCK II cells in monolayers A) and in small clusters B), with β-actin being localized in basal stressfibers (A,B, left panel) and γ-actin being localized at the apical cortex (A,B, right panel). An orthogonal view (A,B, bottom panel) shows, that the cell-cell-boundaries mainly consist of β-actin. These findings are consistent with [12]. In addition, SK-OV-3 cells C) show the same segregation (scale bar: 20 µm). D) The main differences between the isoforms are located at the N-terminus. E) Although those differences appear insignificant by themselves, the N-termini of actin monomers are located at very exposed positions along the filament (adapted from [181]).

However, purely entangled networks are not a very realistic model for the cytoskeleton, since the structure of cellular actin networks is mostly modulated by the influence of actin-binding proteins [171]. Therefore, the network structure of each F-actin isoform cross-linked by fascin as well as rigor myosin II or branched by Arp2/3 is examined to imitate the structures and also dynamics prevalent in cells. Cell motility and structural integrity are mainly controlled by the cortex, filopodia and connecting stress fibers. All these processes are mediated by different actin isoforms in association with specific ABPs [171]. Therefore, the attempted is to select representative isoform and ABP combinations as a bottom-up model.

These networks exhibit (at the chosen concentrations) pronounced structural

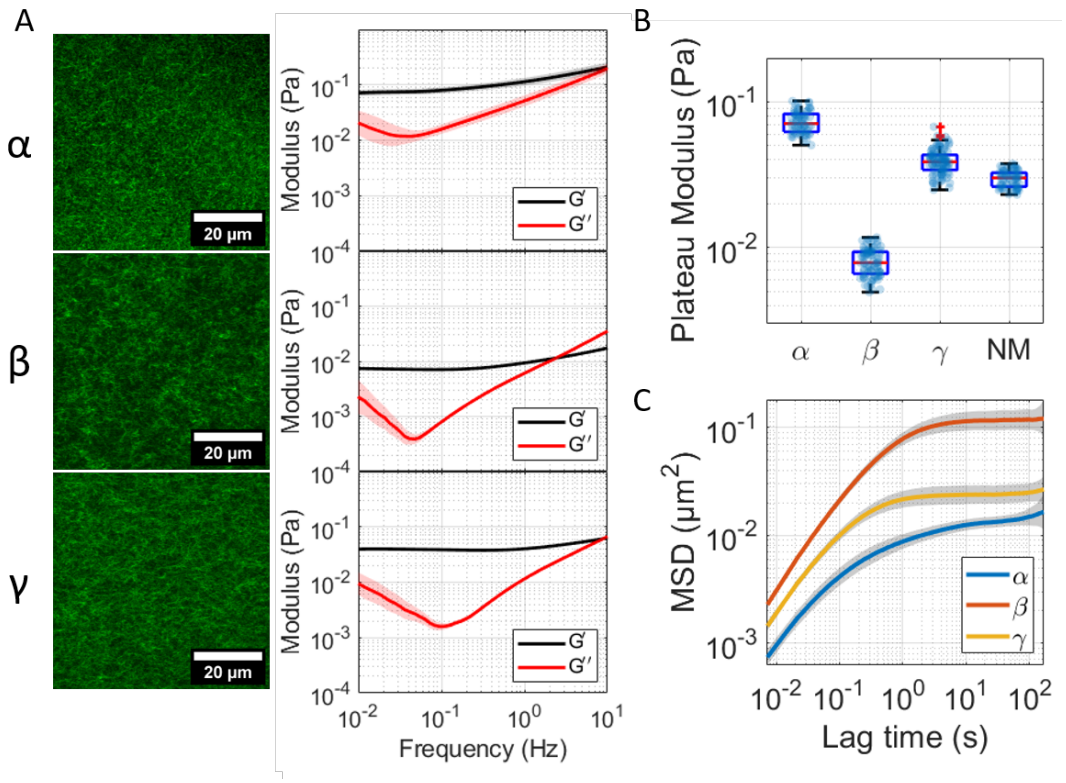

Figure 26: The architecture of purely entangled actin networks does not depend on the isoform. However, upon probing the microrheological properties via hVPT significant differences can be identified. Panal A) shows confocal images of actin networks (12 µM) for the different isoforms as indicated. B) Corresponding shear moduli with the elastic modulus ind black and the loss modulus in red. C) Scatter plot of the plateau moduli for the three isoforms and the mixture nm-actin with mean values. Mean-squared displacements for the three isoforms in different colors as indicated. Scale bars are 20 µM.

differences between isoforms when polymerized together with Arp2/3 or myosin II, but not in the presence of fascin (Figure 27). Fascin fosters the formation of short, straight bundles (around $10\,\mu\text{m}$ in length) with all isoforms [183]. Conversely, Arp2/3 binds to the sides of pre-existing actin filaments and generates a new nucleation site from which a new actin branch is formed at an angle of 70° [184]. Thereby, a dense, highly branched actin network is obtained. Addition of Arp2/3 to the different isoform networks resulted in visible isoform-specific differences in network organization (Figure 27 A). Muscle actin does not display any significant deviation in the visible structure from purely entangled networks in the presence of Arp2/3. But all non-muscle isoforms show a heterogeneous density distribution that can be attributed to a local accumulation of branched networks. Specifically, γ-actin displays a pronounced clustering, pointing towards a stronger interaction with Arp2/3 compared to the other isoforms. In contrast, β-actin is found in a slightly heterogeneous, but filamentous arrangement, akin to bundles formed by low cross-linker concentrations.

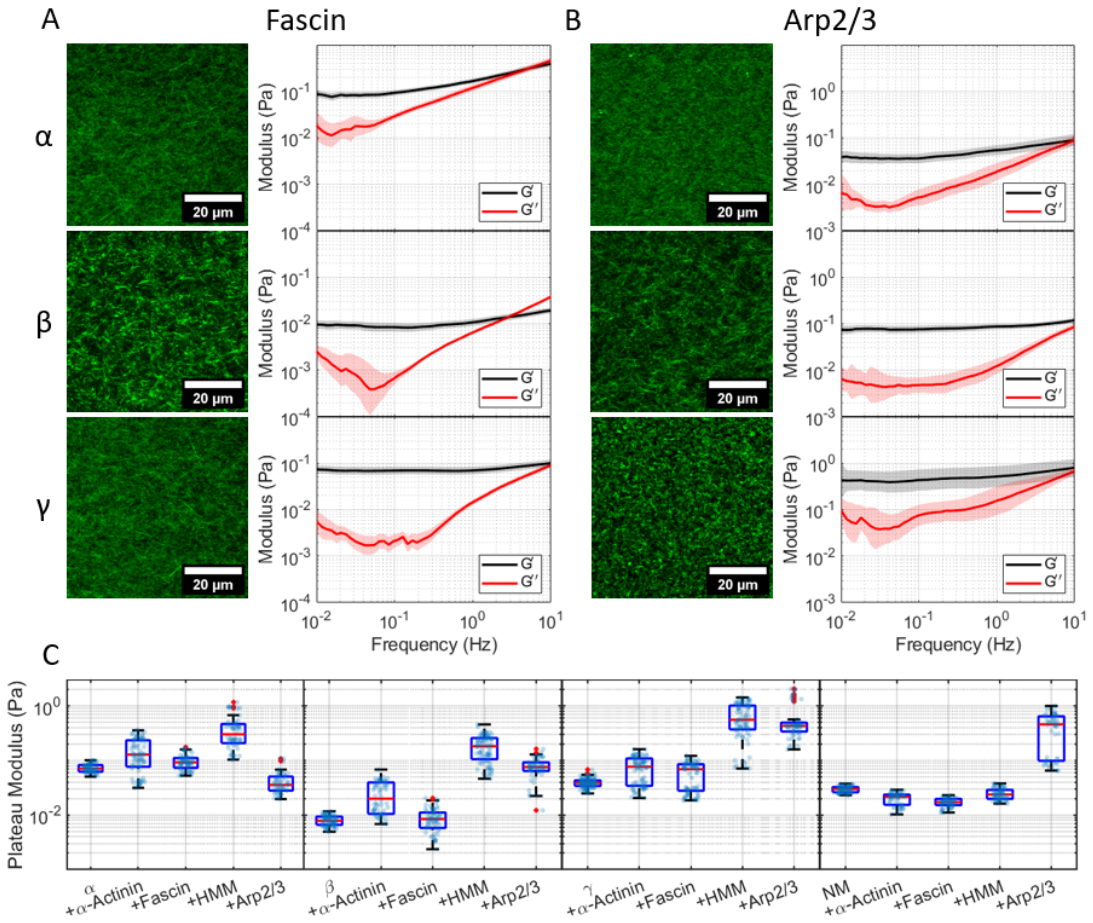

Figure 27: The architecture of ABP-supplemented networks does not display significant differences, however, hVPT measurements reveal microrheological differences of such actin networks depending on the probed isoform (A,B for 120 nM fascin and 180 nM Arp2/3 + 930 nM nWASP). C) Further isoform-specific properties become noticable upon closer inspection of the respective plateau moduli G_0 of each reconstituted network.

3.5 Isoform-Specific Protein Interaction Promotes Individual Network Mechanics

After observing how the choice of actin isoform in combination with an ABP affects the resulting network structure, the next step is to examine how this impacts their mechanical properties. Therefore, entangled actin networks are created in the presence of a number of ABPs: α-actinin (120 nM), fascin (120 nM), heavy meromyosin (HMM) (120 nM) and Arp2/3 (180 nM, with 930 nM nWASP). These ABPs are assessed for each actin isoform at an actin concentration of 12 µM.

To compare the network mechanics of each of those combinations, holographic video particle tracking measurements are conducted. From these measurements, the plateau modulus G_0 is extracted to compare individual network mechanics.

3.5.1 Fascin

As mentioned before, the aligned actin filaments of filopodia are bundled via the crosslinker fascin [183]. The imaged actin networks of each isoform together with fascin don't display any noteworthy differences at a ratio of 100:1. Therefore, no differences in network stiffness are expected for the different isoforms in the presence of fascin. Indeed, the network stiffness of each isoform is only marginally increased by the incorporation of fascin compared to merely entangled networks (compare Figure 27). It should be noted that bundling processes result in different actin filament densities in the sample (network inhomogeneities), which in some cases leads to a reduction in plateau moduli (Figure 27).

3.5.2 α-Actinin

Two of contractile stress fibers' main components are α-actinin and myosin II, in which the former is promoting antiparallel bundling of filaments into straight, higher order structures and the other intercalating into the resulting gaps and contracting them through motor activity [185].
However, bundling of actin with α-actinin at a ratio of 100:1 only alters the network properties slightly (Figure 27). Upon addition of the cross-linker, the plateau modulus increases by a factor of two to three. In summary, no significant isoform specific differences are found.

3.5.3 Heavy Meromyosin II

Heavy meromyosin II (HMM), a non-contractile, dimerizing and artificial variant of myosin II is chosen due to an unchanged architecture of the active sites compared to full length myosin II. It also promotes the formation of a very homogeneous network structure [121]. This enables the quantification of mechanical properties at high motor protein concentrations, in contrast to the native form. The choice of the skeletal muscle isoform is for accessibility and the focus on divergence between the cytoplasmic actins. The non-cytoskeletal origin of this crosslinker has to be pointed out here though. α-actin and nm-actin show only a small increase in the plateau modulus compared to pure actin

networks in the absence of crosslinkers (α-actin around $5\times$ and no change for nm-actin). Conversely, networks formed from β- and γ-actin filaments show a huge increase in stiffness (around $25\times$ and $15\times$, respectively) in the presence of HMM compared to plain networks or networks bundled by the presence of fascin or α-actinin, respectively. Unlike the previous crosslinkers, HMM forms dynamic crosslinks, depending on the availability of ATP. If ATP is available, HMM will undergo the same stroking motion as its uncleaved version muscle myosin II and the HMM complex will move along a filament. Upon depletion of ATP, HMM will remain bound to actin. As such, the HMM complex will most probably remain at an intersection of two filaments, which is responsible for the mesh-like appearance of the network. The dimers are distributed randomly, while not being able to contract or bundle the network.

3.5.4 Arp2/3

Arp2/3 is an important nucleator for daughter filament branching and thus required for lamellipodia formation.
Lamellipodia are mainly found in motile cells and form a thin sheet ($\approx 200\,\mathrm{nm}$ [186]) that is subject to strong undulations without breaking, indicating their mechanical stability. Therefore, at least for the cytoplasmic actin isoforms, a rather strong increase in stiffness is to be expected, which is indeed confirmed by our hVPT measurements as well as by the clustered network architectures (Figure 27). In contrast, the networks formed by α-actin in the presence of Arp2/3 shows no significant stiffness changes compared to a regular entangled network (Figure 27).
Actin networks consisting of β- and γ-actin, branched by Arp2/3 show approximately a 10-fold increase in stiffness compared to purely entangled actin networks. At the same time, nm-actin shows a 20-fold increase in the presence of Arp2/3.

3.6 Myosin-II-Mediated Aster Formation

It has been shown that the interaction of myosin with actin depends on the particular isoform [187, 188]. It is usually characterized by ATPase activity or duty cycle, i.e., the fraction of the ATPase cycle in which the motor protein remains tightly bound to an actin filament. This strongly influences contraction and thereby generation of tension. For example, muscle tissue has been shown to have a short duty cycle for rapid muscle contraction, whereas cytoplasmic actomyosin is known to build tension more slowly [187]. With this in mind, the

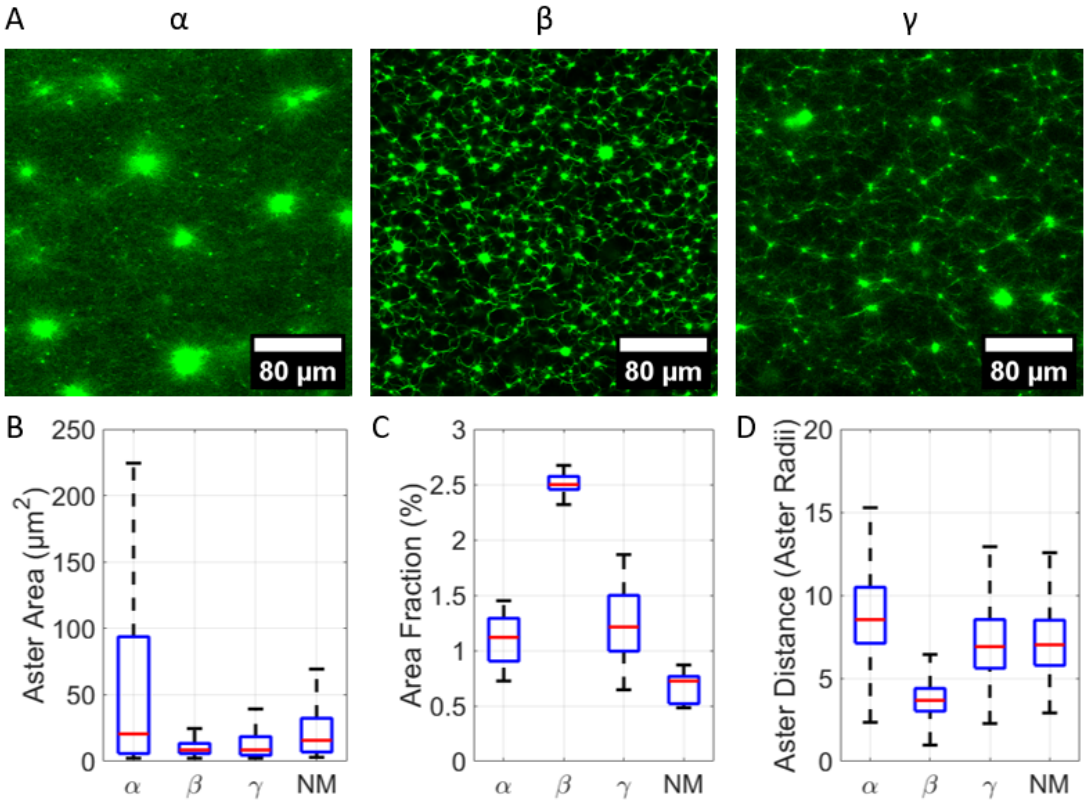

Figure 28: Analysis of contraction based structure formation for different actin isoforms. A) Actomyosin networks constituted from the different isoforms display significant variety in their appearance. B) Clusters of actomyosin, also called asters, are visible in all samples, however, their size distribution and C) area occupation largely depend on the isoform. D) Asters deplete their surrounding of actomyosin, however, this depletion depends on the range of myosin mediated pulling as well as on the size of the aster.

distinct actomyosin activities will probably translate into actin isoform specific contraction dynamics and thus into different emerging actomyosin structures [188].

As shown in Figure 28, the addition of myosin to purely entangled actin networks results in the appearance of contraction foci, referred to as asters. These aster formations are distinguished here between the isoforms by aster size and aster connectivity, which show significant variations depending on the particular isoform. Both α- and nm-actin are characterized by a sparse amount of asters. However, the aster size in the case of α-actin is generally much larger than for the cytoplasmic actins (Figure 28). In contrast, especially β-actin displays the smallest contraction foci, shortest distance and highest density (or area fraction, Figure 28 B/C/D).

Softer Actin networks composed of β-actin filaments display smaller contraction foci, but also a higher density of them. These are spatially closer together, which can be explained in terms of the contractility-connectivity phase dia-

gram. There, a higher connectivity of the network leads to a higher propensity for global collapse at preserved motor activity [189]. If motor forces exceed the unbinding threshold of the cross-links or entanglement points, these constraints eventually fail across the entire network. Well-connected actomyosin gels respond to motor activity by undergoing a global contraction, where large asters emerge with very high actin density. However, depending on the connectivity, contraction events do not necessarily span system length scales. Assuming identical motor activity, so-called local collapse is expected for less connected networks found, for instance in networks consisting of β-actin. The condition of preserved motor activity holds, since identical myosin motors and ATP concentrations are used.
Contraction foci are also frequently observed *in vivo* such as those found in the cortex of developing *C. elegans* embryos and the cell equator of mitotic cells. It was postulated that contraction of the actomyosin cortex affects the spatial distribution of lipid-tethered proteins and thereby influences signalling [189].

3.7 Properties of Single Actin Filaments

To explain the different, isoform-specific properties of purely entangled networks, a few possible reasons for this behavior need to be considered. First, it is conceivable that different polymerization and nucleation dynamics may cause unique filament length distributions. Second, due to the variations of the amino acid sequence, the persistence length of actin filaments reflecting their bending stiffness may become isoform-dependent. Lastly, due to variations of the amino acid sequence and subsequent post-translational modifications, a unique surface charge distribution may lead to peculiar inter-filament interactions and friction as well as modified binding affinities to ABPs. While the latter has been demonstrated above, it has not yet been possible to rule out the possibility of the first two arguments being responsible for our observations.

3.7.1 Filament Length Distribution

The distribution of filament lengths in a network has a non-negligible influence on the plateau modulus $G_0 = \frac{6 \cdot k_B T \cdot l_p^2}{\zeta^2 \cdot l_e^3}$ [90].
This and the potential to win insight into the polymerization dynamics, which control filament length, is considered. A length distribution for surface-adhered

Isoform	l_P(µm)
α	15.4 ± 0.4
β	16.4 ± 0.5
γ	16.8 ± 0.4
NM	15.5 ± 0.4

(a)

Isoform	m(µm)	v(µm)
α	3.8	7.6
β	5.4	56.8
γ	4.4	40.0
NM	1.3	1.4

(b)

Isoform	G_0(mPa)
α	71
NM	31
Rhod-α	3800
Rhod-NM	3900

(c)

Table 8: a) Persistence length l_P measured and calculated using a two-dimensional angular cosine correlation for the different isoforms. b) Mean m and variance v calculated from the lognormal distribution fitted to the filament length histograms for each isoform. c) Plateau moduli G_0 measured for commercially available α- and nm-actin, as well as rhodamine-labeled versions of α- and nm-actin at a concentration of 12 µM.

filaments is presented here. . A lognormal distribution with the density

$$f(x) = \frac{1}{x\sigma\sqrt{2\pi}} \exp\left(-\frac{(\log(x) - \mu)^2}{2\sigma^2}\right), \quad x > 0,$$

and the fitting parameters μ and σ are used to fit the corresponding histograms. The mean m and variance v can be calculated according to

$$m = \exp\left(\mu + \frac{\sigma^2}{2}\right)$$

and

$$v = \exp\left(2\mu + \sigma^2\right)\left(\exp\left(\sigma^2\right) - 1\right).$$

All tested isoforms display a rather short mean filament length of around $4\,\mu m$. It is very similar to comparable findings from Burlacu *et al.* [190].
This small value is due to the inclusion of very small filaments into the calculation. Considering this and the exponentially increasing relevance of filaments for the network properties with their contour length, a weighed average is reasonable.

The commercially available nm-actin features the shortest filaments on average, with a mean of $1.3\,\mu m$. However, the variance of the distributions is found to depend heavily on the specific isoform: While the pure isoforms β- and γ-actin display a rather large variance from presumably inhomogeneous nucleation processes, the commercially available actins and especially the nm-actin show rather small variations in length. This indicates different and isoform-specific nucleation dynamics.

3.7.2 Persistence Length

The persistence length of semi-flexible filaments directly reports on their mechanical properties and might be responsible for the observed isoform-specific network mechanics. Here, we employ imaging of single, fluorescently labeled filaments to determine their persistence length. To visualize the filaments and also estimate the known [75, 191] effect of labeling on their persistence length, different approaches are taken.

Persistence lengths of the various isoforms and mixtures are measured in thin ($2\,\mu m$) glass chambers. Labeled filaments are pipetted into those thin chamber to record quasi-2D-fluctuations, from which the persistence length can be determined. This is necessary to suppress thermal undulations in three dimensions, which would artificially decrease the measured contour length of the filaments. Also and more importantly, twisting and twist-bend-coupling is suppressed this way. Those would also artificially decrease the measured persistence length [91].

The persistence length is calculated via a two-dimensional angular cosine correlation. Preparation and analysis are described in chapter 1.2.8 and 7.4, the calculation in theory chapter 1.2.8. All four phalloidin-labeled actins show very similar persistence lengths around $16\,\mu m$, which is in good agreement with previous results for α- and nm-actin (table 8). This rules out the possibility of a significant difference between the persistence lengths of γ- and β-actin, which could explain the difference in network stiffness. However, using fluorescent probes in the context of actin frequently raises the question, whether it impacts the physical properties of the filaments. It is well-known that phalloidin is stabilizing F-actin by binding between three different monomers [192]. It is also possibly changing the actin D-loop conformation, which is thought to have a major effect on filament persistence length [193]. Therefore, rhodamine-labeled α- and nm-actin as well as γ- and β-actin are examined regarding their persistence length. This is done on a polylysine-coated surface. In some measurements, the filaments are prelabeled prior to adhesion. As comparison, non-labeled actin filaments are also pipetted onto the polylysine-coated surface. They are labeled afterwards to avoid an influence on the filament conformation and to study the influence of the label on the persistence length.

3.7.3 Inter-Filament-Interactions

The mechanical properties of individual filaments are ruled out as a possible reason for the observed significant differences in network stiffness between

different actin isoforms. Sequence-dependent filament-filament interactions have to be considered at this point. The greatest amino acid sequence divergence between γ- and β-actin is found at the N-terminus of the protein. This is located at a protrusion on the outer filament (Figure 25). It also increases the charge density at this position, which might be relevant to network formation and friction between filaments. The associated electrostatic interactions could take the role of weak, transient crosslinks and therefore increase network stiffness, similar to a dedicated crosslinker protein like fascin. This is also discussed in chapter 2.3. Something similar was reported for non-crosslinked microtubule networks [194]. This effect being mainly responsible for the higher network stiffness of γ-actin compared to β-actin, is therefore conceivable. To demonstrate how even subtle changes in charge density can alter network mechanics, rhodamine-labeled, reconstituted m- and nm-actin filaments are polymerized. These have positively charged protrusions in the biologically relevant pH regime [195, 196] associated with random lysine residues on the monomer surface to mimic electrostatic changes of the N-terminus. Their network stiffnesses are subsequently compared to unlabeled, entangled networks. A considerable increase in network stiffness represented by the plateau modulus G_0 upon introduction of rhodamine-labeled actin is found. This indicates that indeed, small changes in the amino acid sequence and thereby the filaments' surface charge structure alter the filament-filament interaction. This leads to substantial alterations in network stiffness (compare table 8.

Small-angle X-ray scattering (SAXS) measurements of bundled actin filaments reveal the formation of charge density waves (CDW) between the filaments [111, 119]. The filaments form a hexagonal tunnel with divalent cations in between within a CDW. These waves are shaped by the electrostatic potential of the filament backbones, their helical twist and their orientation to each other. Angelini *et al.* report the formation of knots in these waves. These are comprised of ions, which are restricted in their mobility compared to free ions in solution. They are localized to some degree in so-called "liquid ion patches" (LIPs). A higher density of these is found at actin subdomain 1, where the N-terminus is located [19]. As already mentioned, this is also the location of the highest variance in the AAS of different actin isoforms.

For entangled networks, the orientation of filaments to each other at entanglement points must statistically be closer to orthogonal than parallel. This is in contrast to bundles, but at entanglements, filaments have a short distance to each other and their undulations are dampened. This makes the formation of LIPs of divalent cations at entanglement points reasonable. An influence of the

specific AAS (for different isoforms of actin) at the N-terminus and thereby the charge density on these LIPs is very likely.
To explain different viscoelastic shear moduli for the investigated isoforms, there are multiple possible explanations.
Inter-filament complexation of cations via the N-termini. A few findings make this option likely. First, the significant difference in affinities of the amino acids Asp and Glu to Mg^{2+} and other divalent cations [197, 198].
Looking at the N-terminal AAS, a higher G_0 for one of the cytoplasmic isoforms of actin would make sense through a decrease in the deflection length (compare point three). But an even higher G_0 for α-actin with its alternating N-terminal occurrence of Asp and Glue is puzzling. This complexation would be something like a transient quasi crosslinking. This would not only mean an increase of G_0, but also imply a stretching of the plateau into the lower frequency regime and a significant shift of the reptation frequency. The on-off rate of the crosslinkers would dictate this shift, which is not observed. But since the divalent cations would most likely show very fast binding and unbinding compared to larger, protein based crosslinkers, this might not be noticeable. The extreme increase in G_0 for the rhodamine labeled actin does not support this hypothesis or at least favor another one. The exposed, positively charged rhodamine can't support complexation of cations, but should rather destabilize it and decrease the cation density in its vicinity.
Steric interactions by different surface structures. The isoforms have been shown to possess different 3D-structures due to the AAS modifications [199]. This could be understood as differences in friction between the filaments, and thereby different shear responses. Due to the relatively smooth surface of the filaments compared to the filament size (compare Figure 25), this seems unlikely. Also, fast thermal undulations of the filaments (µs-ms [96, 95, 97]) are not supporting this explanation.
Different deflection lengths l_d caused by electrostatic interaction of charged protrusions (like the N-terminus or a rhodamine label) with knots of CDWs at entanglement points of the network. Going by the tube model, l_d is the distance, a filament can reptate through a tube of surrounding filaments before it collides with the wall. The collision means a penalty in free energy in the range of $k_\mathrm{B}T$ [74, 72], which is the root cause of the shear resistance of the network here compared as G_0. A decrease of l_d would have an effect similar to an increase in the concentration [72, 89]. The tube walls would get thicker or rougher depending on the charge distribution. Different charge densities at the N-terminus interacting with LIPs (since these would be formed by the same

electrostatic interactions) could reasonably result in different interaction potentials of the filaments and different l_d. The strongly increased G_0 for rhodamine labeled actin also supports this hypothesis. Positively charged protrusions between LIPs would introduce an even rougher tube surface due to repulsion of positive charges and suppression of negative charge repulsion.

3.8 Summary

Actins belong to a structurally conserved family of proteins found in eukaryotic cells. They are mainly involved in the generation of contractile forces, cell motility, cell shape, and mechanical stability. Because all mammalian actin isoforms share a high degree of sequence similarity, the existence of isoforms has been largely ignored in *in vitro* studies. As a result, α-actin from skeletal muscle became the most commonly studied actin isoform [200] because of its abundant availability. However, even though muscle- and cytoplasmic actins display relatively small sequential differences, it is easy to imagine structural and mechanical peculiarities between them, due to their localization and functional distinction [12, 201]. One isoform constitutes large muscle tissues, while the others forms numerous types of filigree structures. Altogether, they fulfill roles ranging from structural integrity to cellular motion and signal transduction within a - compared to the filament dimension - small compartment [12, 15, 13]. Additionally, there are many ABPs [171], among them also muscle and non-muscle myosin II, which are specifically found to interact with only one of these isoforms [202]. Interchangeability of the cytoplasmic isoforms was experimentally shown to some degree in cell experiments [174, 17], but conversely also clear fatality of single knockouts [203]. A purely genetic and thus kinetic reason for different isoforms occupying overlapping spaces has also been proposed and shown to be conceivable [173, 174].
Here, subtle changes of the sequence at the N-terminus of α-, β-, and γ-actin, which is part of an exposed arm originating in the subdomain 1 of G-actin, are demonstrated to be indeed relevant for network mechanics. It is also shown that the interaction of the corresponding filaments with ABPs depends specifically on the isoform and gives rise to an altered network architecture (see Figure 27).
To explain these phenomena, the mechanical properties of actin filaments formed from different isoforms are quantified. This is done across different length scales and states of organization, from single filaments to interconnected and eventually contractile networks. Concretely, persistence length, fil-

ament length and isoform-specific filament-filament-interactions are compared to explain the variations in network mechanics (see table 8).
Single filament properties could be excluded because no significant differences between the persistence lengths of the different isoforms are found. To explain the differences in network stiffness, much larger differences in the persistence length are necessary (compare equation 17). In addition, a very similar filament length distributions for γ- and β-actin is found. However, because of the differences in the filament length of α- and nm-actin, the filament length is normalized to $1\,\mu m$ using gelsolin. After shortening the filaments, the stiffness of nm-actin is not affected, whereas the stiffness of the α-actin network approaches that of nm-actin, although a significant difference remains.

Taken together, isoform-specific filament-filament interactions appear to explain the substantial differences in network stiffness, connectivity and cross-linking with ABPs. Although the amino acid sequences differ only slightly between the isoforms, the greatest differences are found at the highly exposed N-terminus of the actin protein. β- and γ-actin have very similar N-terminal amino acids, e.g., β-actin has a sequence of Asp^1-Asp^2-Asp^3 and Val^{10}, while γ-actin Glu^1-Glu^2-Glu^3 and Ile^{10} [204, 205]. One could infer similar filament growth dynamics and thus similar filament length distribution from these minor differences at the periphery of filaments. Albeit the charge density at the N-terminus of γ-actin and β-actin is most likely very similar, its ability to form complexes with magnesium is expected to be altered already by slight changes in their non-protonated state and especially the flexibility of the ligand. It was found that the sidechains of Asp and Glu show different pKa values for the exposed carboxyl groups (Asp 1.88 and Glu 2.19 [206]), originating from a longer side chain donating more electron density into the residual carboxyl group of Glu, which essentially increases the charge density at the oxigen atoms and destabilizes the negative charge. A stronger interaction with small, highly charged ions like Mg^{2+} is expected. Also importantly, the longer chain of Glu compared to Asp allows for a higher degree of rotational freedom and fewer steric hindrances, allowing for more stable multidentate complexes with divalent cations. Therefore, the complexation of Mg^{2+} cations by Glu is expected to be favored over Asp.
Thus, when two actin filaments collide in an entangled network, their highly exposed N-termini deliberately form temporary complexes with Mg^{2+} ions ($Mg(Glu)_2$ for γ-actin and $Mg(Asp)_2$ for β-actin, respectively). Due to the limited flexibility of the sidechain of Asp and a less exposed N-terminus for β-actin [207, 181],

this complexation is probably less likely to be formed, therefore more short-lived or even fully suppressed. Also $Mg(Glu)_2$ complexes can be expected to be more stable because of stronger metal-ligand binding of electron-denser carboxy groups with the small, highly charged Mg^{2+}. Within the framework of a sticky tube model [208, 209], such complexation can be interpreted as weak quasi-crosslink. The presence of these crosslinks leads to an increased network stiffness as a new length scale - the distance between the adhesion points - is introduced. A particularly suitable model for actin solutions with this kind of interactions is the glassy wormlike chain (GWLC) model introduced by Glaser and Kroy [210]. The GWLC model is derived from the WLC by adding an exponential stretching of the relaxation spectrum reminiscent of generic trap models used to explain the rheology of soft glassy materials. The model includes weak attractive interactions and a so-called stretching parameter $\mathcal{E}$, which controls the slow-down of relaxation due to the presence of weakly crosslinked filaments. Permanently crosslinked filaments through ABP correspond to $\mathcal{E} \to \infty$. The attractive interaction between the filaments of a GWLC leads to a shift of G' and G'' at low and intermediate frequencies to higher values. In their model Glaser and Kroy pointed out that it is conceivable that direct interactions of cytoskeletal elements can approximately be represented by a pair potential, which features a rather narrow energy barrier slowing down the mode relaxation by an Arrhenius factor, which scales exponentially in the barrier height. These barriers would thus yield substantial contributions to $\mathcal{E}$ through their short-ranged 'patchy' character of the molecular interactions, but without consequences for the thermodynamics of the system. This does not lead to macroscopic phase separation. The conclusion is excellently supported by the measurements, and therefore the parameter $\mathcal{E}$ is interpreted as the "stickiness" between actin filaments modulated by the N-terminus.

The importance of filament-filament interactions is further demonstrated by rhodamine-labeled α- and nm-actin as a model system. The labeling exposes a positive surface charge by covalently binding rhodamine to a random lysine residue on the filament surface. An increase of at least $50\times$ in the average plateau modulus compared to non-labeled networks is found (table 8). This result suggests on the one hand a considerable contribution of ionic interactions to network stiffness, on the other hand a general caution in actin experiments with rhodamine or comparable labels, where network structure or mechanical properties are relevant. The strong influence of both could strongly bias the results.

The strong increase in G_0 does not support the hypothesis of Mg^{2+}-complexation

being the main cause of the differences between γ-actin and β-actin. Instead, it points towards a more complex explanation. The two different processes (short lived complexation and CDWs) are most likely both increasing network stiffness, depending on the Mg^{2+}-concentration. At lower concentrations, complexation is dominant and differences between γ-actin and β-actin are highlighted. At higher concentrations, the CDWs dominate until the filament structure collapses to bundles. The rhodamine-labeled filaments could be seen as equipped with non-mobile Mg^{2+} ions. Rather than collapsing the network, the small but localized effective positive charge concentration pins filaments at entanglement points.

In summary, this chapter presents evidence for isoform-specific mechanical properties of actin filaments. In light of the high degree of conservation in the actin AAS, this degree of fine-tuning is conceivable. Eukaryotic life requires substantial adaptability to meet the various extrinsic and intrinsic requirements for proper function, ranging from the response to environmental factors to the generation of motion, growth and development. Actin is among the key molecules to enable such variability and responses. The presence of isoforms with subtle sequence alterations is an important factor to provide the necessary variability. The minute differences between cytoplasmic actin isoforms regarding their translation dynamics and amino acid sequences seem to serve as the starting point for differential post-translational modifications, which in turn initiate the different emerging cytoskeletal substructures. Despite the complexity encountered in living cells, these results demonstrate the importance of subtle differences between isoforms and how the associated weak interactions translate into substantial changes on larger length scales in network architecture, stiffness and contractility.

4 Post-Translational Modifications of Actin Isoforms: Arginylation

4.1 Introduction

As discussed in the previous chapters, actin is not just one type of filament with a smooth and unreactive surface. Of the six mammalian isoforms, the cytosolic β- and γ-actin are shown to differ in their viscoelastic properties and function from α-skeletal muscle actin and from each other as well. This is despite a very high similarity in the amino acid sequences with only four changes (between γ- and β-actin), which are mainly located at the N-terminus. So the actin pool of one mammal can consist of multiple isoforms with unique AAS (compare theory chapter 1.2.2), which differ in their biological functions. A single cell can also have two isoforms of actin present in the cytoplasm at the same time. Additionally, one of these isoforms can be distinguished further into a variety of post-translationally modified variants with likewise unique AAS, which also can potentially fulfil specific functions. There are way more distinguishable types of actin than commonly known. They appear to play important roles in basic cellular processes, but are still poorly understood (compare theory chapter 1.2.3). As an example for its biological relevance, arginylated β-actin was reported to play an important role in the regulation of lamella formation, therefore cell motility and is mainly found in lamellipodia [56, 211].
So shining light on this topic, which is underrepresented in current literature, has a direct relevance for the understanding of biological cells in general, but it is also relevant for the theoretical understanding of bio-polymers. Tube model predictions are examined for DNA networks as well as DNA-actin composite networks in chapter 2. The viscoelastic properties of the two semi-flexible filaments are not described completely accurately by the tube model for semi-flexible filaments. At similar mesh sizes, shear moduli should be the same for filaments with similar bending moduli and filament lengths, when considering them to show hard-body interactions (or something similar like a harmonic potential) with each other. The predictions get worse for composite networks. This is taken as a clear sign of a more complex interaction between the filaments. Further investigation is done in chapter 3.2. Different isoforms of actin also seem to display different shear moduli at the same mesh size. They are treated as different semi-flexible polymers, which allows an expansion of the experiments from chapter 2 to polymers with a more similar and better understood structure. The goal is an understanding of the interaction involved

in creating deviations from the tube model predictions. The focus is on cytoplasmic β- and γ-actin. These differ in four amino acids at the N-terminus (β: 3× Asp and γ: 3× Glu and an N-terminal acetylation for both). A purely electrostatic interaction as well as steric interactions and complexation, causing a change in the deflection length are discussed. Steric interactions are discarded as possibility. The other ones appear to be supported quite well. The formation of charge density waves between filaments, which are influenced by the ionic properties of the N-terminus is likely as well as complexation. The interaction of charged, N-terminal amino acid residues with these CDWs is assumed to change the effective tube diameter, filaments are gliding through, and thereby the deflection length of the filaments. This means more collisions per unit of length and thereby a higher energy penalty for the filaments fluctuations, which ultimately leads to a higher shear modulus (compare chapter 3.7.3). Rhodamine-labeled actin filaments have also been measured with microrheological methods. A positive charge is exposed on the surface of those filaments with every attached label by the binding of rhodamine to random lysine residues. This increases shear moduli by a factor of 50 or more compared to a non-labeled variant. A more controlled, but similar experiment is presented in this chapter. The typically occurring acetylated β-actin is compared to an arginylated variant. It is an investigation of the effects of this post-translational modification on the mechanical properties of β-actin and possible implications for cellular mechanics on the one hand. On the other hand, it explores the mentioned deviations from tube model predictions further in a controlled way. In contrast to rhodamine-labeled actin, here the position of the modified charge is known. Also for rhodamine actin the exact number of rhodamine molecules per actin is not clearly known.
The differences in amino acid sequences relevant in this chapter:
β_{ac}-actin: Ac-Asp1-Asp2-Asp3 and Val10
β_{arg}-actin: Arg-Asp2-Asp3 and Val10

So arginylated β-actin is chosen to investigate the influence of electrostatic interactions on the viscoelastic shear properties of entangled semi-flexible filament networks. Again, single filament properties are analyzed first to determine their influence on the shear properties and make sure, that the semi-flexible regime is not transgressed by a modification. The viscoelastic shear properties are then compared to a tube model prediction and deviations are discussed in the context of a change in deflection length.

4.2 Single Filament Properties

Characterizing the mechanical properties of β_{arg}-actin networks requires an understanding of the single filament properties first. To compare network shear moduli to β_{ac}-actin and tube model predictions, it is necessary to confirm semi-flexibility of single filaments (compare chapter 2.2.2). So for that purpose, β_{arg}-actin filaments are polymerized, labeled and diluted to low concentrations for imaging. Persistence lengths are determined like described in the previous chapter 7.4 by confocal laser scanning microscopy of labeled filaments. This is done in solution in very thin sample chambers (2 µm) to only allow 2D-bending fluctuations of the filaments. This arginylated actin has the same origin as the acetylated one. It has been extracted from modified yeast (compare chapter 7.2).

4.2.1 Persistence Length

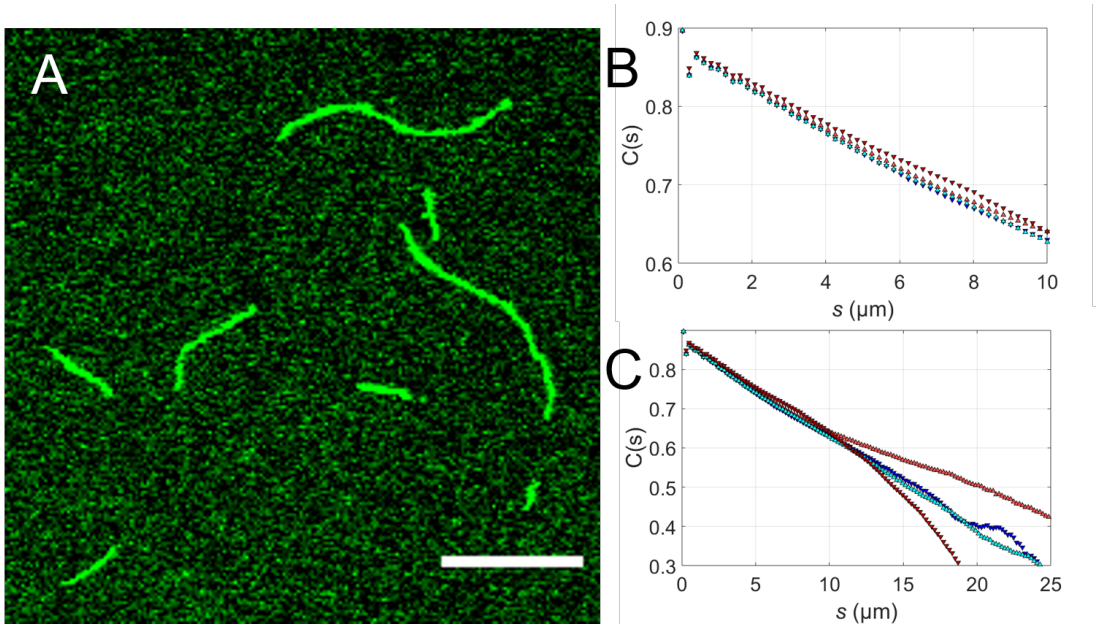

Figure 29: Single filament mechanics analysis of β_{arg}- and β_{ac}-actin. A) CLSM micrograph of labeled β_{arg}-actin filaments in a thin sample chamber to suppress undulations out of the focal plane. B) Angular cosine correlation against the segment length s for β_{arg}-actin at low (red) and high (orange) cation concentrations and β_{ac}-actin as well at low (green) and high (blue) cation concentrations. C) Zoom out for B) to larger s. Scale bar is 10 µm.

Persistence lengths are determined like described in chapter 7.4 and 1.2.8 with a very high number of filaments (5000+) for each condition to ensure good enough statistics for an angular cosine correlation analysis. Also, two different ionic conditions are tested to ensure no relevant influence of the Mg^{2+} concentration on the filaments' bending stiffness. A weakening of the repulsion

between negative charges on the monomers by divalent cations could possibly change the bending properties [212, 213]. Figure 29 (A) shows labeled β_{arg}-actin filaments in solution. They are not adhered to a surface and display 2D-bending fluctuations, which was ensured by taking time series of each location. From the filaments' bending it is already conceivable, that they are in fact semi-flexible. They are obviously not straight over their contour length, but also don't curl up like flexible ones. The 2D-angular cosine correlations displayed in (B) and (C) confirm this. The overlap is very high until a fragment length s of ~15 µm is reached. At that point, two of the four correlation graphs start deviating from the others. The corresponding persistence lengths resulting from a fit like explained in 1.2.8 are presented in table 9.

PTM	total cation concentration (mM)	Mg^{2+} concentration (mM)	l_p
Ac	100	0.2	13.9 ± 0.5
Ac	0.5	0.02	14.4± 0.5
Arg	100	0.2	15.9± 0.5
Arg	0.5	0.02	17.2± 0.6

Table 9: Persistence lengths for β_{ac}-actin and β_{arg}-actin filaments in solution and 2D-confinement. l_p is calculated from a 2D-angular cosine correlation. Different ionic conditions are investigated. Cation concentrations are generally kept low (compare chapter 7.2 and table 7.8) and the Mg^{2+}-ion concentration is varied.

No significant difference between the different ionic conditions is found. So it appears very likely that l_p is not significantly effected by the concentration of magnesium ions. This is true for the compared two orders of magnitude in Mg^{2+}-concentration, close to physiological ones [214, 215, 216]. A slight increase in the persistence length of β_{arg}-actin filaments is found compared to β_{ac}-actin (~15 %). This would also not effect the overall network stiffness noticeably (compare equation 17). It is significant, but considering the general accuracy of the method, not very reliable. The mainly important information gathered from this data, is the clear semi-flexibility of the filaments ($l_p \approx l_c$).

4.3 Network Properties of Arginylated β-Actin

To characterize networks of β_{arg}-actin filaments and compare their viscoelastic shear properties to tube model predictions, entangles networks of the filaments are polymerized. These networks are measured with microrheological methods (VPTMR) at different concentrations. Similar to the characterization of DNA-networks presented in chapter 2, concentration dependencies for plateau moduli and the relaxation behavior (the crossover points of G' and G'') are compared to tube model predictions and the non-arginylated β_{ac}-actin.

4.4 Polymerization of Arginylated β-Actin

To characterize network properties of the semi-flexible β_{arg}-actin filaments, the first step is to polymerize them into entangled networks. The main difference between this experiment and the single filament measurements is the much higher actin concentration (12 µM for the first experiments compared to nM). While the polymerization conditions for the other entangles networks are the same between the different isoforms and labeled filaments, β_{arg}-actin behaves rather peculiar. At Mg^{2+} concentrations of 2 mM (compare chapter 7.2) β_{arg}-actin forms small (1-2 µm) clustered structures, which evolve over a few hours into inhomogeneous networks of larger (5-10 µm), connected clusters. CLSM images of this process are shown in Figure (30) for labeled actin. The inter-filament interaction appears to be much stronger for the arginylated actin. This would explain the very early cluster-formation. Instead of forming long ($l_p \approx l_c$), entangled filaments, very short filaments seem to bundle chaotically and form clusters with randomly oriented filaments.

Actin monomers are polymerized by the addition of divalent cations (mainly Mg^{2+}). Increasing the concentration of these leads to bundling caused by counter-ion condensation [118, 111]. This is due to the high negative charge of actin monomers [98], which gets shielded by the cations. So the way to create entangled networks of β_{arg}-actin appears to be a decrease of the Mg^{2+} concentration. A new buffer (compare chapter 7.2) with orders of magnitude lower ion concentrations is used for this. Figure 30 shows labeled networks at different Mg^{2+} concentrations. At 12 µM actin and 2 mM Mg^{2+} the acetylated actin (D) forms an entangled, homogeneous filament network. The arginylated variant (A) in contrast is already completely bundled under the same ionic conditions and at 6 µM actin. Upon the addition of EDTA, which is a strong chelating agent for Mg^{2+}-ions, bundles disintegrate back into filaments (B). At significantly lower ion concentrations (compare chapter 7.2) 3 µM of arginylated actin are stable in an entangled network (C). This clearly demonstrates how on the one hand Mg^{2+}-ions (like shown before) have a significant influence on inter-filament interactions and on the other, charges at the actin's N-terminus too. The letter appears to have the more relevant contribution, though. With an increase in the ion concentration, repulsive interactions are suppressed by a shielding of negative charges. This effect ultimately leads to counter-ion condensation and bundling. This is true for all isoforms, but the strong change in charge density at the N-terminus for β_{arg}-actin seems to shift the onset for bundling by orders of magnitude in the ion concentration. The effective charge

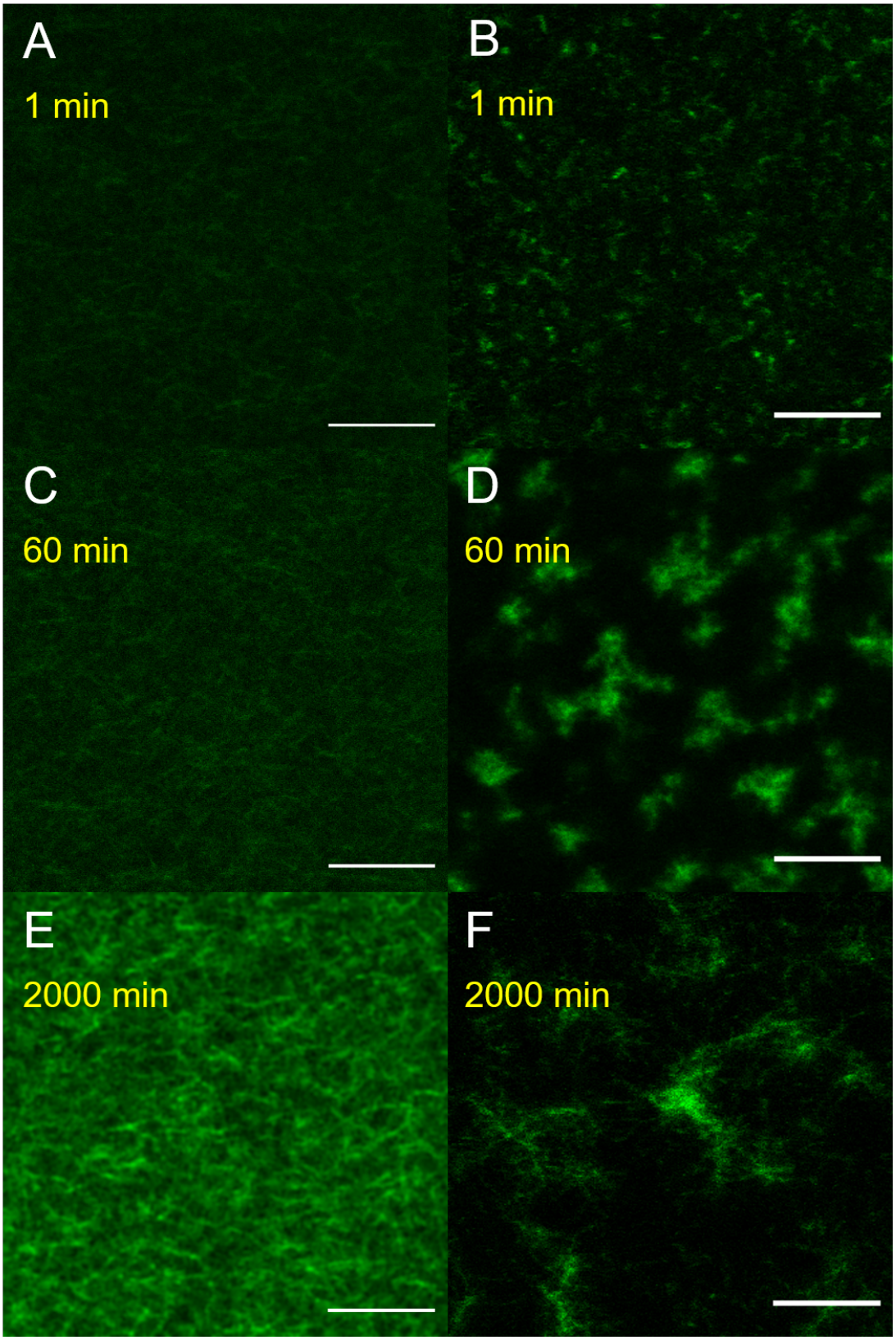

Figure 30: Cluster-formation of arginylated actin compared to the polymerization of acetylated β-actin. CLSM images of acetylated (A, C and E) and arginylated (B, D and F) actin networks at different times (1 min, 60 min and 2000 min in yellow) after initialization of the polymerization.

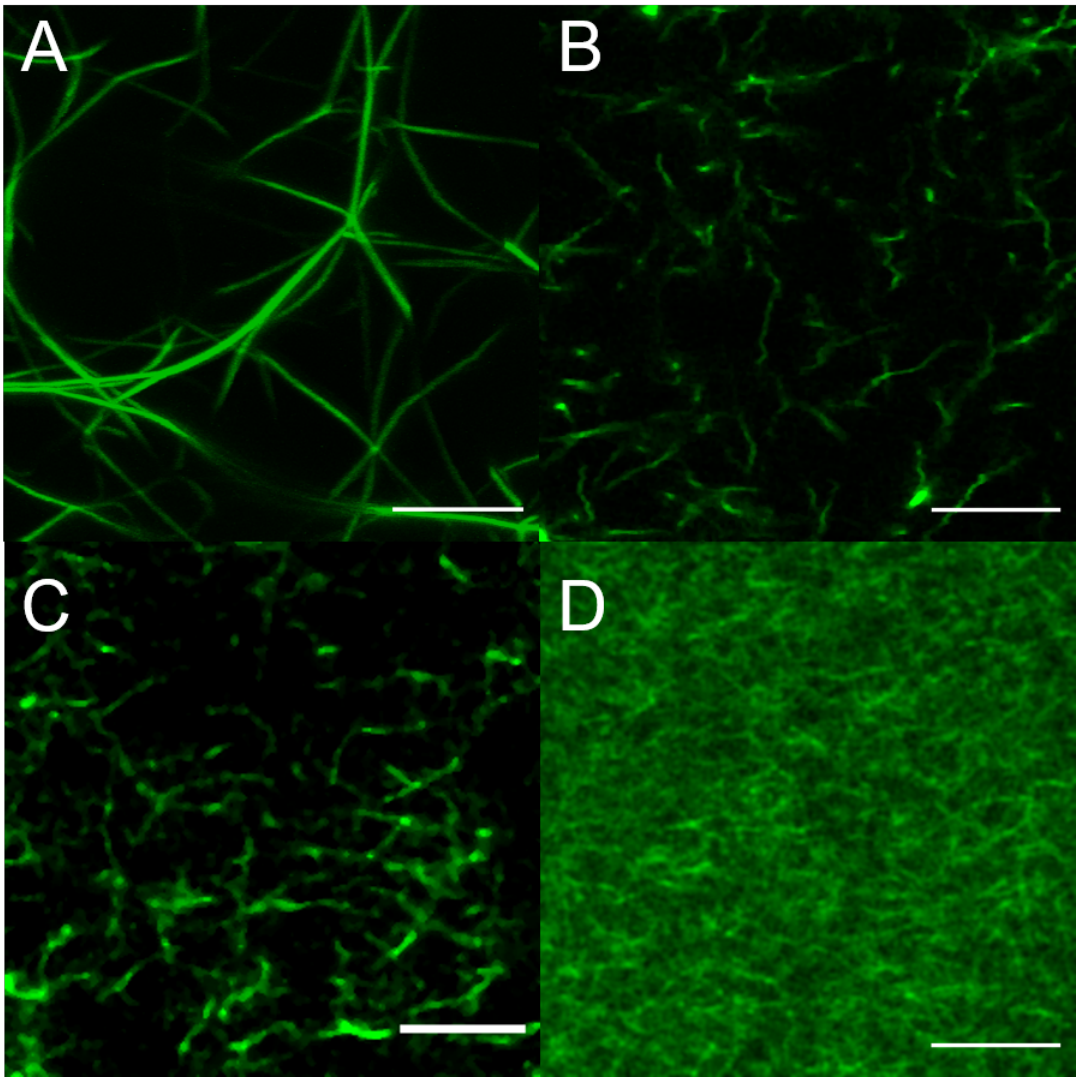

Figure 31: Formation of entangled networks of arginylated actin after the reduction of cation concentrations in the buffers. CLSM images of arginylated actin networks (A, B and C) polymerized at different actin concentrations and buffer conditions. A) shows arginylated actin at 6 µM and 2 mM Mg^{2+}, B) the same conditions after the addition of EDTA, which reduces the effective concentration of divalent ions by chelating them. C) shows a filament network of 3 µM arginylated actin at significantly lower cation concentrations. An entangled network of acetylated actin at 12 µM is shown in D) for comparison. Scale bars are 10 µm.

difference to acetylated actin is +3. A negative charges is removed (an acetyl group and one Asp) and two positive ones are added (an arginyl group with the N-terminal amine group). Bundling happens at much lower ion concentrations since there is less negative charge to shield. This is a valid conclusion, but it appears to not be enough to explain the extreme difference. The onset for bundling of α-skeletal muscle actin for example is at about 24 µM actin and Mg^{2+} concentrations of 25 mM or more [86]. For the β_{arg}-actin (6 µM) it is at <0.2µM Mg^{2+}. Considering the concentration too, there are three orders of magnitude in ion concentration between the two isoforms.

When trying to explain this phenomenon with pure electrostatic interactions, one could start with a comparison of the involved charges. Three charges per actin monomer would give a total molarity of 3 $\times 6$ µM = 16 µM. Compared to the 2 $\times$ 2 mM Mg^{2+} ions, this is 200 $\times$ lower and the N-terminal charges seem to be insignificant. A change in the deflection length caused by charge density waves forming between the filaments (compare chapter 3.7.3) could explain this phenomenon too. With an increase in the number of collisions between filaments and an increased energy penalty for thermal fluctuations, filaments could be bundled by a combination of counterion condensation and an effect similar to that of molecular crowding. With decreased bending fluctuations at higher concentrations of actin and more collisions, the probability of the filaments aligning and forming a bundle should increase. The additional positive charges help to overcome repulsive potentials.
In summary, structural properties of actin networks are clearly influenced by small differences in the amino acid sequence at the N-terminus. In this case (for β_{arg}-actin) the differences in charge density (compared to β_{ac}-actin) are stronger than for the cytosolic isoform (compare chapter 3.2) and so are the effects on the network structure. Under the same conditions (Figure 30 and 31) arginylated actin forms very different structures compared to the unmodified variants. Bundles and small bundle-clusters appear at orders of magnitude lower Mg^{2+} concentrations. This is further indication for the importance of N-terminal charge density for inter-filament interactions, which have a significant impact on structural and viscoelastic properties. The latter will be explored in the following subchapter. The expectation is a significantly higher plateau modulus for arginylated actin filament networks compared to acetylated ones, due to stronger inter-filament interactions.

4.4.1 Viscoelastic Shear Properties of Arginylation β-Actin Networks

In parallel to the DNA-network measurements presented in chapter 2.2, the viscoelastic shear properties of β_{arg}-actin networks are explored in this subchapter. They are compared to β_{ac}-actin networks.
Figure 32 (A) shows an exemplary measurement of the viscoelastic behavior for a 3 mM arginylated actin network. The shear moduli show a typical shape for entangled networks (compare theory chapter 1.2.9). The low frequency regime is dominated by viscous behavior. This transforms to an elastic plateau at frequencies between 0.5 and 50 Hz and then again in the high frequency regime to viscous behavior with a $\omega^{3/4}$ power law scaling. This is another indication for semi-flexible filaments and also reptation. The second crossover of

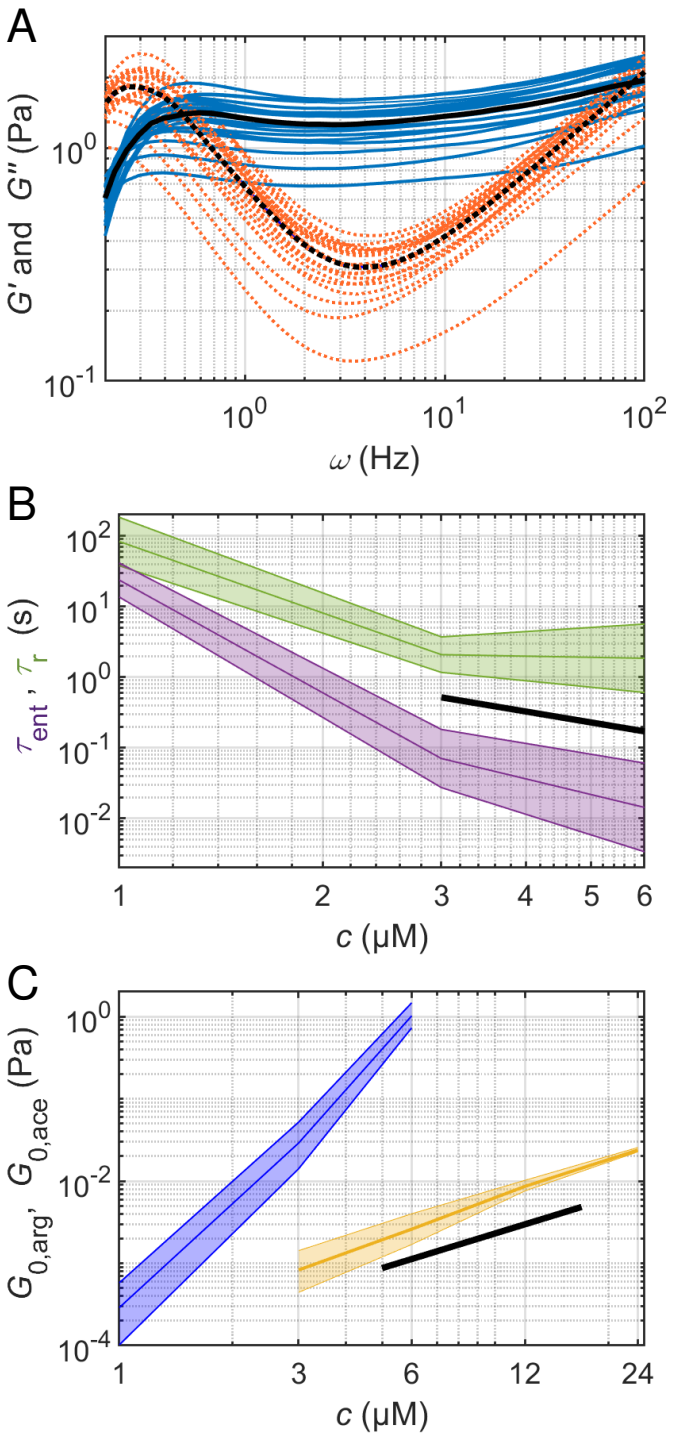

Figure 32: Viscoelastic shear properties of β_{arg}-actin in comparison to β_{ac}-actin. A) shows an exemplary measurement of the viscoelastic behavior for an entangled arginylated actin network (6 µM). The shear moduli show a typical shape for entangled networks. The black lines are a mean of the single measurements for G' (dark blue) and the dotted one of G'' (dark orange). B) entanglement times (purple) and reptation times (green) for different concentrations of arginylated actin. A black line indicates a slope of $c^{-8/5}$. C) Plateau moduli for different concentrations of arginylated (blue) and acetylated (orange) actin.

G' and $G'\prime$ at lower frequencies shows quick relaxation of the network, so no relevant bundling or crosslinking are observable.

The power law behavior for the reptation time t_r, as well as the entanglement time t_e shown in (B) confirm that. They are not very close to the tube model expectation of $t_e \propto c^{-8/5}$ and $t_r \propto c^{0-1}$. This is probably due to a very inaccurate measurement of 1 µM actin. The mesh size is only $2\times$ smaller than the microparticle size at that point, which can have an impact on shear moduli [129]. Lastly, (C) shows plateau moduli for different concentrations of β_{arg}- and β_{ac}-actin. The power-law behavior of the acetylated actin deviates with $\alpha = 1.5 \pm 0.3$ a little bit from the tube model expectation of 7/5, but is still reasonably close for very low actin concentrations. The arginylated actin has a much steeper increase with $\alpha = 4.52 \pm 0.33$. This is again, confirming the previous results generally. It is a good indication for stronger inter-filament interactions of the arginylated actin, since a value of $\alpha = 7/5$ is an indication for purely entangled semi-flexible filament structures. An increased inter-filament interactions could be interpreted as the formation of CDWs at entanglement points. The stronger concentration dependency and generally higher plateau moduli would support this. The clear filament reptation is a good indication for this(compare chapter 3.7.3). Although, an α value significantly higher than 11/5 [158], which is the expectation for crosslinked networks, is puzzling. This discrepancy can be explained with the extremely low concentration of the arginylated actin in the filamentous regime. At 1 and 3 µM, the networks have mesh sizes very close to the probe size, so the measured MSDs might be effected by cage hopping. An overestimation and thereby and underestimation of G_0 at lower concentration is likely. This of cause artificially increases α. An explanation could also be small scale bundling between the filaments and thereby an increase of the mesh size. Still this potential bundling and the much higher absolute G_0 compared to β_{ac}-actin prove higher inter-filament interactions.

So in summary, the viscoelastic shear properties confirm the results of the previous subchapter. The β_{arg}-actin has a stronger inter-filament interaction due to the modification and the change in charge density at the N-terminus coming with it. Compared to β_{ac}-actin the networks are significantly stiffer (at least one order of magnitude), but still behave like entangled networks. This confirms the assumptions of the previous chapters regarding a change in effective concentrations (compare chapter 3.7.3).

4.4.2 Nonlinear Viscoelastic Behavior of β_{arg}-Actin Networks

Non-linear viscoelastic behavior is discussed in chapter 2.4 for actin-DNA composite networks. Strain-stiffening is emerging from the interaction of the two

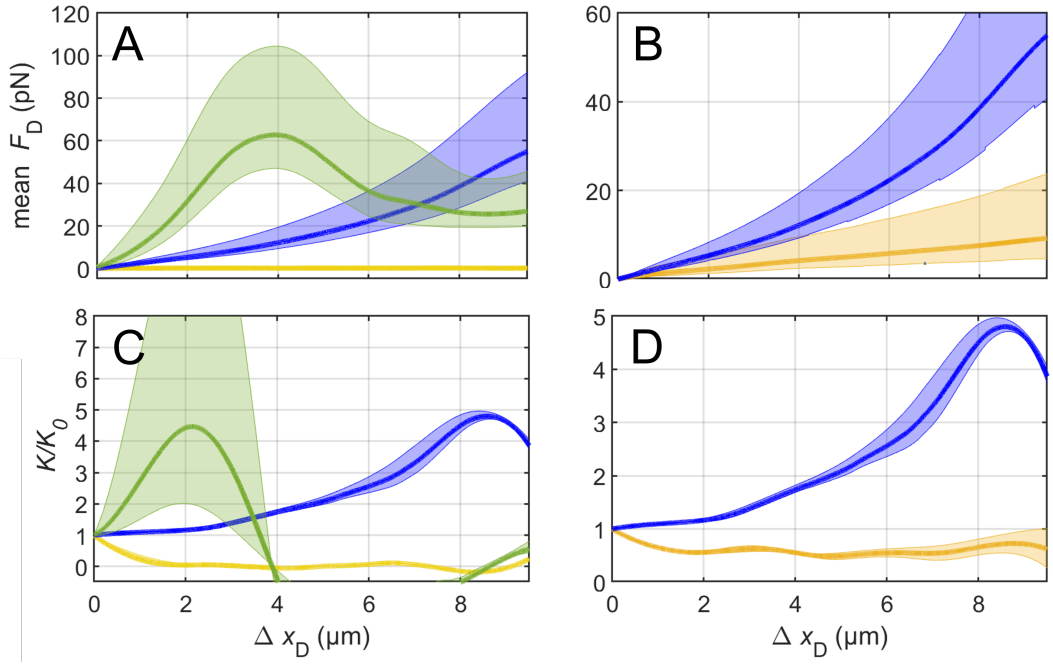

Figure 33: Drag experiments with microparticles pulled through acetylated and arginylated actin networks with optical tweezers. A) and B) show drag forces against displacements. In A) different concentrations of arginylated actin are shown (1 µM: yellow, 3 µM: blue and 6 µM: green). B) compares data for arginylated (blue) and acetylated (orange) actin at a concentration of 3 µM. The corresponding relative differential moduli K/K_0 are depicted in C) and D) in the same colors.

types of filaments. As described there, it is a very important property for the cellular response to external strains. It is only found at high actin concentrations and high strain rates for entangled networks of actin filaments (compare chapter 2.4).

Figure 33 shows the results for drag experiments with β_{arg}-actin as well as β_{ac}-actin. Microparticles significantly larger than the mesh size (d = 2 µm and $\xi = 776$ nm) are dragged with an optical tweezers setup through the actin sample ($c = 3$ µM). The force acting on the microparticle is calculated from the displacement of the microparticle compared to the displacement of the laser trap with the force constant of the laser. Drag forces F_D are shown in (A) against particle displacements Δx_D for different concentrations of arginylated beta actin (1 µM in yellow, 3 µM in blue and 6 µM in green). For very thin networks (1 µM), no force-increase is noticeable. The particles probably slip through the network meshes, which are on average not much smaller than the particle diameter ($\xi \approx$ 1350 nm, d $\approx$ 2000 nm). A continuous and increasing slope from 0 to 60 pN and up to a displacement of 10 µm is found for 3 µM. 6 µM show an even steeper slope with a peak at $\approx$ 60 pN. The comparison of arginylated and acetylated beta actin (B) reveals a lower continuous and con-

stant slope for the latter. Strain stiffening is visualized with the unitless relative differential modulus K/K_0, a modulus above 1 is considered strain stiffening, below strain softening. $\big(\mathrm{C}\big)$ and $\big(\mathrm{D}\big)$ confirm the first impression from the force curves.

For arginylated actin, strain-stiffening appears at 3 µM and is completely absent at 1 µM. For 6 µM the peak height does not increase further, it is just shifted to smaller trap displacements from 9 µm (3 µM) to 2 µm (6 µM). Only 3 and 6 µM show strain stiffening $\big(\mathrm{C}\big)$. The measured forces for 1 µM are very small due to the microparticle size. This, together with the peak shift between 3 and 6 µM supports the assumption of an entangled network, which can relax rather quickly. Filaments are pushed into each other by the microparticle, it comes to shear thickening and the network response becomes more elastic. The filaments (many of them significantly longer than the particle at a diameter of 2 µm), being entangled in the network, experience a counter force. It is stemming from an entropic effect (they are semi-flexible and bent in a thermal bath), enthalpic stretching and the same effects in the surrounding network. At a certain strain, this restoring force becomes larger than the drag force of the trap, the filaments glide through each other and the network relaxes. This critical force not increasing significantly with increasing actin concentration (from 3 to 6 µM), can be interpreted as indication for an entangled network. For the rupture of crosslinks or bundles, one would expect a similarly quick (similar displacement for different actin concentrations) increase in the force, due to the small mesh size (a few hundred nm) and the filaments not being able to glide trough each other or relax by straightening. So the peak for 3 µM would not be shifted compared to 6 µM, just lower due to less links having to be broken.

The found strain stiffening is again an indication for stronger inter-filament interactions of the arginylated compared to the acetylated actin. Acetylated beta actin does not show any strain stiffening in contrary to the arginylated variant. This is similar to the results for DNA networks.

4.5 Summary

Arginylation at the N-terminus of actin is one of its possible post-translational modifications. One central question, that arose for the different Isoforms (Which are very similar regarding their amino acid sequence) is, if changing an amino acid or modifying it has a significant influence on the properties of a protein with 374 or 375 amino acids. Arginylated β-actin has one amino acid less than

the most prevalent acetylated β-actin and a different modification. This results in a difference of about 0.5%. Is that enough to have a measurable impact on the viscoelastic properties?
Concluding from the results presented in this chapter, the influence of this small modification at the N-terminus of actin on structural and viscoelastic properties of filament networks and inter-filament interactions is actually very strong. The single filament properties are shown to be very similar to those of β_{ac}-actin. The filaments are semi-flexible with persistence lengths of around 16 µm. These l_p differ less than 15% from the ones for β_{ac}-actin and are barely dependent on the ion concentrations investigated here (less than 15% change over two orders of magnitude in the Mg^{2+} concentration). So arginylated and acetylated actin filaments are both semi-flexible and have very similar bending properties. This means, their network properties can be compared directly to each other and to predictions from the tube model for semi-flexible filaments.

At typical conditions for the polymerization of β_{ac}-actin (compare chapter 7.2), β_{arg}-actin does not likewise form homogeneous, entangled networks, but clusters of very small (<1µm), chaotically bundled filaments. These structures evolve over an hour to loosely connected, larger cluster structures. The viscoelastic shear properties of the arginylated actin network reflect this. G_0 is slowly increasing with a final plateau significantly lower than that of β_{ac}-actin. This happens under conditions, at which β_{ac}-actin forms entangled networks, comprised of visibly (in confocal images) long filaments (>3 µm). Lowering the overall cation concentrations and especially the Mg^{2+} concentration, removes this cluster-formation and entangled networks are created like for the acetylated actin. Interestingly, in between the ion concentrations leading to entangled and to clustered networks, bundle formation happens (Figure 31). Typically, F-actin structure formation follows a simple pattern in a phase-diagram with actin and divalent cation concentrations on the axes with 0 in the Origin. Coming from low concentrations diagonally through the diagram, F-actin filaments form solutions, loosely entangled networks, then entangled networks with mesh sizes ~<1 µm. Filaments start to form bundled structures at actin concentrations of ~48 µM (2 mg/ml) or a Mg^{2+} concentration of ~25 mM. At even higher concentrations, a nematic phase is formed [217]. This is heavily shifted for β_{arg}-actin by orders of magnitude to lower concentrations of actin as well as cations. A liquid crystalline phase is not observed. Clusters of short bundles emerge instead probably due to stronger, attractive inter-filament interactions and lower actin densities. The collapsed structures (bundles and

clusters) must have a very similar actin density to those formed by other types of actin, but they are formed at much lower actin concentrations, so clusters with a lot of empty space (buffer solution) around them are formed. The strong inter-filament interactions additionally start this process very quickly during the actin polymerization, leading to clusters of small filaments. This thesis clearly demonstrates the importance of actin isoforms and PTMs for the understanding of cellular properties and their modification. The viscoelastic response of living cells to external strain is still not fully understood. Studies investigating this topic are still very much underrepresented. It is possible and even probable that these variants of actin play an important role in the regulation of cellular viscoelastic shear properties.

At higher cation concentrations (compare chapter 7), the attraction between the filaments appears to be too strong for longer filaments to form. Filaments in proximity to each other collapse to clusters before that happens. This is already a clear sign for the strong effect of the charge density at the N-terminus of actin on inter-filament interactions.
Entangled networks of β_{arg}-actin were analyzed with microrheological methods. They show typical behavior for semi-flexible entangled filament networks with a plateau in G', two crossover points with G'' and typical high frequency power law behavior (compare chapter 1.2.9). The comparison with β_{ac}-actin networks reveals much stiffer networks for the arginylated actin. The plateau moduli are at least one order of magnitude higher for all measured concentrations.
The power law scaling behavior for the entanglement time and the reptation time against the actin concentration follows tube model predicts quite well. This again shows relaxation of the network, typical for an entangled network without permanent crosslinking or bundling present.
The power law scaling behavior of the plateau modulus against the actin concentration does not follow tube model predictions. With α= 4.52 , the slope is higher than the expected $G \propto c^{7/5}$. It is even higher than $G \propto c^{11/5}$, which would be expected for crosslinked networks [158]. This can be explained by lower accuracy for MR measurements at small actin concentration, which are partially (1 µM actin) necessary for β_{arg}-actin, due to it bundling at concentrations above 6 µM.
The viscoelastic shear properties of β_{arg}-actin networks resemble those of rhodamine labeled actin (chapter 3.7.3) to a high degree. G_0 is increased at least 50-fold compared to regular β_{ac}-actin networks at the same concentration.

As an explanation for the high plateau moduli, crosslinking or short-lived transient crosslinking can not be ruled out completely, but it seems unlikely. The relaxation behavior of the network (compare chapter 1.2.6 and 2.3) does not support this. The positive charge at the N-terminus makes the hypothesis, that divalent cations bind in a complex between two filaments also unlikely. The positive charge would decrease the stability of bridging $Mg(Asp_x)$-complexes and therefore decrease inter-filament attraction, leading to a lower G_0. A comparison to rhodamin-labled actin (compare chapter 3.8 reveals high similarity.
All together, these results support the hypothesis from chapter 3.7.3. Charge density waves of divalent cations form between filament entanglement points and decrease the effective diameter of the tube consisting of other filaments, it is reptating through. This causes the deflection length of the network to decrease and thereby the number of collisions between filaments to increase. This again means a higher energy penalty for fluctuating filaments. They interact with each other more because of attractive, electrostatic forces on the one hand and friction caused by repeating, charged protrusions gliding over a partially localized wave of divalent cations on the other. This results in increased shear moduli compared to β_{ac}-actin networks.
Another interesting finding is the non-linear behavior of β_{arg}-actin networks. They show strain stiffening at actin concentrations and particle displacement speeds, where the acetylated ones don't. This is again a clear indication for a stronger interaction between the filaments and a potential way for cells to regulate non-linear behavior with small modifications of actin.
An important effect of cellular resistance to external stresses is non-linear stiffening of their viscoelastic filament networks. The crosslinked actin cortex for example has the ability to stiffen under sudden strain and vimentin networks around the nucleus stiffen under compression (in contrast to entangled actin, which softens) to protect the DNA and keep the nucleus at its place [23]. These are features arising from the single protein level in the case of vimentin (high density of surface charges and low l_p compared to the mesh size). The cortex stiffens mainly through inter-filament connections, set up by crosslinkers or motor proteins. Entangled actin filaments only display strain stiffening in very high concentrations and under high strain rates. β_{arg}-actin is an exception here, in that it shows significant strain stiffening at very low concentrations (3 µM) and under smaller strain rates (2 cms^{-1}). Drag forces for β_{arg}-actin are generally 1-2 orders of magnitude higher than for the acetylated protein.

The stiffness of cellular protein filament networks can be increased or de-

creased by orders of magnitude without ABP-crosslinking, just with small modifications of actin itself. Controlling nonlinear viscoelastic behavior like strain stiffening is also possible. Structural properties and interactions with divalent cations show a similarly strong influence of this comparably small modification. It sheds light on the previous question regarding the mechanism by which different isoforms generate different network shear properties and favors the effect of electrostatic interactions.

To answer another question, asked at the beginning, there are different types of semi-flexible filament networks *in vivo* within the cytoplasmic isoforms of actin alone. PTMs add a variety of possible further semi-flexible filament networks with different shear properties. Research in this area is still underrepresented, considering the relevance of PTMs for many different cellular processes. They also seem to play a role in the seemingly well understood shear properties of actin networks.

5 Summary

This study is separated into three parts:
1. Viscoelastic shear properties of DNA networks and actin-DNA composite networks.
2. Viscoelastic shear properties of actin networks consisting of different actin isoforms.
3. Viscoelastic shear properties of actin networks consisting of different post-translationally modified actin types of one isoform.
The overall aim of it is twofold. On the one hand, **semi-flexible** filament networks are explored in general. The viscoelastic shear properties, the relaxation behavior and structure are compared between different semi-flexible polymer filament networks and theoretical model predictions. The **tube model** for semi-flexible filaments is a commonly applied tool to explain viscoelastic shear properties. It simplifies semi-flexible filaments with a uniform, smooth surface, which undergoes hard-body interactions and the viscoelastic properties of entangled networks are explained as result of filament collisions, which are the cause of energy penalties (compare chapter 1.2.6). It has been used successfully to describe and predict the viscoelastic shear properties of entangled **F-actin** networks [5, 6, 7]. But is it actually that simple? Are semi-flexible filaments of comparable sizes similar enough to use this assumption generally? The second chapter is focused on the comparison of actin filaments and also semi-flexible **DNA filaments** [8, 9]. They get compared to tube model prediction. If the assumption of the filaments interacting only via hard body collisions holds up, a mixture of different semi-flexible filaments should only change the concentration of filaments in the model and still be predictable. To investigate that, entangled composite networks of actin and DNA are co-polymerized.
The type of DNA used here is artificially synthesized and does not exist *in vivo*. But are there different types of semi-flexible polymer networks in cells and more specifically in mammalian cells? The cytoskeletal filaments are typically separated into flexible (intermediate filaments), stiff rod like (microtubules) and semi-flexible filaments (F-actin). There is only one cytosolic, semi-flexible type of filament in mammalians, F-actin. But is that actually correct? α-skeletal muscle actin is used for the overwhelming majority of *in vitro* experiments to represent cytoskeletal actin. This is mainly done because of the easier accessibility of muscle actin. It can simply be purchased in a pure form and is the cheapest variant. But there are two cytosolic **isoforms** of actin, which differ in their amino acid sequence from the muscular actin and also from each

other. So these two cytosolic isoforms (β- and γ-actin) of actin are investigated in the third chapter. There are different types of interacting actins (of semi-flexible filaments) present in the cytoplasm. So the main focus of the chapter is the question, if these different isoforms possess different viscoelastic shear properties. They have been shown to be locally separated despite close proximity and very high evolutionary conservation of the amino acid sequence [11, 12]. It has also been reported, that their interaction with other proteins (mainly actin binding proteins) is isoformspecific [171]. Since the main purposes of actin filaments are structural integrity of the cell and force generation [218], the assumption of different mechanical properties for the isoforms is not too far-fetched.
And finally the fourth chapter is investigating **post-translational modifications** of actin (**arginylated** and **acetylated** β-actin). There are not only two unique types of cytosolic actin filaments, but a huge number of modified variants of β- and γ-actin [219, 20, 38]. These modifications have been shown to be biologically very relevant for a multitude of cellular processes [39, 40, 41, 42, 43, 44, 45, 46, 47, 48]. But are they also relevant for the viscoelastic shear properties of actin filaments? The differences in amino acid sequences between the modified variants are mostly even smaller than between the isoforms. Do they in the context of cellular mechanics?

Results: In the second chapter, DNA-filaments are characterized as semi-flexible. This is achieved via a comparison of the average filament length (6.8 $\pm$ 4.3 µm) and their persistence length (6.46 $\pm$ 0.26 µm [8], estimation: 17-34 µm, chapter 2.2.4). They form homogeneous, entangled networks with viscoelastic shear properties, which can mostly be predicted by the tube model. The comparison with F-actin networks of the same mesh size (compare chapter 1.2.6) reveals significantly lower (2 $\times$ or more) plateau moduli for the DNA-networks. So there must be something else than just filament length and persistence length, determining the plateau modulus. Entangled homogeneous composite networks are formed. They are shown to not be bundled or crosslinked. This is necessary to use the correct type of model to predict viscoelastic properties from the shape of $G')$ and $G'')$ as well as the position of their crossover points. These and their concentration dependency can be used to detect filament reptation and crosslinking (compare chapter 2.2.4). The entangled networks show an increase in G_0 emerging from their co-entanglement. This is determined for different relative mesh sizes of actin and DNA networks. The strongest deviation from tube model predictions is

found at the same mesh size for both filament types (chapter 2.3). These composite networks also show non-linear strain-stiffening, which is not present in the separate networks (chapter 2.4). And the interaction of actin with actin binding proteins is changed by the interaction of the two networks too. Contraction by myosin II as well as bundling by crosslinkers and divalent cations is significantly reduced compared to the separate networks (chapter 2.5). These results clearly show a stronger interaction between heterogeneous than homogeneous filament types, which can not be explained with the tube model. Electrostatic inter-filament interactions, which are assumed to explain this peculiarity, are explored in the following two chapters. Another important discovery from the presented experiments is a difference in the viscoelastic shear behavior of muscular and non-muscular actin, which is explored in the third chapter.

Chapter three investigates differences in the viscoelastic shear properties of β- and γ-actin. These cytoplasmic isoforms are shown to be spatially separated. Similar to the proceedings with DNA networks, the actin isoforms are characterized by their single filament properties. Both are shown to be semi-flexible with very similar persistence lengths ($\sim$16 µm with phalloidin, compare table 8). The plateau modulus for entangled γ-actin networks was found to be at least $2\times$ higher than the one for β-actin at concentrations of 12 µM actin (chapter 3.4). Nm-actin networks (chapter 7.2) have a G_0 between that of β- and γ-actin, which is expected for a mixture of both. But since β- and γ-actin are harvested from genetically modified yeast and then modified to resemble human actin, this is a good indication for the artificially created actin to be very similar compared to naturally occurring cytoplasmic actin. α-skeletal muscle actin is found to be slightly stiffer than γ-actin ($1.5-2\times$). The interaction with ABPs (fascin, α-actinin, Arp2/3 and rigor HMM) is also shown to be different for some ABPs between the isoforms. Especially rigor HMM and Arp2/3 induce a very strong increase in G_0 for some isoforms (compare Figure 27). The network clustering effect of full length myosin II is isoform-specific (compare Figure 28). Isoform-specific interaction with myosin has been reported in the literature [187, 188]. The main difference between β- and γ-actin lies in a few amino acids at the proteins N-terminus. The final three amino acids are exposed on the surface of the filament (Figure 25). The amino acid residues show different electron densities, which is assumed to cause different electrostatic interactions with each other and divalent cations [206]. Additionally the N-terminus of γ-actin is more exposed than that of β-actin [207, 181].

β-actin: Ac-Asp1-Asp2-Asp3
γ-actin: Ac-Glu1-Glu2-Glu3
To examine the influence of electrostatic interaction on shear moduli, rhodamine labeled actin is chosen. Rhodamin is covalently bound to a random lysine residue on the filaments surface. It exposes a positive charge and should have an influence on G_0. This is confirmed (table 8) and the increase compared to non- or plalloidin-labeled actin is very strong (at least 50 $\times$).
The most probable reason for these deviations in the viscoelastic shear behavior from tube model predictions is, concluding from the presented findings is presented in chapter 3.7.3. Charge density waves of divalent cations (Mg^{2+}) form at entanglement points between filaments and decrease the effective diameter of the tube (from the perspective of a single filament: a tube-like void between other filaments, defined by the interaction with them). This decreases the deflection length of the network and thereby the number of collisions between filaments increases. This again means a higher energy penalty for thermal fluctuations of filaments. Their interaction increases because of attractive, electrostatic forces on the one hand and increased friction on the other. This friction is caused by repeating charged protrusions (N-termini with a high density of negative charges) gliding over a partially localized wave of divalent cations on the other. This results in increasing shear moduli. But this would not explain the differences between β- and γ-actin at lower Mg^{2+} concentrations (2 mM), because of the small electrostatic differences between the amino acids and the generally low ion concentrations. So complexation, which is stronger and longer lived for γ-actin (due to higher electron density in the carboxy group and stronger interaction with the very small, highly charged metal cation), in the form of quasi-crosslinking is most likely to also occur.

Chapter four explores the influence of post-translational modifications on the viscoelastic shear properties of actin. Acetylation of β-actin is compared to arginylation. The arginylation modifies β-actin (β_{ac}-actin), which is prevalent *in vivo*, to β_{arg}-actin. Single filament properties are characterized again and found to be very similar for both actins. Arginylated actin filaments are also semi-flexible with persistence lengths of around 16 µm (table 8) at different ion concentrations. Entangled networks of arginylated actin filaments are only formed at very low concentrations of Mg^{2+} (<0.2 mM Mg^{2+}) and also actin concentrations (<6 µM). Above that, bundles are formed and at even higher concentrations, clusters of small(<1 µm), bundled filaments. A nematic phase is not observed above that, due to the extremely quick formation of clusters,

which starts before filaments are fully formed and at very low actin concentrations.
This clearly shows a stronger attractive interaction between the filaments. The homogeneous networks at low cation concentrations are still entangled (no crosslinking or bundling) and show filament reptation. The charge difference at the N-terminus between acetylated and arginylated actin is +3.
β_{ac}-actin: Ac-Asp1-Asp2-Asp3
β_{arg}-actin: Arg-Asp2-Asp3
Looking at the strong increase in G_0 from rhodamine-labled actin, stemming from a positive charge at the outer filament, one would also expect a significant change in G_0 resulting from the arginylation. A positive charge at the N-terminus of β-actin should have a comparable effect on the network stiffness. That is confirmed by microrheological analysis. Compared to the acetylated networks, a strong increase of G_0 comparable to the one for rhodamine labeled entangled actin networks is found (at least one order of magnitude). Like actin-DNA composite networks, arginylated networks are shown to possess non-linear strain stiffening at very low concentrations and strain-rates. These results combined also confirm the hypothesis from chapter 3.7.3. The entangled filaments have the viscoelastic shear properties of a theoretical tube model network with additional quasi crosslinking from complexation of divalent cations or the formation of CDWs at entanglement points, which could be predicted by the GWLC model.
This study clearly demonstrates how an understanding of actin isoforms and PTMs is necessary for a representative model of cellular mechanical properties and more complex derivative properties like cell motility or structural integrity. The viscoelastic response of living cells to external strain for example is still not fully understood. Studies investigating this topic are very much underrepresented. It is possible and even probable, that these variants of actin play an important role in the regulation of viscoelastic shear properties.

6 Correction

In the name of good scientific practice: the data in chapter 2 was collected from two batches of DNA filaments and most experiments many samples with hundreds of particle trajectories (rheometer measurements typically only included 5 samples due to the large sample volume necessary). New batches of DNA filaments showed very similar network properties for pure DNA networks, but different results regarding the composite properties of 50:50 DNA-actin networks (compare Figure 19). The increase in G_0 compared to tube model expectations was not confirmed. It turned out to be a result of small inhomogeneities in the DNA network, which didn't effect the network stiffness significantly, but the interaction with actin filaments. This is interesting in its own right and doesn't effect the unexpectedly low plateau modulus of pure DNA networks (which contradicts tube model predictions) or observations from other chapters, but still has to be addressed.

7 Materials and Experimental Procedures

7.1 Cell culture and immunostaining

MDCK II cells (Madin-Darby canine kidney; Health Protection Agency Salisbury, UK) and SK-OV-3 cells (ovarian adenocarcinoma; ATCC) were cultivated in minimal essential medium (MEM with Earl's salts, containing Glutamax™ (Gibco™, Thermo Fisher Scientific) and $10\,\%$ fetal calf serum (FCS; BioWest, Nuaillé, France). Stem and samples were kept at $37\,^{\circ}\mathrm{C}$ and $5\,\%$ CO_2 (Heracell 150i; Thermo Fisher Scientific, Waltham, MA). Subcultivation was performed using standard culture flasks (TPP, Trasadingen, Switzerland) by addition of $0.25\,\%$ trypsin and $0.02\,\%$ EDTA (BioWest) and short incubation to remove the adherent cells from the culture surface. Suspended cells were mixed with FCS and centrifuged, and the pellet was dissolved in MEM and seeded into fresh flasks.

Cells destined to serve in experiments of confluent cells were taken in the last step. Cells were seeded into petri dishes (Ibidi, Martinsried, Germany) and kept at $37\,^{\circ}\mathrm{C}$ and $5\,\%$ CO_2 for 24 h, unless stated otherwise. MDCK II cells were seeded at 1.5×10^5 cells per dish for confluent cell layers or 1.5×10^4 cells per dish for cell clusters.
Primary antibodies (Anti-β-actin antibody, clone SP124; anti-γ-actin antibody, clone 2A3) were purchased (Sigma-Aldrich Chemie GmbH, Taufkirchen, Germany) and immunostaining was conducted in accordance to [12]: Prior to fixation, cells were rinsed with preheated ($37\,^{\circ}\mathrm{C}$) MEM supplemented with $20\,\mathrm{mM}$ HEPES. Cells were then incubated with preheated ($37\,^{\circ}\mathrm{C}$) MEM supplemented with $1\,\%$ PFA for $30\,\mathrm{min}$ at $37\,^{\circ}\mathrm{C}$ and $7.5\,\%$ CO_2. Afterwards, cells were treated for $5\,\mathrm{min}$ with cooled MeOH ($-20\,^{\circ}\mathrm{C}$) and were then washed $3\times$ with PBS ($20\,^{\circ}\mathrm{C}$). Fixed cells were then treated with $0.1\,\%$ Triton in PBS for $5\,\mathrm{min}$, washed $3\times$ with PBS and then incubated for $30\,\mathrm{min}$ with Blocking/Dilution Buffer (BDB) at $20\,^{\circ}\mathrm{C}$. Liquid was then aspirated from the cells and $200\,\mu\mathrm{L}$ BDB with primary antibodies for β-actin and γ-actin (dilution of $1:200$) was added on top of the cells and incubated at $20\,^{\circ}\mathrm{C}$ for $1\,\mathrm{h}$. Cells were then rinsed $3\times$ with PBS and subsequently incubated with $200\,\mu\mathrm{L}$ BDB with secondary antibodies (dilution of $1:400$) at $20\,^{\circ}\mathrm{C}$ for $1\,\mathrm{h}$.

7.2 Sample Preparation

All proteins (**rabbit skeletal muscle:** α-actinin, skeletal muscle α-actin, rhodamine labeled skeletal muscle α-actin, myosin II, heavy meromyosin; **porcine brain:** Arp2/3; **human platelet:** non-muscle actin (a mixture of 15% γ- and 85% β-actin, also referred to as NM-actin), rhodamine labeled α- and NM-actin) except for pure γ-, β_{ac}-actin and β_{arg}-actin (*vide infra*) were purchased from Cytoskeleton, Inc (Denver, CO). Organisms of origin are marked in bold letters.

7.2.1 Skeletal Muscle and Commercial Non-Muscle Actin

G-actin (rabbit skeletal muscle and human platelet non-muscle) samples were prepared from lyophilized actin monomers by dissolving the powder in deionized water up to a concentration of 10 mg/ml. Solutions were further diluted by the addition of G_2-buffer (2 mM Tris HCl, 0.2 mM adenosine triphosphate (ATP), 0.5 mM dithiothreitol (DTT), 0.1 mM $CaCl_2$, 0.001 mM NaN_3, pH 7.8). Carboxylated probe particles (2 µm, L4530, Sigma) were coated with bovine serum albumin (BSA) by incubation with a BSA solution (1 mg/ml BSA in G-buffer (2 mM Tris HCl, 0.1 mM $CaCl_2$, 0.001 mM NaN_3, pH 7.8), Thermo Fisher Scientific) and subsequent washing with G-buffer (3x). The polymerization of G-actin to F-actin was achieved by adding 1/10 of the final volume in polymerization solution (F_E) (20 mM $MgCl_2$, 1000 mM KCl, 50 mM EGTA, 0.001 mM NaN_3, pH 7.4).

7.2.2 Cytoplasmic β-,γ-actin and arginylated β-actin

Cytoplasmic γ- and β-actin was obtained from yeast as described previously [205]. They modified a strain of yeast to express actin isoforms with specific post-translational modifications to approach a synthetic recreation of organism specific proteins.
In the case of γ- and β-actin, further dilution and polymerization was done like for the commercially available actins. Arginylated actin was diluted with G_L-buffer (50 mM KCl, 2 mM Tris HCl, 0.2 mM ATP, 1 mM DTT, 0.001 mM NaN_3, pH 8) and deionized water to ensure very low cation concentrations. Polymerization was initialized with the addition of 0.1 or 1% of the final volume F_E.
The degree of polymerization was verified by ultracentrifugation of polymerized networks and measurement of the residual concentration in the supernatant

with a NanoDrop^{TM} 2000c spektralphotometer.

7.2.3 General Sample Preparation

Lyophilized and diluted (to 10 mg/ml) actin was stored at -80°C. It was further diluted (from 10 mg/ml) in G_2-buffer on ice for measurements. For depolymerisation the G-actin solution was kept on ice for an hour and then centrifuged to remove actin oligomers in the supernatant. The Polymerization was initiated in a glass chamber with a volume of approximately 10 µl by adding 1/10 of the sample volume in F_E-solution. Crosslinkers, motor proteins and probe particles (dv= 2 µm, BSA-coated, fluorecent green, polystyrene microparticles, L4530) were purchased (Sigma-Aldrich Chemie GmbH, Taufkirchen, Germany) and also added quickly in this step to avoid the buildup of inhomogeneities in the polymerized network.

7.2.4 Sample Chambers

Sample chambers were prepared from cleaned glass microscopy slides (#1, 60$\times$24 mm, Carl Roth, Karlsruhe, Germany). Double-sided tape was cut to form a chamber and glued on the slides. The filled chamber was sealed with cleaned glass coverslips (#1, 22$\times$22 mm, Carl Roth, Karlsruhe, Germany).

7.3 Microrheology

7.3.1 OT Measurements

For active and passive microrheological measurements with optical tweezers (Nanotracker 2, Bruker JPK) glass chambers with samples were placed in the optical tweezers setup. The laser was focused in the center of probe particles with a laser intensity tuned to the elastic properties of the network. For example, probing nonlinear behavior of highly crosslinked networks requires high force constants and therefore higher laser intensities than a passive measurement where dampening effects of the laser have to be minimized in order to record particle motion. For active rheology, the laser-focus was oscillated with an acousto-optic device (AOD) and the dampened motion of the trapped particle was recorded with a quadrant photodiode (QPD) in dependence of frequency and driving amplitude. Passive measurements were performed by turning the laser intensity to a minimum and recording particle positions with the QPD. Calibration of the trap's force constant was done with the same kind of microspheres in pure G-buffer.

7.3.2 Passive Measurements - hVPT

Passive microrheology data was collected via holographic video particle tracking (hVPT) using monochromatic light from a light-emitting diode ($\lambda = 660\,\mathrm{nm}$) in a bright-field setup with a 60x objective (CFI Achromat FF, numerical aperture [NA] = 0.80, working distance = 0.3 mm; Nikon) at a frame rate of $138\,\mathrm{s}^{-1}$. Two-dimensional microparticle trajectories were recorded with a commercial tracking software (AFS, Lumicks B.V., Amsterdam, the Netherlands) in real time.

7.3.3 Plateau Modulus

Mechanical properties of the samples were compared in the form of storage moduli G' at a specific frequency $\omega = 0.1\,\mathrm{s}^{-1}$. This value was chosen due to the proximity of most observed plateau moduli. For some very fluid like samples, these are hard to determine and the small slope of G' in this frequency regime allows a fixed frequency for comparison.
Storage moduli were calculated from mean squared displacements and those from trajectories. The MSDs were converted to shear moduli as described previously in chapter 1.3.2.
Particle tracks were collected via hVPT and data was captures at 138 fps in the technical data management streaming format (*.tdms). These were converted to MATLAB R2020b [220] files (*.mat) with a custom made code, accessing function originally published by Jim Hokanson [221]. MSDs were then calculated from the trajectories and Laplace transformed by accessing function originally published by the Kilfoil laboratory [222]. The result was plugged in the generalized Stokes-Einstein equation to obtain the complex shear modulus G^*.

7.3.4 Drag Experiments with Optical Tweezers

Drag experiments for the comparison of non-linear network mechanics were performed with optical tweezers very similarly to active microrheology. The only difference is wider displacement of the trapped microparticle (20 µm instead of a few hundred nm) and a linear displacement with high force constants (high laser intensity).

7.4 Measurement of Persistence Lengths and Length Distributions

F-actin was prepared with at a concentration of 1 mg/ml and polymerized like described before and then further diluted by a factor of 1000 in G-buffer to enable the observation of non-overlapping, single filament fluctuations.
Two different approaches were taken for the visualization of these. The first is direct observation of pre-labled filaments in solution in thin chambers, which suppress z-undulations. They consist of a microscope glass slide (#1, 60×24 mm^2, Carl Roth), washed spacer particles (2 µm, L4530, Sigma) scattered around the sample and a cover slide (#1, 24×24 mm^2, Carl Roth). The slides are plasma-cleaned, passivated by coating with PLL-g-PEG-coated (2 kDa, SuSoS AG) and sealed with two-component silicone (eco-sil, Picodent GmBH) to reduce drift and avoid evaporation. The sample volume is 0.3 µl. Labeling is done via an excess of Alexa Fluor^{TM} 488 phalloidin (Cytoskeleton, Inc, Denver, CO) for all isoforms and a covalent rhodamine labeling for α-actin and nm-actin.
For the second approach, filaments adhere to a surface, which fixates their position and enables the comparison of the bending stiffness of pre-labeled and unlabeled filaments.
Microscope glass slides (#1, 60×24 mm^2, Carl Roth) were plasma-cleaned and coated with poly-d-lysine (PDL, Sigma-Aldrich). A diluted F-actin filament sample (1 µl) was carefully added to the slide and spread. The sample was either pre-labeled (saturated with Alexa Fluor^{TM} 488 phalloidin) or unlabeled, in which case phalloidin was added after adhesion of the filaments. Finally, the droplet was covered with a saturated sucrose solution to avoid quick evaporation.
Data for filament length distributions was collected equivalently
Images of filaments were taken with a confocal laser scanning unit (FluoView FV10, Olympus) connected to an inverted microscope (Olympus IX 83) with a 100× oil-immersion objective (UPLFLN100XO2PH, Olympus)). Raw images were binarized and skeletonized with the ImageJ plugin Ridge detection [223]. The resulting minimal filaments are combined to stacks and analyzed via the MATLAB based software Persistence (De La Cruz Lab) as cosine correlation.

So, persistence lengths of actin filaments were determined by imaging of fluorescently labeled filaments in thin (diameter >2 µm) glass chambers like described before [65]. The persistence lengths were then determined by skele-

tonization of the filaments and analysis of the angular cosine correlation like described by De La Cruz *et. al*. [71, 153].

7.5 Network Structure Analysis

7.5.1 Imaging

Images of filaments, networks and cell structures were taken with a confocal laser scanning unit (FluoView FV10, Olympus) connected to an inverted microscope (Olympus IX 83) with a $100\times$ oil-immersion objective (UPLFLN100XO2PH, Olympus).

7.5.2 Aster Analysis

Reconstituted actin networks ($12\,\mu\mathrm{M}$) were polymerized together with myosin II ($600\,\mathrm{nM}$). The emerging actomyosin asters were imaged as described before. Images were then further processed using the open source software FIJI [224] and a custom written MATLAB [220] program.

7.6 Measuring Protein Concentrations

To make sure, protein concentrations were correctly adjusted, an UV-VIS spectrophotometer (Thermo Scientific NanoDrop 2000c) was used at different sample dilutions. The results were averaged over 10+ measurements. Microrheological properties like the plateau modulus G_0 are highly dependent on the actin concentration (compare equation 14, [88, 76], so comparing these properties requires high accuracy with protein concentrations.

7.7 Measuring the Degree of Actin Polymerization

Similar to the actin concentration, the degree of polymerization is also very important for the same reason. Non-polymerizing actin monomers would also influence the effective concentration, which is that of F-actin. Usually the introduced G-actin concentration is assumed to fully polymerize and used as concentration for F-actin. This is a good approximation for measurements after a dynamic equilibrium is reached, since the critical concentrations for polymerization are quite low under typical experimental conditions. To confirm this, G-actin was polymerized at a known concentration. The samples reached dynamic equilibrium after 1 h, were centrifuged at 50000 g for 20 min

with an Ultracentrifuge to remove polymerized actin as a pellet and the supernatant was measured with an UV-VIS spectrophotometer (Thermo Scientific NanoDrop 2000c). The remaining concentration subtracted from the initial one and then divided by the initial concentration gives the degree of polymerization and should be very close to 1. It was confirmed to be between 0.95 and 0.98.

7.8 Buffers and Polymerization Solutions

buffer	substance	concentration [mM]	pH
G-buffer	Tris HCl	2	7.8
	$CaCl_2$	0.1	
	NaN_3	0.001	
G_2-buffer	Tris HCl	2	7.8
	ATP	0.2	
	DTT	0.5	
	$CaCl_2$	0.1	
	NaN_3	0.001	
G_L-buffer	Tris HCl	2	8
	KCl	50	
	ATP	0.2	
	DTT	1	
	NaN_3	0.001	
F-solution	$MgCl_2$	20	7.4
	KCl	1000	
	NaN_3	0.001	
F_E-solution	$MgCl_2$	20	7.4
	KCl	1000	
	EGTA	50	
	NaN_3	0.001	
F_{125}-solution	$MgCl_2$	125	7.4
	KCl	1000	
	EGTA	50	
	NaN_3	0.001	

References

[1] Griselda Cooper and Robert E. Hausman. *The cell ; a molecular approach*. Sinauer Associates, 2000.

[2] Masao Doi and Sam F. Edwards. *The theory of Polymer Dynamics*. Clarendon Press, 1986.

[3] Jan Wilhelm and Erwin Frey. "Elasticity of stiff polymer networks". In: *Physical review letters* 91.10 (2003), p. 108103. ISSN: 0031-9007. DOI: 10.1103/PhysRevLett.91.108103.

[4] Mohau J. Mateyisi et al. "Influence of weak reversible cross-linkers on entangled polymer melt dynamics". In: *The Journal of chemical physics* 148.24 (2018), p. 244901. DOI: 10.1063/1.5019277.

[5] P. A. Janmey et al. "The mechanical properties of actin gels. Elastic modulus and filament motions". In: *The Journal of biological chemistry* 269.51 (1994), pp. 32503–32513. ISSN: 0021-9258. DOI: 10.1016/S0021-9258(18)31663-6.

[6] D. H. Wachsstock, W. H. Schwarz, and T. D. Pollard. "Cross-linker dynamics determine the mechanical properties of actin gels". In: *Biophysical Journal* 66.3 (1994), pp. 801–809. ISSN: 00063495. DOI: 10.1016/s0006-3495(94)80856-2.

[7] Jingyuan Xu et al. "Mechanical Properties of Actin Filament Networks Depend on Preparation, Polymerization Conditions, and Storage of Actin Monomers". In: *Biophysical Journal* 74.5 (1998), pp. 2731–2740. ISSN: 00063495. DOI: 10.1016/S0006-3495(98)77979-2.

[8] Kevin Jahnke et al. "Bottom-Up Assembly of Synthetic Cells with a DNA Cytoskeleton". In: *ACS nano* (2022). DOI: 10.1021/acsnano.1c10703.

[9] Paul W. K. Rothemund et al. "Design and characterization of programmable DNA nanotubes". In: *Journal of the American Chemical Society* 126.50 (2004), pp. 16344–16352. ISSN: 0002-7863. DOI: 10.1021/ja044319l.

[10] Benjamin J. Perrin and James M. Ervasti. "The actin gene family: function follows isoform". In: *Cytoskeleton (Hoboken, N.J.)* 67.10 (2010), pp. 630–634. DOI: 10.1002/cm.20475.

[11] Perrin BJ, Ervasti JM. "The actin gene family: function follows isoform". In: *Cytoskeleton (Hoboken)* 67(10) (2010).

[12] Vera Dugina, Ingrid Zwaenepoel, Giulio Gabbiani, Sophie Clément, Christine Chaponnier. “β- and -cytoplasmic actins display distinct distribution and functional diversity”. In: *J. Cell. Sci.* 122 (2009), pp. 2980–2988.

[13] Dugina VB, Shagieva GS, Shakhov AS, Alieva IB. “The Cytoplasmic Actins in the Regulation of Endothelial Cell Function”. In: *Int J Mol Sci* 22(15) (2021).

[14] Pasquier E, Tuset MP, Sinnappan S, Carnell M, Macmillan A, Kavallaris M. “-Actin plays a key role in endothelial cell motility and neovessel maintenance”. In: *Vasc Cell* 7:2 (2015).

[15] Lechuga S, Baranwal S, Li C, Naydenov NG, Kuemmerle JF, Dugina V, Chaponnier C, Ivanov AI. “Loss of -cytoplasmic actin triggers myofibroblast transition of human epithelial cells”. In: *Mol Biol Cell* 25(20) (2014).

[16] Baranwal S, Naydenov NG, Harris G, Dugina V, Morgan KG, Chaponnier C, Ivanov AI. “Nonredundant roles of cytoplasmic β- and γ-actin isoforms in regulation of epithelial apical junctions”. In: *Mol Biol Cell* 23(18) (2012).

[17] Belyantseva IA, Perrin BJ, Sonnemann KJ, Zhu M, Stepanyan R, McGee J, Frolenkov GI, Walsh EJ, Friderici KH, Friedman TB, Ervasti JM. “Gamma-actin is required for cytoskeletal maintenance but not development”. In: *Proc Natl Acad Sci USA* 106(24) (2009).

[18] Furness DN, Katori Y, Mahendrasingam S, Hackney CM. “Differential distribution of beta- and gamma-actin in guinea-pig cochlear sensory and supporting cells”. In: *Hear Res* 207(1-2) (2005).

[19] Sylvia Varland, Joël Vandekerckhove, and Adrian Drazic. “Actin Post-translational Modifications: The Cinderella of Cytoskeletal Control”. In: *Trends in biochemical sciences* 44.6 (2019), pp. 502–516. ISSN: 0968-0004. DOI: 10.1016/j.tibs.2018.11.010.

[20] Jonathan R. Terman and Anna Kashina. “Post-translational modification and regulation of actin”. In: *Current opinion in cell biology* 25.1 (2013), pp. 30–38. DOI: 10.1016/j.ceb.2012.10.009.

[21] Wylie W. Ahmed, Étienne Fodor, and Timo Betz. “Active cell mechanics: Measurement and theory”. In: *Biochimica et biophysica acta* 1853.11 Pt B (2015), pp. 3083–3094. ISSN: 0006-3002. DOI: 10.1016/j.bbamcr.2015.05.022.

[22] R. C. Hibbeler. *Mechanics of Materials*. Pearson, 2022.

[23] Alison E. Patteson et al. “Vimentin protects cells against nuclear rupture and DNA damage during migration”. In: *The Journal of cell biology* 218.12 (2019), pp. 4079–4092. DOI: 10.1083/jcb.201902046.

[24] Bekele Gurmessa et al. “Entanglement density tunes microscale nonlinear response of entangled actin”. In: *Macromolecules* 49.10 (2016), pp. 3948–3955. DOI: 10.1021/acs.macromol.5b02802.

[25] T. D. Pollard, L. Blanchoin, and R. D. Mullins. “Molecular mechanisms controlling actin filament dynamics in nonmuscle cells”. In: *Annual review of biophysics and biomolecular structure* 29 (2000), pp. 545–576. ISSN: 1056-8700. DOI: 10.1146/annurev.biophys.29.1.545.

[26] Ming Guo et al. “Cell volume change through water efflux impacts cell stiffness and stem cell fate”. In: *Proceedings of the National Academy of Sciences of the United States of America* 114.41 (2017), E8618–E8627. DOI: 10.1073/pnas.1705179114.

[27] Enrico Grazi. “What is the diameter of the actin filament?” In: *FEBS Letters* 405.3 (1997), pp. 249–252. DOI: 10.1016/s0014-5793(97)00214-7.

[28] Kenji Murakami et al. “Structural basis for actin assembly, activation of ATP hydrolysis, and delayed phosphate release”. In: *Cell* 143.2 (2010), pp. 275–287. DOI: 10.1016/j.cell.2010.09.034.

[29] Anja M. Swenson et al. “Magnesium modulates actin binding and ADP release in myosin motors”. In: *Journal of Biological Chemistry* 289.34 (2014), pp. 23977–23991. DOI: 10.1074/jbc.m114.562231.

[30] T. D. Pollard. “Rate constants for the reactions of ATP- and ADP-actin with the ends of actin filaments”. In: *The Journal of cell biology* 103.6 Pt 2 (1986), pp. 2747–2754. DOI: 10.1083/jcb.103.6.2747.

[31] Vera Dugina et al. “Beta and gamma-cytoplasmic actins display distinct distribution and functional diversity”. In: *Journal of cell science* 122.Pt 16 (2009), pp. 2980–2988. ISSN: 0021-9533. DOI: 10.1242/jcs.041970.

[32] Roberto Dominguez and Kenneth C. Holmes. “Actin structure and function”. In: *Annual review of biophysics* 40 (2011), pp. 169–186. DOI: 10.1146/annurev-biophys-042910-155359.

[33] Hugo Sanabria et al. “βCaMKII regulates actin assembly and structure”. In: *Journal of Biological Chemistry* 284.15 (2009), pp. 9770–9780. DOI: 10.1074/jbc.m809518200.

[34] Hyeran Kang et al. “Identification of cation-binding sites on actin that drive polymerization and modulate bending stiffness”. In: *Proceedings of the National Academy of Sciences of the United States of America* 109.42 (2012), pp. 16923–16927. DOI: 10.1073/pnas.1211078109.

[35] Toshiro Oda et al. “The nature of the globular- to fibrous-actin transition”. In: *Nature* 457.7228 (2009), pp. 441–445. DOI: 10.1038/nature07685.

[36] Brittany MacTaggart and Anna Kashina. “Posttranslational modifications of the cytoskeleton”. In: *Cytoskeleton (Hoboken, N.J.)* 78.4 (2021), pp. 142–173. DOI: 10.1002/cm.21679.

[37] Thomas D. Pollard and John A. Cooper. “Actin, a central player in cell shape and movement”. In: *Science (New York, N.Y.)* 326.5957 (2009), pp. 1208–1212. DOI: 10.1126/science.1175862.

[38] E. GAETJENS and M. BARANY. “N-acetylaspartic acid in G-actin”. In: *Biochimica et Biophysica Acta (BBA) - General Subjects* 117.1 (1966), pp. 176–183. ISSN: 03044165. DOI: 10.1016/0304-4165(66)90164-4.

[39] Philipp Mertins et al. “Ischemia in tumors induces early and sustained phosphorylation changes in stress kinase pathways but does not affect global protein levels”. In: *Molecular & cellular proteomics : MCP* 13.7 (2014), pp. 1690–1704. DOI: 10.1074/mcp.M113.036392.

[40] Philipp Mertins et al. “Proteogenomics connects somatic mutations to signalling in breast cancer”. In: *Nature* 534.7605 (2016), pp. 55–62. DOI: 10.1038/nature18003.

[41] Francis Impens et al. “Mapping of SUMO sites and analysis of SUMOylation changes induced by external stimuli”. In: *Proceedings of the National Academy of Sciences of the United States of America* 111.34 (2014), pp. 12432–12437. DOI: 10.1073/pnas.1413825111.

[42] Alicia Lundby et al. “Proteomic analysis of lysine acetylation sites in rat tissues reveals organ specificity and subcellular patterns”. In: *Cell reports* 2.2 (2012), pp. 419–431. DOI: 10.1016/j.celrep.2012.07.006.

[43] Ivo A. Hendriks et al. “Uncovering global SUMOylation signaling networks in a site-specific manner”. In: *Nature structural & molecular biology* 21.10 (2014), pp. 927–936. DOI: 10.1038/nsmb.2890.

[44] Ryan J. Lumpkin et al. “Site-specific identification and quantitation of endogenous SUMO modifications under native conditions”. In: *Nature communications* 8.1 (2017), p. 1171. DOI: 10.1038/s41467-017-01271-3.

[45] Chia-Feng Tsai et al. “Large-scale determination of absolute phosphorylation stoichiometries in human cells by motif-targeting quantitative proteomics”. In: *Nature communications* 6 (2015), p. 6622. DOI: 10.1038/ncomms7622.

[46] Delphine Rolland et al. “Global phosphoproteomic profiling reveals distinct signatures in B-cell non-Hodgkin lymphomas”. In: *The American journal of pathology* 184.5 (2014), pp. 1331–1342. DOI: 10.1016/j.ajpath.2014.01.036.

[47] Isabella Dalle-Donne et al. “Protein carbonyl groups as biomarkers of oxidative stress”. In: *Clinica Chimica Acta* 329.1-2 (2003), pp. 23–38. ISSN: 00098981. DOI: 10.1016/s0009-8981(03)00003-2.

[48] Mutay Aslan et al. “Nitric oxide-dependent generation of reactive species in sickle cell disease. Actin tyrosine induces defective cytoskeletal polymerization”. In: *The Journal of biological chemistry* 278.6 (2003), pp. 4194–4204. ISSN: 0021-9258. DOI: 10.1074/jbc.M208916200.

[49] A. Abe et al. “Acetylation at the N-terminus of actin strengthens weak interaction between actin and myosin”. In: *Biochemical and biophysical research communications* 268.1 (2000), pp. 14–19. ISSN: 0006-291X. DOI: 10.1006/bbrc.1999.2069.

[50] S. Schmitz et al. “Drosophila ACT88F indirect flight muscle-specific actin is not N-terminally acetylated: a mutation in N-terminal processing affects actin function”. In: *Journal of molecular biology* 295.5 (2000), pp. 1201–1210. ISSN: 0022-2836. DOI: 10.1006/jmbi.1999.3407.

[51] Thomas Arnesen. “Towards a functional understanding of protein N-terminal acetylation”. In: *PLoS biology* 9.5 (2011), e1001074. DOI: 10.1371/journal.pbio.1001074.

[52] J. Vandekerckhove and K. Weber. “Mammalian cytoplasmic actins are the products of at least two genes and differ in primary structure in at least 25 identified positions from skeletal muscle actins”. In: *Proceedings of the National Academy of Sciences of the United States of America* 75.3 (1978), pp. 1106–1110. DOI: 10.1073/pnas.75.3.1106.

[53] R. K. Cook, W. T. Blake, and P. A. Rubenstein. “Removal of the amino-terminal acidic residues of yeast actin. Studies in vitro and in vivo”. In: *The Journal of biological chemistry* 267.13 (1992), pp. 9430–9436. ISSN: 0021-9258. DOI: 10.1016/S0021-9258(19)50441-0.

[54] Bogdan Polevoda et al. “Nat3p and Mdm20p are required for function of yeast NatB Nalpha-terminal acetyltransferase and of actin and tropomyosin”. In: *The Journal of biological chemistry* 278.33 (2003), pp. 30686–30697. ISSN: 0021-9258. DOI: 10.1074/jbc.M304690200.

[55] E. Balzi et al. “Cloning and functional analysis of the arginyl-tRNA-protein transferase gene ATE1 of Saccharomyces cerevisiae”. In: *The Journal of biological chemistry* 265.13 (1990), pp. 7464–7471. ISSN: 0021-9258. DOI: 10.1016/S0021-9258(19)39136-7.

[56] Sougata Saha et al. “Arginylation regulates intracellular actin polymer level by modulating actin properties and binding of capping and severing proteins”. In: *Molecular biology of the cell* 21.8 (2010), pp. 1350–1361. DOI: 10.1091/mbc.E09-09-0829.

[57] Pirta Hotulainen et al. “Defining mechanisms of actin polymerization and depolymerization during dendritic spine morphogenesis”. In: *The Journal of cell biology* 185.2 (2009), pp. 323–339. DOI: 10.1083/jcb.200809046.

[58] Marina Karakozova et al. “Arginylation of beta-actin regulates actin cytoskeleton and cell motility”. In: *Science (New York, N.Y.)* 313.5784 (2006), pp. 192–196. DOI: 10.1126/science.1129344.

[59] Fangliang Zhang et al. “Differential arginylation of actin isoforms is regulated by coding sequence-dependent degradation”. In: *Science (New York, N.Y.)* 329.5998 (2010), pp. 1534–1537. DOI: 10.1126/science.1191701.

[60] Reena Rai et al. “Arginyltransferase regulates alpha cardiac actin function, myofibril formation and contractility during heart development”. In: *Development (Cambridge, England)* 135.23 (2008), pp. 3881–3889. ISSN: 0950-1991. DOI: 10.1242/dev.022723.

[61] Satoshi Kurosaka et al. “Arginylation-dependent neural crest cell migration is essential for mouse development”. In: *PLoS genetics* 6.3 (2010), e1000878. DOI: 10.1371/journal.pgen.1000878.

[62] Satoshi Kurosaka et al. “Arginylation regulates myofibrils to maintain heart function and prevent dilated cardiomyopathy”. In: *Journal of molecular and cellular cardiology* 53.3 (2012), pp. 333–341. DOI: 10.1016/j.yjmcc.2012.05.007.

[63] Yong Tae Kwon et al. “An essential role of N-terminal arginylation in cardiovascular development”. In: *Science (New York, N.Y.)* 297.5578 (2002), pp. 96–99. DOI: 10.1126/science.1069531.

[64] L. D. Landau. *Theory of Elasticity: Volume 7*. 3rd ed. Oxford: Elsevier Science, 1984. ISBN: 978-0-08-057069-3. URL: http://gbv.eblib.com/patron/FullRecord.aspx?p=1179792.

[65] Ott et al. “Measurement of the persistence length of polymerized actin using fluorescence microscopy”. In: *Physical review. E, Statistical physics, plasmas, fluids, and related interdisciplinary topics* 48.3 (1993), R1642–R1645. ISSN: 1063-651X. DOI: 10.1103/PhysRevE.48.R1642.

[66] Olivier Pelletier et al. “Structure of actin cross-linked with α-actinin: a network of bundles”. In: *Physical review letters* 91.14 (2003), p. 148102.

[67] Mireille Maria Anna Elisabeth Claessens et al. “Helical twist controls the thickness of F-actin bundles”. In: *Proceedings of the National Academy of Sciences* 105.26 (2008), pp. 8819–8822.

[68] Toshihiro Toyota et al. “Non-Gaussian athermal fluctuations in active gels”. In: *Soft Matter* 7.7 (2011), pp. 3234–3239.

[69] Daisuke Mizuno. “Levy statistics and dynamics in active cytoskeletons”. In: *Proceedings of the Samahang Pisika ng Pilipinas* (2013), SPP2013–BP.

[70] P. G. de Gennes and Thomas A. Witten. “Scaling Concepts in Polymer Physics”. In: *Physics Today* 33.6 (1980), pp. 51–54. ISSN: 0031-9228. DOI: 10.1063/1.2914118.

[71] Enrique M. de La Cruz and Margaret L. Gardel. “Actin Mechanics and Fragmentation”. In: *The Journal of biological chemistry* 290.28 (2015), pp. 17137–17144. ISSN: 0021-9258. DOI: 10.1074/jbc.R115.636472.

[72] Theo Odijk. “The statistics and dynamics of confined or entangled stiff polymers”. In: *Macromolecules* 16.8 (1983), pp. 1340–1344. ISSN: 0024-9297. DOI: 10.1021/MA00242A015.

[73] Alexander N. Semenov. “Dynamics of concentrated solutions of rigid-chain polymers. Part 1.—Brownian motion of persistent macromolecules in isotropic solution”. In: *J. Chem. Soc., Faraday Trans. 2* 82.3 (1986), pp. 317–329. ISSN: 0300-9238. DOI: 10.1039/F29868200317.

[74] Theodore W. Burkhardt. “Free energy of a semiflexible polymer in a tube and statistics of a randomly-accelerated particle”. In: *Journal of Physics A: Mathematical and General* 30.7 (1997), pp. L167–L172. ISSN: 0305-4470. DOI: 10.1088/0305-4470/30/7/004.

[75] H. Isambert et al. “Flexibility of actin filaments derived from thermal fluctuations. Effect of bound nucleotide, phalloidin, and muscle regulatory proteins”. In: *The Journal of biological chemistry* 270.19 (1995), pp. 11437–11444. ISSN: 0021-9258. DOI: 10.1074/jbc.270.19.11437.

[76] B. Hinner et al. “Entanglement, Elasticity, and Viscous Relaxation of Actin Solutions”. In: *Physical review letters* 81.12 (1998), pp. 2614–2617. ISSN: 0031-9007. DOI: 10.1103/PhysRevLett.81.2614.

[77] D. C. Morse. “Tube diameter in tightly entangled solutions of semiflexible polymers”. In: *Physical review. E, Statistical, nonlinear, and soft matter physics* 63.3 Pt 1 (2001), p. 031502. ISSN: 1539-3755. DOI: 10.1103/PhysRevE.63.031502.

[78] Jizeng Wang and Kai Li. “Statistical Behaviors of Semiflexible Polymer Chains Stretched in Rectangular Tubes”. In: *Polymers* 11.2 (2019). DOI: 10.3390/polym11020260.

[79] Christoph F. Schmidt et al. “Chain dynamics, mesh size, and diffusive transport in networks of polymerized actin: a quasielastic light scattering and microfluorescence study”. In: *Macromolecules* 22.9 (1989), pp. 3638–3649. ISSN: 0024-9297. DOI: 10.1021/ma00199a023.

[80] PB Moore, HE Huxley, and DJ DeRosier. “Three-dimensional reconstruction of F-actin, thin filaments and decorated thin filaments”. In: *Journal of molecular biology* 50.2 (1970), pp. 279–292.

[81] Matthias D. Koch and Alexander Rohrbach. “Label-free Imaging and Bending Analysis of Microtubules by ROCS Microscopy and Optical Trapping”. In: *Biophysical Journal* 114.1 (2018), pp. 168–177. ISSN: 00063495. DOI: 10.1016/j.bpj.2017.10.036.

[82] O. Kratky and G. Porod. “Röntgenuntersuchung gelöster Fadenmoleküle”. In: *Recueil des Travaux Chimiques des Pays-Bas* 68.12 (1949), pp. 1106–1122. ISSN: 01650513. DOI: 10.1002/recl.19490681203.

[83] C. P. Broedersz and F. C. MacKintosh. “Modeling semiflexible polymer networks”. In: *Reviews of Modern Physics* 86.3 (2014), pp. 995–1036. ISSN: 0034-6861. DOI: 10.1103/RevModPhys.86.995.

[84] Chenyang Liu et al. “Evaluation of different methods for the determination of the plateau modulus and the entanglement molecular weight”. In: *Polymer* 47.13 (2006), pp. 4461–4479. ISSN: 00323861. DOI: 10.1016/j.polymer.2006.04.054.

[85] Wen Li Kelly Chen and Craig A. Simmons. “Lessons from (patho)physiological tissue stiffness and their implications for drug screening, drug delivery and regenerative medicine”. In: *Advanced drug delivery reviews* 63.4-5 (2011), pp. 269–276. DOI: 10.1016/j.addr.2011.01.004.

[86] Guoyou Huang et al. “Engineering three-dimensional cell mechanical microenvironment with hydrogels”. In: *Biofabrication* 4.4 (2012), p. 042001. DOI: 10.1088/1758-5082/4/4/042001.

[87] Peter Nietmann et al. “Epithelial cells fluidize upon adhesion but display mechanical homeostasis in the adherent state”. In: *Biophysical journal* 121.3 (2022), pp. 361–373. DOI: 10.1016/j.bpj.2021.12.042.

[88] Isambert Groupe De, H. Isambert, and A. C. Maggs. “Dynamics and Rheology of Actin Solutions”. In: *Macromolecules* 29 (1996), pp. 1036–1040. ISSN: 0024-9297.

[89] Theo Odijk. “Theory of lyotropic polymer liquid crystals”. In: *Macromolecules* 19.9 (1986), pp. 2313–2329. DOI: 10.1021/ma00163a001.

[90] F. Gittes and F. C. MacKintosh. “Dynamic shear modulus of a semiflexible Polymer Network”. In: *Physical Review E* 58.2 (1998). DOI: 10.1103/physreve.58.r1241.

[91] Enrique M. de La Cruz et al. “Origin of twist-bend coupling in actin filaments”. In: *Biophysical journal* 99.6 (2010), pp. 1852–1860. DOI: 10.1016/j.bpj.2010.07.009.

[92] Clifford P. Brangwynne et al. “Bending dynamics of fluctuating biopolymers probed by automated high-resolution filament tracking”. In: *Biophysical journal* 93.1 (2007), pp. 346–359. DOI: 10.1529/biophysj.106.096966.

[93] Brad A. Krajina et al. “Dynamic Light Scattering Microrheology Reveals Multiscale Viscoelasticity of Polymer Gels and Precious Biological Materials”. In: *ACS central science* 3.12 (2017), pp. 1294–1303. ISSN: 2374-7943. DOI: 10.1021/acscentsci.7b00449.

[94] David C. Morse. “Viscoelasticity of Concentrated Isotropic Solutions of Semiflexible Polymers. 1. Model and Stress Tensor”. In: *Macromolecules* 31.20 (1998), pp. 7030–7043. ISSN: 0024-9297. DOI: 10.1021/ma9803032.

[95] J. Käs et al. “F-actin, a model polymer for semiflexible chains in dilute, semidilute, and liquid crystalline solutions”. In: *Biophysical journal* 70.2 (1996), pp. 609–625. DOI: 10.1016/S0006-3495(96)79630-3.

[96] Andre Palmer et al. “Diffusing Wave Spectroscopy Microrheology of Actin Filament Networks”. In: *Biophysical journal* 76.2 (1999), pp. 1063–1071. DOI: 10.1016/S0006-3495(99)77271-1.

[97] T. G. Mason et al. “Rheology of F-actin solutions determined from thermally driven tracer motion”. In: *Journal of Rheology* 44.4 (2000), pp. 917–928. ISSN: 0148-6055. DOI: 10.1122/1.551113.

[98] Anna V. Glyakina and Oxana V. Galzitskaya. “Bioinformatics Analysis of Actin Molecules: Why Quantity Does Not Translate Into Quality?” In: *Frontiers in genetics* 11 (2020), p. 617763. ISSN: 1664-8021. DOI: 10.3389/fgene.2020.617763.

[99] Nicholas Castaneda, Jinho Park, and Ellen Hyeran Kang. “Regulation of Actin Bundle Mechanics and Structure by Intracellular Environmental Factors”. In: *Frontiers in physics* 9 (2021). ISSN: 2296-424X. DOI: 10.3389/fphy.2021.675885.

[100] A. Mogilner and B. Rubinstein. “The physics of filopodial protrusion”. In: *Biophysical Journal* 89.2 (2005), pp. 782–795. ISSN: 00063495. DOI: 10.1529/biophysj.104.056515.

[101] Laurent Blanchoin et al. “Actin dynamics, architecture, and mechanics in cell motility”. In: *Physiological reviews* 94.1 (2014), pp. 235–263. DOI: 10.1152/physrev.00018.2013.

[102] T.J Mitchison and L.P Cramer. “Actin-Based Cell Motility and Cell Locomotion”. In: *Cell* 84.3 (1996), pp. 371–379. DOI: 10.1016/S0092-8674(00)81281-7.

[103] Vilmos Zsolnay et al. “Structural basis for polarized elongation of actin filaments”. In: *Proceedings of the National Academy of Sciences of the United States of America* 117.48 (2020), pp. 30458–30464. DOI: 10.1073/pnas.2011128117.

[104] Praveena Narayanan et al. “Length regulation of mechanosensitive stereocilia depends on very slow actin dynamics and filament-severing proteins”. In: *Nature communications* 6 (2015), p. 6855. DOI: 10.1038/ncomms7855.

[105] Florian Rückerl et al. “Adaptive Response of Actin Bundles under Mechanical Stress”. In: *Biophysical Journal* 113.5 (2017), pp. 1072–1079. ISSN: 00063495. DOI: 10.1016/j.bpj.2017.07.017.

[106] M. Hosek and J. X. Tang. “Polymer-induced bundling of F actin and the depletion force”. In: *Physical review. E, Statistical, nonlinear, and soft matter physics* 69.5 Pt 1 (2004), p. 051907. ISSN: 1539-3755. DOI: 10.1103/PhysRevE.69.051907.

[107] Mireille M. A. E. Claessens et al. “Actin-binding proteins sensitively mediate F-actin bundle stiffness”. In: *Nature materials* 5.9 (2006), pp. 748–753. ISSN: 1476-1122. DOI: 10.1038/nmat1718.

[108] Jörg Schnauß, Tina Händler, and Josef A. Käs. “Semiflexible Biopolymers in Bundled Arrangements”. In: *Polymers* 8.8 (2016). DOI: 10.3390/polym8080274.

[109] Nicholas Castaneda et al. “Cations Modulate Actin Bundle Mechanics, Assembly Dynamics, and Structure”. In: *The journal of physical chemistry. B* 122.14 (2018), pp. 3826–3835. DOI: 10.1021/acs.jpcb.8b00663.

[110] Silvia Jansen et al. “Mechanism of actin filament bundling by fascin”. In: *The Journal of biological chemistry* 286.34 (2011), pp. 30087–30096. ISSN: 0021-9258. DOI: 10.1074/jbc.M111.251439.

[111] Thomas E. Angelini et al. “Structure and dynamics of condensed multivalent ions within polyelectrolyte bundles: a combined x-ray diffraction and solid-state NMR study”. In: *Journal of Physics: Condensed Matter* 17.14 (2005), S1123–S1135. ISSN: 0953-8984. DOI: 10.1088/0953-8984/17/14/001.

[112] Laura A Sherer and Naomi Courtemanche. “Cooperative bundling by fascin generates actin structures with architectures that depend on filament length”. In: *Frontiers in Cell and Developmental Biology* 10 (2022), p. 974047.

[113] Dennis Breitsprecher et al. “Cofilin cooperates with fascin to disassemble filopodial actin filaments”. In: *Journal of cell science* 124.19 (2011), pp. 3305–3318.

[114] Sumra Shahid et al. “Size-dependent studies of macromolecular crowding on the thermodynamic stability, structure and functional activity of proteins: in vitro and in silico approaches”. In: *Biochimica et Biophys-*

ica Acta (BBA) - General Subjects 1861.2 (2017), pp. 178–197. ISSN: 03044165. DOI: 10.1016/j.bbagen.2016.11.014.

[115] Allen P. Minton. “Implications of macromolecular crowding for protein assembly”. In: *Current Opinion in Structural Biology* 10.1 (2000), pp. 34–39. ISSN: 0959440X. DOI: 10.1016/S0959-440X(99)00045-7.

[116] Martin Streichfuss et al. “Measuring forces between two single actin filaments during bundle formation”. In: *Nano letters* 11.9 (2011), pp. 3676–3680. DOI: 10.1021/nl201630y.

[117] Florian Huber et al. “Formation of regularly spaced networks as a general feature of actin bundle condensation by entropic forces”. In: *New Journal of Physics* 17.4 (2015), p. 043029. DOI: 10.1088/1367-2630/17/4/043029.

[118] Thomas E. Angelini et al. “Like-charge attraction between polyelectrolytes induced by counterion charge density waves”. In: *Proceedings of the National Academy of Sciences of the United States of America* 100.15 (2003), pp. 8634–8637. DOI: 10.1073/pnas.1533355100.

[119] Thomas E. Angelini et al. “Counterions between charged polymers exhibit liquid-like organization and dynamics”. In: *Proceedings of the National Academy of Sciences of the United States of America* 103.21 (2006), pp. 7962–7967. DOI: 10.1073/pnas.0601435103.

[120] O. Lieleg et al. “Transient binding and dissipation in cross-linked actin networks”. In: *Physical review letters* 101.10 (2008), p. 108101. ISSN: 0031-9007. DOI: 10.1103/PhysRevLett.101.108101.

[121] Oliver Lieleg, Mireille M. A. E. Claessens, and Andreas R. Bausch. “Structure and dynamics of cross-linked actin networks”. In: *Soft Matter* 6.2 (2010), pp. 218–225. DOI: 10.1039/b912163n. URL: https://doi.org/10.1039%2Fb912163n.

[122] R. Tharmann, M. M. A. E. Claessens, and A. R. Bausch. “Viscoelasticity of isotropically cross-linked actin networks”. In: *Physical review letters* 98.8 (2007), p. 088103. ISSN: 0031-9007. DOI: 10.1103/PhysRevLett.98.088103.

[123] Yuxia Luan et al. “Micro- and macrorheological properties of isotropically cross-linked actin networks”. In: *Biophysical Journal* 94.2 (2008), pp. 688–693. ISSN: 00063495. DOI: 10.1529/biophysj.107.112417.

[124] F. Gittes and F. C. MacKintosh. “Dynamic shear modulus of a semi-flexible polymer network”. In: *Physical Review E* 58.2 (1998), R1241–R1244. ISSN: 1063-651X. DOI: 10.1103/PhysRevE.58.R1241.

[125] O. Lieleg et al. “Cytoskeletal polymer networks: viscoelastic properties are determined by the microscopic interaction potential of cross-links”. In: *Biophysical Journal* 96.11 (2009), pp. 4725–4732. ISSN: 00063495. DOI: 10.1016/j.bpj.2009.03.038.

[126] Thomas G. Mezger. *The rheology handbook: For users of rotational and oscillatory rheometers*. Vincentz Network, 2020.

[127] M. T. Valentine et al. “Colloid surface chemistry critically affects multiple particle tracking measurements of biomaterials”. In: *Biophysical Journal* 86.6 (2004), pp. 4004–4014. ISSN: 00063495. DOI: 10.1529/biophysj.103.037812.

[128] James L. McGrath, John H. Hartwig, and Scot C. Kuo. “The Mechanics of F-Actin Microenvironments Depend on the Chemistry of Probing Surfaces”. In: *Biophysical Journal* 79.6 (2000), pp. 3258–3266. ISSN: 00063495. DOI: 10.1016/S0006-3495(00)76558-1.

[129] Qiang Lu and Michael J. Solomon. “Probe size effects on the microrheology of associating polymer solutions”. In: *Physical review. E, Statistical, nonlinear, and soft matter physics* 66.6 Pt 1 (2002), p. 061504. ISSN: 1539-3755. DOI: 10.1103/PhysRevE.66.061504.

[130] Alex J. Levine and T. C. Lubensky. “One- and Two-Particle Microrheology”. In: *Phys. Rev. Lett.* 85 (8 Aug. 2000), pp. 1774–1777. DOI: 10.1103/PhysRevLett.85.1774. URL: https://link.aps.org/doi/10.1103/PhysRevLett.85.1774.

[131] Manlio Tassieri et al. “Microrheology with optical tweezers: data analysis”. In: *New Journal of Physics* 14.11 (2012), p. 115032. DOI: 10.1088/1367-2630/14/11/115032.

[132] Daryl Preece et al. “Optical tweezers: wideband microrheology”. In: *Journal of Optics* 13.4 (2011), p. 044022. ISSN: 2040-8978. DOI: 10.1088/2040-8978/13/4/044022.

[133] Andrew Resnick. “Use of optical tweezers for colloid science”. In: *Journal of Colloid and Interface Science* 262.1 (2003), pp. 55–59. ISSN: 00219797. DOI: 10.1016/S0021-9797(03)00193-0.

[134] Eric M. Furst. “Applications of laser tweezers in complex fluid rheology”. In: *Current Opinion in Colloid & Interface Science* 10.1-2 (2005), pp. 79–86. ISSN: 13590294. DOI: 10.1016/j.cocis.2005.04.001.

[135] T. G. Mason et al. “Particle Tracking Microrheology of Complex Fluids”. In: *Physical review letters* 79.17 (1997), pp. 3282–3285. ISSN: 0031-9007. DOI: 10.1103/PhysRevLett.79.3282.

[136] T. G. Mason, Hu Gang, and D. A. Weitz. “Diffusing-wave-spectroscopy measurements of viscoelasticity of complex fluids”. In: *Journal of the Optical Society of America A* 14.1 (1997), p. 139. ISSN: 1084-7529. DOI: 10.1364/josaa.14.000139.

[137] Mason and Weitz. “Optical measurements of frequency-dependent linear viscoelastic moduli of complex fluids”. In: *Physical review letters* 74.7 (1995), pp. 1250–1253. ISSN: 0031-9007. DOI: 10.1103/PhysRevLett.74.1250.

[138] Robert Byron Bird, Robert C. Armstrong, and Ole Hassager. *Fluid mechanics*. 2. ed. Vol. Vol. 1. Dynamics of polymeric liquids / R. Byron Bird. New York: Wiley, 1987. ISBN: 978-0-471-80245-7.

[139] Bivash R. Dasgupta et al. “Microrheology of polyethylene oxide using diffusing wave spectroscopy and single scattering”. In: *Physical review. E, Statistical, nonlinear, and soft matter physics* 65.5 Pt 1 (2002), p. 051505. ISSN: 1539-3755. DOI: 10.1103/PhysRevE.65.051505.

[140] David Lopez-Diaz and Rolando Castillo. “Microrheology of solutions embedded with thread-like supramolecular structures”. In: *Soft Matter* 7.13 (2011), p. 5926. ISSN: 1744-683X. DOI: 10.1039/C1SM05274H.

[141] Tobias Paust. “New Methods for Passive and Active Microrheology”. PhD thesis. Universität Ulm, 2013. DOI: 10.18725/OPARU-2611.

[142] B. Fabry et al. “Scaling the microrheology of living cells”. In: *Physical review letters* 87.14 (2001), p. 148102. ISSN: 0031-9007. DOI: 10.1103/physrevlett.87.148102.

[143] Ji Yeon Huh and Eric M. Furst. “Colloid dynamics in semiflexible polymer solutions”. In: *Physical review. E, Statistical, nonlinear, and soft matter physics* 74.3 Pt 1 (2006), p. 031802. ISSN: 1539-3755. DOI: 10.1103/PhysRevE.74.031802.

[144] Qi Li et al. “The Laplace approach in microrheology”. In: *Soft Matter* 16.14 (2020), pp. 3378–3383. ISSN: 1744-683X. DOI: 10.1039/c9sm02242b.

[145] Michael A. Taylor, Joachim Knittel, and Warwick P. Bowen. “Fundamental constraints on particle tracking with optical tweezers”. In: *New Journal of Physics* 15.2 (2013), p. 023018. DOI: 10.1088/1367-2630/15/2/023018.

[146] R. M. L. Evans et al. “Direct conversion of rheological compliance measurements into storage and loss moduli”. In: *Physical review. E, Statistical, nonlinear, and soft matter physics* 80.1 Pt 1 (2009), p. 012501. ISSN: 1539-3755. DOI: 10.1103/PhysRevE.80.012501.

[147] M. L. Gardel et al. “Microrheology of Entangled F-Actin Solutions”. In: *Physical Review Letters* 91.15 (Oct. 2003). DOI: 10.1103/physrevlett.91.158302. URL: https://doi.org/10.1103%2Fphysrevlett.91.158302.

[148] A. C Maggs and S Leibler. “Adsorption and Fluctuations of Two-Dimensional Vesicles”. In: *Europhysics Letters (EPL)* 12.1 (May 1990), pp. 19–24. DOI: 10.1209/0295-5075/12/1/004. URL: https://doi.org/10.1209/0295-5075/12/1/004.

[149] Lucas Lamparter and Milos Galic. “Cellular Membranes, a Versatile Adaptive Composite Material”. In: *Frontiers in cell and developmental biology* 8 (2020), p. 684. ISSN: 2296-634X. DOI: 10.3389/fcell.2020.00684.

[150] Nisha Bte Mohd Rafiq et al. *The cytoskeleton as a smart composite material: A unified pathway linking microtubules, myosin-II filaments and integrin adhesions*. 2017. DOI: 10.1101/195495.

[151] Shea N. Ricketts, Jennifer L. Ross, and Rae M. Robertson-Anderson. “Co-Entangled Actin-Microtubule Composites Exhibit Tunable Stiffness and Power-Law Stress Relaxation”. In: *Biophysical Journal* 115.6 (Sept. 2018), pp. 1055–1067. DOI: 10.1016/j.bpj.2018.08.010. URL: https://doi.org/10.1016%2Fj.bpj.2018.08.010.

[152] Mikkel H. Jensen et al. “Emergent properties of composite semiflexible biopolymer networks”. In: *BioArchitecture* 4.4-5 (2014), pp. 138–143. DOI: 10.4161/19490992.2014.989035.

[153] John S. Graham et al. “Multi-platform compatible software for analysis of polymer bending mechanics”. In: *PloS one* 9.4 (2014), e94766. DOI: 10.1371/journal.pone.0094766.

[154] F. Gittes et al. “Flexural rigidity of microtubules and actin filaments measured from thermal fluctuations in shape”. In: *The Journal of cell biology* 120.4 (1993), pp. 923–934. DOI: 10.1083/jcb.120.4.923.

[155] Osigwe Esue et al. “A direct interaction between actin and vimentin filaments mediated by the tail domain of vimentin”. In: *The Journal of biological chemistry* 281.41 (2006), pp. 30393–30399. ISSN: 0021-9258. DOI: 10.1074/jbc.M605452200.

[156] Tom Golde et al. “Glassy dynamics in composite biopolymer networks”. In: *Soft Matter* 14.39 (2018), pp. 7970–7978. DOI: 10.1039/c8sm01061g.

[157] Cornelis Storm et al. “Nonlinear elasticity in biological gels”. In: *Nature* 435.7039 (2005), pp. 191–194. DOI: 10.1038/nature03521.

[158] M. L. Gardel et al. “Elastic Behavior of Cross-Linked and Bundled Actin Networks”. In: *Science* 304.5675 (2004), pp. 1301–1305. DOI: 10.1126/science.1095087.

[159] J. P. Mills et al. “Nonlinear elastic and viscoelastic deformation of the human red blood cell with optical tweezers”. In: *Mechanics & chemistry of biosystems : MCB* 1.3 (2004), pp. 169–180. ISSN: 1546-2048.

[160] Philip Kollmannsberger and Ben Fabry. “Linear and Nonlinear Rheology of Living Cells”. In: *Annual Review of Materials Research* 41.1 (2011), pp. 75–97. ISSN: 1531-7331. DOI: 10.1146/annurev-matsci-062910-100351.

[161] Yi-Chia Lin et al. “Control of non-linear elasticity in F-actin networks with microtubules”. In: *Soft matter* 7.3 (2011), pp. 902–906. DOI: 10.1039/C0SM00478B.

[162] Matthew D. Welch and Michael Way. “Arp2/3-Mediated Actin-Based Motility: A Tail of Pathogen Abuse”. In: *Cell Host and Microbe* 14.3 (2013), pp. 242–255. DOI: 10.1016/j.chom.2013.08.011.

[163] Congying Wu et al. “Arp2/3 Is Critical for Lamellipodia and Response to Extracellular Matrix Cues but Is Dispensable for Chemotaxis”. In: *Cell* 148.5 (2012), pp. 973–987. DOI: 10.1016/j.cell.2011.12.034.

[164] Praveen Suraneni et al. “The Arp2/3 complex is required for lamellipodia extension and directional fibroblast cell migration”. In: *Journal of Cell Biology* 197.2 (2012), pp. 239–251. DOI: 10.1083/jcb.201112113.

[165] Claire Wilhelm. “Out-of-Equilibrium Microrheology inside Living Cells”. In: *Physical Review Letters* 101.2 (2008). DOI: 10.1103/physrevlett.101.028101.

[166] Priyamvada Chugh et al. “Actin cortex architecture regulates cell surface tension”. In: *Nature cell biology* 19.6 (2017), pp. 689–697.

[167] Andrea Cordes et al. “Prestress and area compressibility of actin cortices determine the viscoelastic response of living cells”. In: *Physical Review Letters* 125.6 (2020), p. 068101.

[168] Roberto Dominguez, Kenneth C. Holmes. “Actin Structure and Function”. In: *Annu. Rev. Biophys.* 40 (2011), pp. 169–186.

[169] Ott A, Magnasco M, Simon A, Libchaber A. “Measurement of the persistence length of polymerized actin using fluorescence microscopy”. In: *Phys Rev E* 48(3) (1993).

[170] McCullough BR, Blanchoin L, Martiel JL, De la Cruz EM. “Cofilin Increases the Bending Flexibility of Actin Filaments: Implications for Severing and Cell Mechanics”. In: *J Mol Biol* 381(3) (2008).

[171] Thomas D. Pollard. “Actin and Actin-Binding Proteins”. In: *Cold Spring Harb. Perspect. Biol.* 8(8) (2016).

[172] Samandar Eweis D, Plastino J. “Roles of Actin in the Morphogenesis of the Early Caenorhabditis elegans Embryo”. In: *Int J Mol Sci* 21(10) (2020).

[173] Pavan Vedula, Satoshi Kurosaka, Brittany MacTaggart, Qin Ni, Garegin Papoian, Yi Jiang, Dawei W. Dong, Anna Kashina. “Different translation dynamics of β- and -actin regulates cell migration”. In: *Elife* (2021). DOI: 10.7554/eLife.68712.

[174] Pavan Vedula Satoshi Kurosaka Nicolae Adrian Leu Yuri I Wolf Svetlana A Shabalina Junling Wang Stephanie Sterling Dawei W Dong Anna Kashina. “Diverse functions of homologous actin isoforms are defined by their nucleotide, rather than their amino acid sequence”. In: *Elife* (2017). DOI: https://doi.org/10.7554/eLife.31661.

[175] Köhler S, Schaller V, Bausch AR. “Collective dynamics of active cytoskeletal networks”. In: *PLoS One* 6(8) (2011).

[176] Humphrey D, Duggan C, Saha D, Smith D, Käs J. “Active fluidization of polymer networks through molecular motors”. In: *Nature* 416(6879) (2002).

[177] Strehle D, Mollenkopf P, Glaser M, Golde T, Schuldt C, Käs JA, Schnauß J. “Single Actin Bundle Rheology”. In: *Molecules* 22(10) (2017).

[178] Cabrales Fontela Y, Kadavath H, Biernat J, Riedel D, Mandelkow E, Zweckstetter M. “Multivalent cross-linking of actin filaments and microtubules through the microtubule-associated protein Tau”. In: *Nat Commun* 8(1) (2017).

[179] Andreas Janshoff. “Viscoelastic properties of epithelial cells”. en. In: *Biochem. Soc. Trans.* 49.6 (Dec. 2021), pp. 2687–2695.

[180] Peter Nietmann et al. “Epithelial cells fluidize upon adhesion but display mechanical homeostasis in the adherent state”. en. In: *Biophys. J.* 121.3 (Feb. 2022), pp. 361–373.

[181] Cong Y, Topf M, Sali A, Matsudaira P, Dougherty M, Chiu W, Schmid MF. “Crystallographic conformers of actin in a biologically active bundle of filaments”. In: *J Mol Biol* 375(2) (2008).

[182] Helen Nöding et al. “Rheology of Membrane-Attached Minimal Actin Cortices”. In: *The Journal of Physical Chemistry B* 122.16 (Mar. 2018), pp. 4537–4545. DOI: 10.1021/acs.jpcb.7b11491. URL: https://doi.org/10.1021%2Facs.jpcb.7b11491.

[183] Jansen S, Collins A, Yang C, Rebowski G, Svitkina T, Dominguez R. “Mechanism of actin filament bundling by fascin”. In: *J Biol Chem* 286(34) (2011).

[184] Chesarone MA, Goode BL. “Actin nucleation and elongation factors: mechanisms and interplay”. In: *Curr Opin Cell Biol* 21(1) (2009).

[185] Edlund M, Lotano MA, Otey CA. “Dynamics of alpha-actinin in focal adhesions and stress fibers visualized with alpha-actinin-green fluorescent protein”. In: *Cell Motil Cytoskeleton* 48(3) (2001).

[186] J. Victor Small, Theresia Stradal, Emmanuel Vignal, KlemensRottner. “The lamellipodium: where motility begins”. In: *Trends in Cell Biology* 12(3) (2002), pp. 112–120.

[187] Christopher B. O’Connell, Matthew J. Tyska, and Mark S. Mooseker. “Myosin at work: Motor adaptations for a variety of cellular functions”. In: *Biochimica et Biophysica Acta (BBA) - Molecular Cell Research* 1773.5 (May 2007), pp. 615–630. DOI: 10.1016/j.bbamcr.2006.06.012. URL: https://doi.org/10.1016/j.bbamcr.2006.06.012.

[188] Mirco Müller et al. “Distinct Functional Interactions between Actin Isoforms and Nonsarcomeric Myosins”. In: *PLoS ONE* 8.7 (July 2013). Ed. by Friedrich Frischknecht, e70636. DOI: 10.1371/journal.pone.0070636. URL: https://doi.org/10.1371%2Fjournal.pone.0070636.

[189] José Alvarado et al. “Force percolation of contractile active gels”. en. In: *Soft Matter* 13.34 (Aug. 2017), pp. 5624–5644.

[190] S. Burlacu, P. A. Janmey, and J. Borejdo. “Distribution of actin filament lengths measured by fluorescence microscopy”. In: *The American journal of physiology* 262.3 Pt 1 (1992), pp. C569–77. ISSN: 0002-9513. DOI: 10.1152/ajpcell.1992.262.3.C569.

[191] Joost van Mameren et al. “Leveraging single protein polymers to measure flexural rigidity”. In: *The journal of physical chemistry. B* 113.12 (2009), pp. 3837–3844. DOI: 10.1021/jp808328a.

[192] Ahmet Mentes et al. “High-resolution cryo-EM structures of actin-bound myosin states reveal the mechanism of myosin force sensing”. In: *Proceedings of the National Academy of Sciences of the United States of America* 115.6 (2018), pp. 1292–1297. DOI: 10.1073/pnas.1718316115.

[193] Zeynep A. Oztug Durer et al. “Structural states and dynamics of the D-loop in actin”. In: *Biophysical Journal* 103.5 (2012), pp. 930–939. ISSN: 00063495. DOI: 10.1016/j.bpj.2012.07.030.

[194] Yi-Chia Lin et al. “Viscoelastic properties of microtubule networks”. In: *Macromolecules* 40.21 (2007), pp. 7714–7720.

[195] Christopher M Lemon et al. “Metabolic tumor profiling with pH, oxygen, and glucose chemosensors on a quantum dot scaffold”. In: *Inorganic chemistry* 53.4 (2014), pp. 1900–1915.

[196] Lukáš Trizna et al. “Rhodamine 6G-ligand influencing G-quadruplex stability and topology”. In: *International Journal of Molecular Sciences* 22.14 (2021), p. 7639.

[197] Shen Tang and Jenny J. Yang. “Magnesium Binding Sites in Proteins”. In: *Encyclopedia of Metalloproteins*. Ed. by Robert H. Kretsinger, Vladimir N. Uversky, and Eugene A. Permyakov. New York, NY: Springer New York, 2013, pp. 1243–1250. ISBN: 978-1-4614-1532-9. DOI: 10.1007/978-1-4614-1533-6{\textunderscore}257.

[198] Zhifeng Jing et al. “Many-body effect determines the selectivity for Ca2+ and Mg2+ in proteins”. In: *Proceedings of the National Academy of Sciences of the United States of America* 115.32 (2018), E7495–E7501. DOI: 10.1073/pnas.1805049115.

[199] Boiero Sanders M, Antkowiak A, Michelot A. “Diversity from similarity: cellular strategies for assigning particular identities to actin filaments and networks”. In: *Open Biol* 10(9) (2020).

[200] Pardee JD, Spudich JA. “Purification of muscle actin”. In: *Methods Enzymol* (1982).

[201] Sarah E. Bergeron, Mei Zhu, Suzanne M. Thiem, Karen H. Friderici, Peter A. Rubenstein. “Ion-dependent Polymerization Differences between Mammalian β- and -Nonmuscle Actin Isoforms”. In: *J. Biol. Chem.* 285(21) (2010), pp. 16087–16095.

[202] Mirco Müller, Ralph P. Diensthuber, Igor Chizhov, Peter Claus, Sarah M. Heissler, Matthias Preller, Manuel H. Taft, Dietmar J. Manstein. “Distinct Functional Interactions between Actin Isoforms and Nonsarcomeric Myosins”. In: *PLoS ONE* 8(7) (2013).

[203] Bunnell TM, Burbach BJ, Shimizu Y, Ervasti JM. “β-Actin specifically controls cell growth, migration, and the G-actin pool”. In: *Mol Biol Cell* 22(21) (2011).

[204] Hatano T, Alioto S, Roscioli E, Palani S, Clarke ST, Kamnev A, Hernandez-Fernaud JR, Sivashanmugam L, Chapa-Y-Lazo B, Jones AME, Robinson RC, Sampath K, Mishima M, McAinsh AD, Goode BL, Balasubramanian MK. “Rapid production of pure recombinant actin isoforms in Pichia pastoris”. In: *J Cell Sci* 131(8) (2018).

[205] Tomoyuki Hatano et al. “Pick-ya actin: a method to purify actin isoforms with bespoke key post-translational modifications”. In: *J. Cell Sci.* (Jan. 2020). DOI: 10.1242/jcs.241406. URL: https://doi.org/10.1242/jcs.241406.

[206] Case DR, Zubieta J, P Doyle R. “The Coordination Chemistry of Bio-Relevant Ligands and Their Magnesium Complexes”. In: *Molecules* 25(14) (2020).

[207] Amandeep S Arora et al. “Structural insights into actin isoforms”. In: *Elife* 12 (2023), e82015.

[208] Leibler L, Rubinstein M, Colby RH. “Dynamics of Reversible Networks”. In: *Macromolecules* 24 (1991).

[209] Rubinstein M, Panyukov S. “Elasticity of Polymer Networks”. In: *Macromolecules* 35 (2002).

[210] Klaus Kroy and Jens Glaser. “The glassy wormlike chain”. In: *New Journal of Physics* 9.11 (Nov. 2007), pp. 416–416. DOI: 10.1088/1367-2630/9/11/416. URL: https://doi.org/10.1088/1367-2630/9/11/416.

[211] Li Chen and Anna Kashina. “Quantification of intracellular N-terminal β-actin arginylation”. In: *Scientific reports* 9.1 (2019), p. 16669. DOI: 10.1038/s41598-019-52848-5.

[212] MN Spiteri et al. “Persistence length for a PSSNa polyion in semidilute solution as a function of the ionic strength”. In: *Physical review letters* 77.26 (1996), p. 5218.

[213] Eric Buhler and Francois Boue. “Chain persistence length and structure in hyaluronan solutions: Ionic strength dependence for a model semi-rigid polyelectrolyte”. In: *Macromolecules* 37.4 (2004), pp. 1600–1610.

[214] Andrea Romani and A Scarpa. “Regulation of cell magnesium”. In: *Archives of biochemistry and biophysics* 298.1 (1992), pp. 1–12.

[215] Hans-Jürgen Apell, Tanja Hitzler, and Grischa Schreiber. “Modulation of the Na, K-ATPase by magnesium ions”. In: *Biochemistry* 56.7 (2017), pp. 1005–1016.

[216] Th Giinther. “Biochemistry and Pathobiochenpstry of Magnesium”. In: (1981).

[217] Jun He et al. “Counterion-dependent microrheological properties of F-actin solutions across the isotropic-nematic phase transition”. In: *Physical Review E* 78.1 (2008), p. 011908.

[218] Allen J Ehrlicher et al. “Alpha-actinin binding kinetics modulate cellular dynamics and force generation”. In: *Proceedings of the National Academy of Sciences* 112.21 (2015), pp. 6619–6624.

[219] Pablo Minguez et al. “PTMcode v2: a resource for functional associations of post-translational modifications within and between proteins”. In: *Nucleic acids research* 43.D1 (2015), pp. D494–D502.

[220] MATLAB. *version 9.0.1538559 (R2020b)*. Natick, Massachusetts: The MathWorks Inc., 2020.

[221] J. Hokanson. *Tdms reading options*. https://gist.github.com/JimHokanson/dfecf21bde0bb7f2484adaf3c646b91a. 2018.

[222] D. Seara. *Kilfoil Lab Microrheology suite*. https://github.com/dsseara/microrheology. 2017.

[223] T Wagner and M Hiner. “Ridge (Line) detection plugin (Fiji)”. In: 20 (2020), p. 20.

[224] Schindelin, J. et al. “Fiji: an open-source platform for biological-image analysis”. In: *Nat. Methods* 9.7 (2012), pp. 676–682.

List of Tables

List of Figures

List of Abbreviations

AA amino acid

AAS amino acid sequence

ABP actin binding protein

AFM atomic force microscopy

Asp aspartate

CDW charge density wave

DLS dynamic light scattering

DNA deoxyribonucleic acid

DWS diffusing wave spectroscopy

EM electron microscopy

GAUSS Georg-August-University School of Scienc

Glu glutamate

HMM heavy meromyosin

hVPT holographic video particle tracking

LIP liquid ion patch

m-actin muscle actin

MSD mean squared displacement

MT magnetic tweezers

nm-actin non-muscle actin

OT optical tweezers

PDL poly-D-lysine

PTM post-translational modification

SAXS small-angle X-ray scattering

VPT video particle tracking

VPT video particle tracking

WLC worm-like chain

List of Variables and Constants

$l_{\mathbf{p}}$	persistence length
l_0	initial length of an object
σ	mechanical stress
A	area
E	elastic modulus
ϵ	mechanical strain
κ	bending stiffness
$k_{\mathbf{B}}$	Boltzmann constant
T	temperature
D	spatial dimensionality of a system
c	concentration
$l_{\mathbf{c}}$	contour length
ω	angular frequency
ν	Poisson's ratio
$\dot{\epsilon}$	strain rate
η	dynamic viscosity
Δs	shift of the parallel planes against each other (shear deformation)
ν	Poisson's ratio
$l_{\mathbf{O}}$	Odijk length or deflection length
$d_{\mathbf{t}}$	tube diameter (tube model)
$\sigma_{\mathbf{d}}$	mean squared deviation from the tube center (tube model)
$N_{\mathbf{w}}$	number of cubes in a volume
$N_{\mathbf{mw}}$	number of molecules in a mesh cubes
$N_{\mathbf{mv}}$	number of molecules in a volume

$l_{\mathbf{m}}$ monomer length

$s_{\mathbf{u}}$ number of subunits per monomer

s coordinate along the filament

ξ mesh size

τ time step

$\vec{r}(s)$ chain segment position

$\hat{r}_{\mathbf{t}}(s)$ unit tangent vector

$E_{\mathbf{b}}$ energy penalty for filament bending

$C(s)$ tangent vector autocorrelation function or cosine correlation in 2D

$\theta(s)$ tangent angle (cosine correlation)

$\omega_{\mathbf{r}}$ reptation frequency

$\omega_{\mathbf{e}}$ entanglement frequency

$\tau_{\mathbf{r}}$ reptation time

$\tau_{\mathbf{e}}$ entanglement time

$F_{\mathbf{D}}$ drag force

$A_{\mathbf{bt}}$ amplitude of bending fluctuations

ζ translational friction coefficient

$k_{\mathbf{on}}, k_{\mathbf{off}}$ binding rated (on and off)

$R_{\mathbf{eff}}$ effectively bound total number of crosslinks

$\sigma_{\mathbf{A}}$ stress amplitude

$\epsilon_{\mathbf{A}}$ strain amplitude

$\delta_{\mathbf{p}}(\omega)$ phase shift

$m\ddot{x}$ mass

$f_{\mathbf{R}}(t)$ random forces

η^* complex viscosity

$\kappa_{\mathbf{t}}$ force constant of the riving force (OT laser)

$A_{\mathbf{d}}$ amplitude driving force

$\zeta_{\mathbf{f}}(t)$ memory function

$\vec{r}$ position verctor

$\tilde{G}(s)$ Laplace transformed shear modulus

Γ gamma function

t time

h distance of parallel planes from each other (shear deformation)

F force

T torque

l length

K differential modulus

K_0 initial differential modulus

G_0 plateau shear modulus

G^* complex shear modulus

G' storage modulus

G" loss modulus

i imaginary uni

V Volume

a edge length of a cube

R number of crosslinks

I moment of inertia

$\Theta(i\omega)$ sample deformation

$k_{\mathbf{g}}$ geometry specific constant for rheometer measurements

x one dimensional particle position in a laser trap (OT)

a particle radius

D dampened amplitude of particle oscillation (OT)

v velocity

Acknowledgments

Ich möchte an dieser Stelle besonders Prof. Andreas Janshoff für die gute Betreuung und Unterstützung danken. Vor allem für die vielen Freiheiten, die eine freie Entfaltung in meiner wissenschaftlichen Arbeit ermöglicht haben.

Prof. Sarah Köster danke ich für die Übernahme des Zweitgutachtens, eine gute Betreuung im Thesis Committee und die gute Kooperation bei wissenschaftlicher Arbeit.
Des Weiteren danke ich Prof. Peter Sollich ebenfalls für eine gute Betreuung im Thesis Committee und zusätzlich die Bereitschaft, Teil des Examination Boardes zu werden.
Genauso danke ich Prof. Tim Salditt, Dr. Tim Schäfer und Prof. Timo Betz für die Beteiligung an meinem Examination Board und das Interesse an meiner Arbeit.
Besonderer Dank gebührt meinem Kollegen Kevin Kaub, mit dem ich gemeinsam einige der hier beschriebenen Experimente durchgeführt und ausgewertet habe. Die Daten im Isoformen-Kapitel (Kapitel 3) sind in gleichberechtigter Kooperation mit ihm gesammelt worden. Daten im DNA-Kapitel (Kapitel 2) wurden teilweise zusammen aufgenommen. Kevin, du bist für mich nicht nur ein guter Kollege, sondern auch ein guter Freund geworden.
Ebenso möchte ich meiner Bachelor-Studentin Susanne Stenz für hervorragende Zusammenarbeit und erfrischendes Interesse an der Forschung danken. Die Daten im PTM-Kapitel (Kapitel 4) sind in Kooperation mit ihr gesammelt und ausgewertet worden.
Gesondert danke ich unseren Kooperationspartnern. Prof. Kerstin Göpfrich, sowie Kevin Jahnke danke ich für gute Zusammenarbeit und das Zusenden von DNA-filamenten. Prof. Mohan Balasubramanian und Andrejus Suchenko danke ich ebenfalls für gute Zusammenarbeit und das Zusenden der in Hefe exprimierten Aktin Varianten.
Dr. Ingo Mey und Dr. Tabea Oswald danke ich für stets gute fachliche und moralische Unterstützung.
Zu guter Letzt danke ich dem restlichen Arbeitskreis der Abteilung Janshoff. Die Arbeit hat mir großen Spaß gemacht und auch nach Feierabend war die Verständigung auch immer gut.
Es waren vier Jahre meines Lebens, die mich sowohl fachlich, als auch menschlich sehr viel weiterentwickelt haben. Dafür bin ich vollkommen aufrichtig dankbar.